Expanding Primary Metabolism for New Bioproducts: Pathway Design, Enzyme Discovery, and Fermentation Optimization

A Dissertation
SUBMITTED TO THE FACULTY OF
UNIVERSITY OF MINNESOTA
BY

Yi-shu Tai

IN PARTIAL FULFILLMENT OF THE REQUIREMENTS
FOR THE DEGREE OF
DOCTOR OF PHILOSOPHY

Kechun Zhang

June 2016

Acknowledgements

I would like to first thank my wife Chin-Ann Yang for her love and encouragement during these long years. I always feel that I am the luckiest to have her as my wife. Without her keeping me sane, I won't be able to complete my PhD degree. I would also like to thank my daughter Amelia Tai. Just seeing her smile makes my day. As a genetic engineer, she is always inspiring to me about how incredible nature is. I would thank my parents and my parents-in-law for their patience and support throughout the process. Especially, I really appreciate my mother-in-law for helping taking care of Amelia for the first several months.

I am thankful to people who have helped me along the way. I am thankful to all colleagues and friends in the department. I also want thank Chi-Ming Tseng and Shu-Yun Tseng for taking care of me when I first arrived at MN. They generously provided a room for me and helped me settle down in Minneapolis. I really appreciate Christopher Peterson for sparing his time every week helping me improve me communication and presentation skills. I would thank Julie Prince for her assistance on various things such as fellowship applications and registration process.

My deepest acknowledgement goes to my PhD advisor Dr. Kechun Zhang. I learnt a great deal from him. Thanks him for letting me have this opportunity to work on the exciting science. His enthusiasm and wisdom on metabolic engineering is always motivating to me. Through his mentorship, I became a better metabolic engineer. Besides, I would like to thank all past and present Zhang lab members, in particular Dr. Mingyong Xiong, Pooja Jambunathan, Maria McClintock, Dr. Jingyu Wang, Dr. Jilong Wang, and Kevin J. Fox. Specifically, I would like to acknowledge all the collaborators in various project including Dr. Chaoqun Zhang, Dr. Tao Cai, and Debbie Schneiderman on the MVL project and Dr. Wenqin Bai on the mesaconate project. I would also like to thank members of Hackel lab who shared lab space with us and helped me a lot on experiments and equipment usage. Financially, The Stephen J. Salter Fellowship and the Doctoral Dissertation Fellowship supported my study. Lastly, I would like to thank my committee members Dr. Xiang Cheng, Dr. Prodromos Daoutidis, and Dr. Michael Smanski for their time and help on the process of completing my degree.

Dedication

This thesis is dedicated to my parents Ping-Hung Tai and Hui-Ling Kuo, my wife Chin-Ann Yang, and my daughter Amelia Tai.

Abstract

Fermentation, like brewing beer, has the potential to produce chemicals and fuels that are currently derived from petroleum via unsustainable and environmentally-unfriendly manufacturing processes. The two main challenges for a fermentation-based chemical industry are the diversity of molecules and the effectiveness of conversion processes. To enable broader applications of fermentation, there is a pressing need to expand the scope of fermentation products and improve the relevant production efficiency. Therefore, my thesis research focuses on expanding the capabilities of microbial biosynthesis in *Escherichia coli*. I designed novel metabolic pathways to enable the production of new bioproducts and to effectively convert abundant but underused biomass sugars into value-added chemicals. The biosynthetic processes were realized by enzyme discovery and then further optimized by metabolic engineering and enzyme engineering. Firstly, I designed and built a medium-chain ester biosynthetic platform and enabled production of two target esters by screening the key enzyme. I also engineered a novel nonphosphorylative metabolism which can effectively convert biomass-derived pentoses or sugar acids into TCA cycle derivatives. Two chemicals, 1,4-butanediol and mesaconate, were successfully produced as demonstrations. Furthermore, an optically active monomer (-)-β-methyl-δ-valerolactone was manufactured via a chemo-enzymatic process and the key enzymes were investigated. Overall, this work has brought new tools and design principles to the field of metabolic engineering and can be served as the cornerstone for future development of economically feasible renewable chemicals.

Table of Contents

List of Tables

List of Figures

Chapter 2

Chapter 3

Chapter 4

Chapter 5

List of Schemes

Chapter 1

Chapter 5

Chapter 1. Overview of Engineering Metabolic Pathways for the Production of Commodity Chemicals

1. Background

Petroleum is the material basis of modern society which not only fuels our vehicles but also provides precursors for innumerable daily consumer products (e.g. cosmetics, sneakers, textiles, and drugs). For over a century, we have been extracting petroleum from oil reservoirs and then performing energy-intensive distillation to refine it into different products. We currently consume more than 90 million barrels of oil each day and the demand will continue to surge with the growing population. Therefore, this resource is nonrenewable and will not be sustainable in the near future. Moreover, the use of petroleum has a negative impact on the environment. For example, the BP oil spill in the Gulf of Mexico in 2010 killed about 800,000 birds, devastated the marine ecosystem, and resulted in health problems for cleanup workers. Globally, CO_2 released by combusting petroleum has caused global warming and climate change. These growing concerns are driving the transition from current petroleum-based economy to a green, bio-based economy.

Fermentation will play a key role in facilitating this significant transition due to its ability of producing a diverse array of products from biomass-derived sugars. The fermentation processes exploit microbes as cellular chemical factories with enzymes as catalysts. Unlike petrochemical processes, fermentation processes are environmentally benign (mild reaction conditions, no toxic heavy-metal catalyst required, fewer production wastes) and cost-effective since the starting materials—biomass—is

abundant and renewable. For example, worldwide production of lignocellulosic biomass (plant dry matter) is estimated to exceed 220 billion tons, equivalent to 60-80 billion tons of crude oil[1], which has the potential to support global oil consumption for more than 15 years. To develop these microbial cell factories that can rival petrochemical industry, technological advances are necessary to address the challenges.

The key challenge that has limited the application of using fermentation for producing chemicals and fuels is the natural metabolic capacity of microorganisms. Most of the daily petroleum-derived chemicals or fuels used are not metabolites found in nature. To address this significant challenge, my thesis focuses on applying synthetic biology and metabolic engineering tools to design and build artificial metabolic pathways to produce new bioproducts in an industrial workhorse *E. coli* (**Fig. 1.1**).

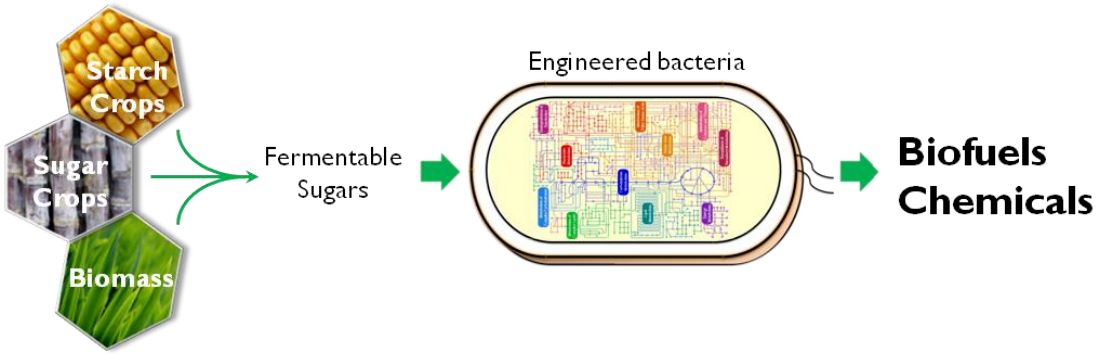

Figure 1.1|Production of non-natural chemicals or biofuels from renewable and sustainable resources by engineered microorganisms.

2. Engineering Artificial Metabolic Pathways for Biosynthesis of Chemicals

2.1 Introduction

The current fossil-based economy is unsustainable considering surging demand from the rapidly increasing world population, coupled with diminishing petroleum reserves and environmental problems associated with chemical processes. Thus, the transformation of traditional chemical processing and production into a green and sustainable future is of critical importance. The U.S. Department of Energy has set goals to replace 30% of transportation fuel with biofuels and to produce 25% of industrial chemicals from biomass by 2025[2]. A shift in the feedstock from hydrocarbons to biomass will fundamentally change the technological basis of the industry. In particular, there is a need for technologies that can convert renewable carbon sources into a diverse array of useful products.

Biosynthesis is powerful tool to facilitate the paradigm shift. As an ancient process dating back thousands of years, biosynthesis plays a pivotal role in human history. For example, winemaking has shaped the development of human civilization[3]; and the production of the "wonder drug" penicillin contributed to victory in World War II, and since then has saved millions of lives[4]. The unique advantage of biosynthesis is its potential to manufacture chemicals from renewable biomass resources or even CO_2[5] in a sustainable, green and cost-effective fashion.

Traditionally, the practice of biosynthesis is through "metabolic engineering"[6], by which enzymatic pathways, regulatory networks and cellular metabolism are optimized to increase the production of a given substance. This process relies on manipulating natural

metabolic capability, and so targets are limited to existing natural metabolites. As a result, decades of research in this field have found success with only a few molecules for large-scale industrial production, such as ethanol, amino acids, lactate, and vitamins[7]. This contrasts starkly with the situation of synthetic organic chemistry, which grew rapidly following the discovery of petroleum, led to the birth of the petrochemical and pharmaceutical industries, and laid the foundation for modern life by providing most of the chemicals which are used daily around the globe.

Recently, to maximize the potential of biosynthesis to replace chemical synthesis, there have been various research efforts directed towards constructing artificial metabolic pathways for novel metabolites[8, 9, 10, 11, 12, 13, 14]. With information provided by genomics, proteomics and bioinformatics, pathway design is facilitated by the availability of suitable enzymes and microorganisms. Some of the recent progress on synthetic pathways to fuels and chemicals are described including three model pathways: ketoacid, fatty acid and isoprenoid. As the key primary and secondary metabolic pathways in nature, these pathways utilize a wide range of chemical reactions and generate various products.

2.2 Ketoacid-based pathways

It is challenging to import and express artificial pathways because they may cause metabolic imbalance. Therefore, the use of existing pathways that are compatible with the host are sometimes necessary. One of the promising candidates is amino acid pathways which produce the building blocks of proteins. Thus, amino acid synthesis pathways are essential to any living organism. Currently, microbial engineering has

enabled the economical production of natural amino acids from glucose[15]. For example, more than two million tons of L-glutamate, L-lysine and L-threonine are produced annually[16]. With knowledge from the fermentation industry, significant progress has been made in artificially expanding the amino acid pathways. Since the common precursors to amino acids are 2-ketoacids, engineering efforts have been focused on building pathways around ketoacids (**Scheme 1.1**).

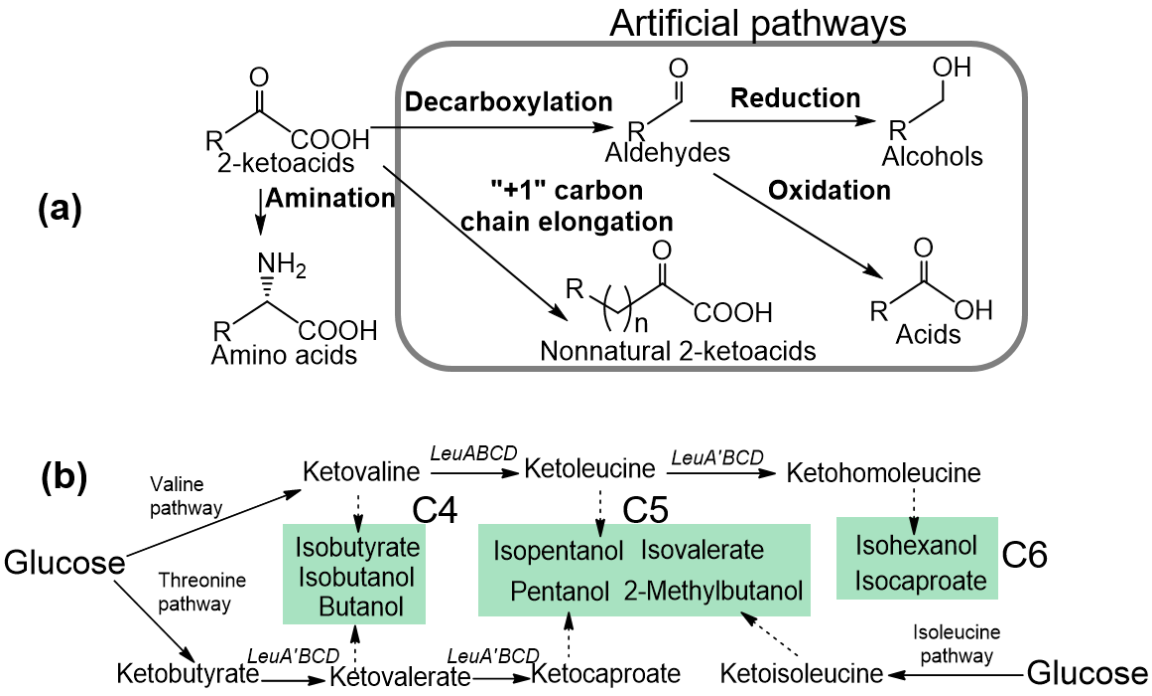

Scheme 1.1| (a) Artificial pathways expanded from 2-ketoacids by combinatorial enzyme screening or engineering. Decarboxylation is catalyzed by 2-ketoacid decarboxylase. Reduction is catalyzed by alcohol dehydrogenase and oxidation is enabled by aldehyde dehydrogenase. Chain elongation is facilitated by engineered LeuABCD "+1" module. **(b) Examples of C4, C5, and C6 compounds produced in *E. coli* with the platform pathways.**

One type of chemical derived from ketoacids is alcohol. Higher alcohols are minor metabolites that exist in the Ehrlich degradation pathway[17]. However, the natural higher alcohol pathway is not optimal given that the alcohol concentration is too low for practical application. To explore the potential of artificial pathways to improve production, Atsumi *et al.* developed a strategy to produce C3-C5 alcohols by enzyme discovery and combinatorial optimization[8]. In their design, 2-ketoacids were converted to aldehydes by 2-ketoacid decarboxylase (KDC), and then reduced to alcohols by alcohol dehydrogenase (ADH). With Adh2 from *Saccharomyces cerevisiae* selected as the alcohol dehydrogenase, five KDCs from different organisms were screened for their ability to produce alcohols. Fermentation results demonstrated that Kivd from *Lactococcus lactis* was the most active decarboxylase, which enabled the synthesis of 1-propanol, 1-butanol, isobutanol, 2-metyl-1-butanol, 3-methyl-1-butanol, and 2- phenylethanol. Increasing the 2-ketoacid flux did enhance the specificity and production levels of alcohols. In particular, isobutanol derived from the valine pathway accumulated to 22 g/l with a yield of 0.35 g/g glucose (86% theoretical maximum). Later the production of other C3-C5 alcohols was also optimized[18, 19, 20].

Artificial pathways have also been constructed to extend the carbon chain of ketoacids. Zhang *et al.* engineered a "+1" metabolic pathway to produce non-natural C6-C9[21] 2-ketoacids. The nature role of the "+1" reaction enzyme (LeuABCD) is to add one more carbon onto ketoisovalerate (C5) and turn it into ketoisocaproate (C6). The synthetic pathway was utilized by protein engineering. Interestingly, only mutation of the first enzyme, LeuA (2-isopropylmalatesynthase), in the LeuABCD elongation pathway

was necessary, while the subsequent enzymes are naturally promiscuous enough to accept bulkier substrates. To enlarge the binding pocket, the authors systematically mutated several residues of the substrate binding pocket into smaller amino acids such as glycine or alanine. Coupled with the alcohol pathway enzymes, a two-residue LeuA mutant produced 793.5 mg/l 3-methyl-1-pentanol, a nonnatural C6 alcohol. Several other LeuA mutations were good for producing a series of C5-C8 alcohols: 1-pentanol (C5), 1-hexanol (C6), 4-metyl-1-pentanol (C6), 4-methyl-1-hexanol (C7), and 5-methyl-1-heptanol (C8). This LeuABCD pathway was later modified to be a universal "+1" metabolic module and enabled the production of 1-heptanol, 1-octanol and even the aromatic compound phenylpropanol[22]. The success of this module to catalyze 5 elongation cycles that involved 25 chemical reaction steps relied on engineering an extremely flexible LeuA with four mutated residues that have better catalytic efficiency towards higher substrates. This work demonstrates the utility of protein engineering in building artificial metabolism for biosynthesis of fuels or chemicals.

In addition to alcohols, the conversion of ketoacids to carboxylic acids was demonstrated[23, 24]. To shift the products from alcohols to acids, nonnatural metabolic pathways were constructed to oxidize rather than reduce aldehydes. With a hypothesis that promiscuous enzymes could facilitate nonnatural biosynthesis, seven candidate enzymes representing the entire aldehyde dehydrogenase family were screened for acid production. It was discovered that *E. coli* phenylacetaldehyde dehydrogenase was the best enzyme to synthesize isobutyrate and isovalerate, and *Burkholderia ambifaria* α-ketoglutaric semialdehyde dehydrogenase was effective for isocaproate production. Carboxylic acids

could be biosynthesized with a higher titer than alcohols. Bioreactor experiments showed that engineered *E. coli* could produce 90 g/l C4 isobutyrate, and 32 g/l C5 isovalerate. In comparison, the concentrations of corresponding alcohols (isobutanol and isopentanol) could only reach 22 g/l and 4.4 g/l respectively in the fermentation broth without in situ removal[25].

2.3 Fatty acid-derived pathways

Fatty acids are the basic components of cell membranes. They constitute a major portion of cell mass in many organisms. These molecules have high energy density and low water solubility because of their long hydrocarbon chain. They are traditionally used to produce biodiesels by esterification. The utility of fatty acid biosynthesis has been broadened by designing novel pathways composed of promiscuous enzymes to synthesize fatty acid derivatives, such as fatty acid esters, fatty alcohols, alkanes, alkenes, and long-chain dicarboxylic acids (**Scheme 1.2**).

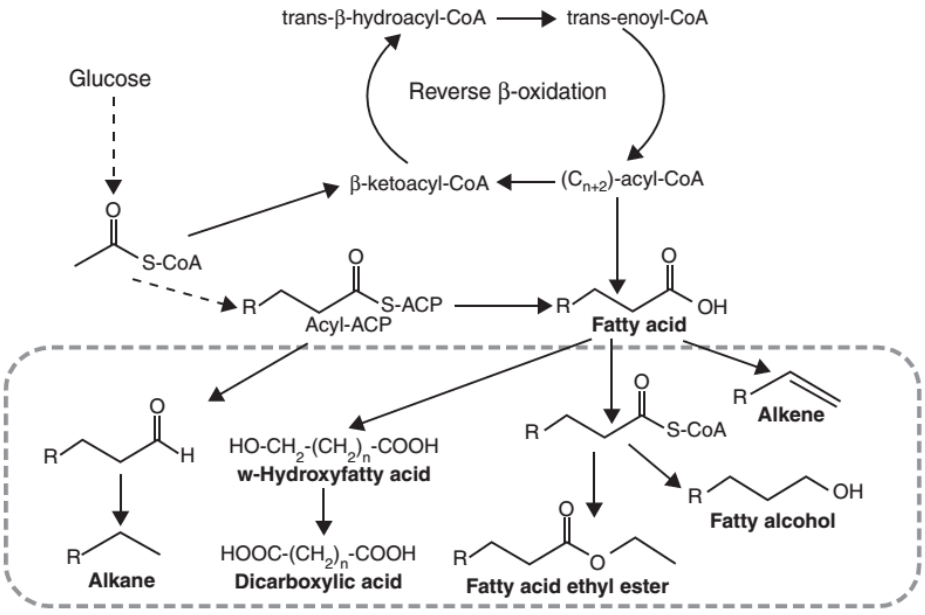

Scheme 1.2| Biosynthesis of chemicals by expanding fatty acid pathways with promiscuous enzymes. Fatty acid can be derived from either the natural fatty acid biosynthetic pathway or the reversal of b-oxidation pathway. Alkanes are derived from the intermediate compound acyl-ACP. Fatty acids can lead to a diverse set of molecules: alkenes, dicarboxylic acids, fatty acid ethyl esters and fatty alcohols.

Two major problems for biodiesel production are transesterification and the separation steps. To abate these effects, a nonnative pathway was constructed in *E. coli* to generate fatty acid ethyl esters[26]. This pathway was enabled by the discovery of a broad-substrate-range acyltransferase (AftA) from *Acinetobacter baylyi*. Combining the ethanol production pathway from *Zymomonas mobilis* (*pdc* & *adhB*), the engineered cell produced 1.28 g/l fatty acid ethyl esters. Steen *et al.* further developed this concept and engineered novel pathways in *E. coli* to overproduce fatty alcohols and esters directly from hemicellulose[9]. In this consolidate bioprocessing scheme, fatty acids were obtained from fatty acyl-ACPs with a native thioesterase (TesA) from *E. coli*, and then activated to acyl-

CoAs with ligase FadD for ester synthesis. Fatty alcohols were also detected by overexpressing *fadD* and an acyl-CoA reductase from *Acinetobacter calcoaceticus*. These pathways could be optimized in *E. coli* strains that hyperproduce fatty acids. For example, Liu *et al.* reported that the productivity of fatty acids reached 4.5 g/l/d with the introduction of a plant thioesterase and the overexpression of acetyl-CoA carboxylase[27].

New synthetic pathways have also been built to biosynthesize other useful chemicals, such as alkanes, alkenes and dicarboxylic acids. In one study, 300 mg/l alkane mixture (C13–C17) was produced in *E. coli* with a combination of the cyanobacteriaenzymes acyl-ACP reductase (AAR) and aldehyde decarbonylase (ADC)[28]. For this pathway, AAR reduced the acyl-ACPs into aldehydes, which were turned into alkanes by ADC. The synthesis followed the "n-1" rule with one carbon loss in the process. In parallel, terminal alkenes were synthesized in *E. coli* by the expression of a functionally promiscuous P450 enzyme from *Jeotgalicoccus spp.*, which decarboxylated free fatty acids into alkenes[29]. The other function of P450 is hydroxylation. Picataggio *et al.* utilized P450 to produce a wide range of C12-C20 dicarboxylic acids in engineered *Candida tropicalis*[30]. Here fatty acids were first ω-hydroxylated, then fully oxidized to ω-acid by long-chain alcohol and aldehyde dehydrogenases. With the right selection of enzymes, the regioselectivity of terminal oxidation and conversion efficiency of fatty acids reached almost 100%. Another study used engineered *C. tropicalis* to produce commercially viable yields of ω-hydroxyfatty acids (174 g/l of 14-hydroxytetradecanoic acid)[31].

In addition, fuels and chemicals were produced by engineering the reversal of the fatty acid β-oxidation pathway. Dellomonaco *et al.* constructed a novel platform in *E. coli* for the production of a series of compounds that included C4–10 alcohols and C10–18 fatty acids[32]. This system reported a production titer of 7 g/l long chain fatty acids. The platform innovatively exploited the reversible nature of enzymatic reactions to drive the carbon-carbon bond formation. A similar strategy was also utilized for the synthesis of butanol and hexanol[33, 34].

2.4 Isoprenoid-derived artificial pathways

Isoprenoids represent structurally and functionally the most diverse group of plant metabolites, with more than 30,000 compounds reported so far[35, 36]. Isoprenoids are synthesized from two basic units, isopentenyl diphosphate (IPP) and its isomer dimethylallyl diphosphate (DMAPP), which are produced via the mevalonate pathway or the methylerythritol pathway. DMAPP and IPP are condensed to generate geranyl diphosphate (GPP, C10), which is further converted to FPP (C15) and GGPP (C20). GPP, FPP and GGPP are the precursors to monoterpenes, sesquiterpenes and diterpenes, respectively. Because most isoprenoids are present in minute amounts in their natural hosts, they do not have wide industrial applications. This situation is being alleviated by the emergence of "synthetic biology", which reconstitutes natural pathways in new hosts for higher-level production, or redesigns novel pathways for product diversification (**Scheme 1.3**).

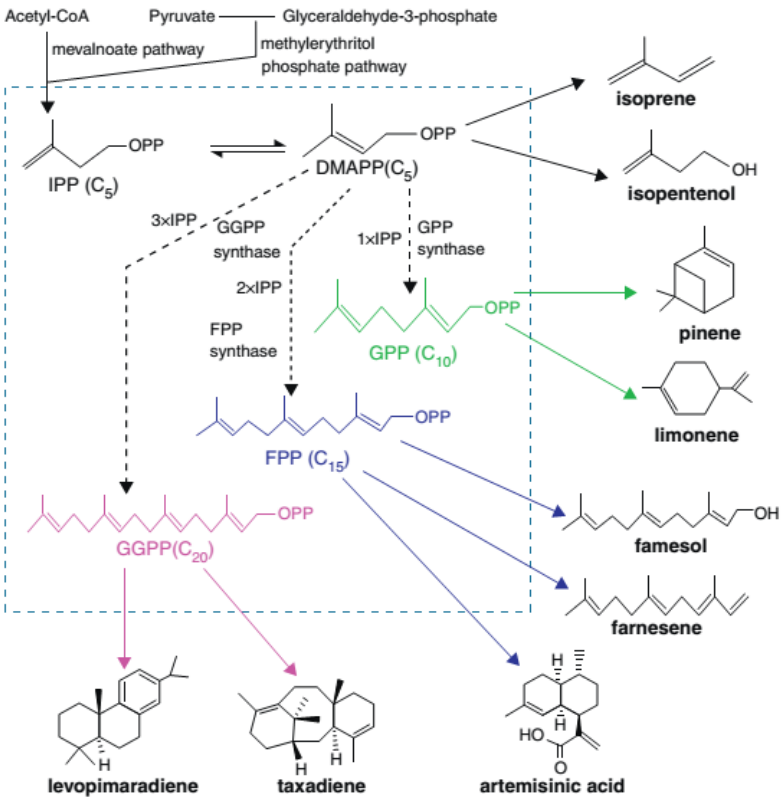

Scheme 1.3| Synthetic pathways derived from isoprenoid biosynthesis. Three basic structural units, GPP, FPP and GGPP, are obtained from DMAPP by prenyltransferases. By further extension of the isoprenoid pathways, DMAPP is converted to isoprene or isopentenol. GPP can be used to synthesize monoterpenes pinene and limonene. Sesquiterpenes such as farnesol, farnesene and artemisinic acid are derived from FPP. Diterpenes levopimaradiene and taxol are synthesized from GGPP.

Biosynthesis of isoprenoid alcohols takes advantage of the promiscuous nature of phosphatases to construct nonnatural metabolic pathways. Recently, two genes, *yhfR* and *nudF*, from *Bacillus subtilis* were discovered to convert IPP or DMAPP to isopentenol based on toxicity screening[37]. Overexpression of such nonspecific pyrophosphatases in *E. coli* with melvonate pathway amplified led to the production of 1.5 mM isopentenol directly from glucose. Similarly, the C15 alcohol farnesol was produced in *E. coli* at a

concentration of 135.5 mg/l by increasing the FPP flux[38]. It was suggested that promiscuous endogenous phosphatases catalyzed the hydrolysis of FPP to farnesol.

Terpene synthases represent another class of promiscuous enzymes that could aid the construction of pathways to produce isoprenoid olefins. For example, the poplar isoprene synthase was characterized and introduced into *E. coli* for the production of isoprene from DMAPP[39]. The pathways to monoterpene olefins such as pinene and limonene were also demonstrated with the overexpression of monoterpene synthase[40]. However, the production level of monoterpenes was very low (<5 mg/l). In contrast, sesquiterpene synthases can be more effectively overexpressed in bacterial hosts and thus can enable the biosynthesis of C15 olefins such as farnesene and bisabolene[41, 42]. In particular, 900 mg/l bisabolene was produced by engineered *E. coli* in shake flask experiments. This was achieved by enzyme screening to identify the best bisabolene synthase, optimizing codons of heterologous pathway genes and overexpressing key mevalonate pathway enzymes.

Isoprenoids are an important source of pharmaceuticals. It is well known that the sesquiterpene artemisinin is the most effective antimalarial drug, and diterpene taxol is a well-known mitotic inhibitor used in ovarian, breast and lung cancer therapy. The low yield from natural sources has limited their usage. Recently, reengineering natural pathways into bacterial hosts has generated exciting results. Ajikumar *et al.* successfully overproduced the first committed taxol intermediate, taxadiene, in *E. coli* with a high titer of 1 g/l[43]. They proposed a "multivariate modular pathway engineering" approach to combinatorially optimize the synthetic pathway. The high titer of taxadiene production

was obtained by balancing the upstream and downstream pathways. In addition, they introduced an engineered P450 fusion enzyme to produce 58 mg/l taxadien-5a-ol from taxadiene. Another diterpene, levopimaradiene, was successfully produced in *E. coli* with a titer of 700 mg/l[44]. The pathway was optimized by generating combinatorial mutations in geranylgeranyl diphosphate synthase and levopimaradiene synthase to remove limitations caused by precursor supply, and therefore enhance the productivity of levopimaradiene. One of the most striking examples for synthetic pathways is engineered biosynthesis of artemisinin precursor[45]. By adjusting protein activity of the pathway enzymes, a transgenic yeast could produce >40 g/l of the artemisinin precursor amorpha-4,11-diene[46].

3. Thesis Overview

Chapter 1. This chapter presents a background for the importance of renewable and sustainable chemicals and shows fermentation as a promising method for a sustainable future. I use three metabolic platforms including ketoacid pathways, fatty acid pathways, and isoprenoid pathways to demonstrate potential products that can be or have been manufactured by expanding natural metabolic pathways.

Chapter 2. This chapter describes my early project on designing and constructing an ester production platform in *E. coli*. Working in collaboration with Dr. Mingyong Xiong, I screened five candidate alcohol acyltransferases and successfully produced two target esters isobutyl acetate and isoamyl acetate. I also characterized the activities of these

alcohol and acyltransferases and scaled up the fermentation process in a 1.3-l bioreactor using the best isobutyl acetate producing strain which resulted in 36 g/l production.

Chapter 3. This chapter describes the design and construction of a nonphosphorylative metabolism in *E. coli*. This novel metabolism has a higher theoretical yield and fewer reaction steps than intrinsic pathways. I worked D-xylose and D-galacturonate pathways and characterized key enzymes. After confirming the activity of this metabolism in *E. coli*, it was expanded to produce 1,4-butanediol.

Chapter 4. This chapter discusses the expansion of the nonphosphorylative metabolism used in the previous chapter to produce a dicarboxylic acid mesaconate. Various pentose transporters and operons were screened for better mesaconate production. Metabolic engineering was applied to optimize mesaconate production. The engineered strain can use glucose, D-xylose, and L-arabinose simultaneously for mesaconate production.

Chapter 5. This chapter describes the attempt to investigate optically active monomer β-methyl-δ-valerolactone. I performed 1.3-l bioreactor fermentation to produce the two enantiomers and characterized the two enol reductases. The polymer produced from optically active (-) monomer showed similar properties as to the atactic counterpart.

Chapter 6. This chapter concludes the work described in the previous chapters and highlights the contribution to the field of microbial metabolic engineering.

Chapter 2. Design and Creation of a Novel Biosynthetic Platform for Medium-chain Esters in *Escherichia coli*

Summary

Medium-chain esters such as isobutyl acetate (IBAc) and isoamyl acetate (IAAc) are high-volume solvents, flavors, and fragrances. I engineered a synthetic metabolic platform in *Escherichia coli* for the total biosynthesis of IBAc and IAAc directly from glucose. The pathways harnessed the power of natural amino acid biosynthesis. In particular, native valine and leucine pathways in *E. coli* were utilized to supply precursors. Alcohol acyltransferases (AATs) from various organisms including *Petunia x hybrida*, *S. cerevisiae*, *Clarkia breweri*, and *Fragaria x ananassa* were investigated on their capability to catalyze esterification reactions between targeted alcohols and acyl-CoAs. It was discovered that ATF1 from *S. cerevisiae* was the best AAT for the formation of both IBAc and IAAc in *E. coli*. *In vitro* biochemical characterization of the five AATs further confirmed the fermentation results and showed that ATF1 is the most active AAT with specific constants (k_{cat}/K_M) at 90.6 $s^{-1}M^{-1}$ and 113.2 $s^{-1}M^{-1}$ towards IBAc and IAAc, respectively. Strain improvement was then performed by removing byproduct pathways (Δ*ldh*, Δ*poxB*, Δ*pta*) and resulted in increasing production of both target chemicals. The best IBAc producing strain was used for scale-up fermentation in a 1.3-L benchtop bioreactor. IBAc was produced at 36g/l after 72 h of fermentation. This work demonstrates the design and creation of a novel ester production platform in *E. coli* and showed the feasibility and scalability of the total biosynthesis of IBAc as a renewable chemical.

1. Introduction

Volatile medium-chain esters (C6-C10) are chemicals with versatile industrial applications. They are flavor components of the majority of fruits and are widely used as flavors and fragrances[47]. For example, isobutyl acetate (IBAc), naturally existing in raspberries, pears, and pineapples, has a fruity scent and can also be used as a colorless solvent[48]. IBAc is an economical and environmentally friendly replacement for methylisobutyl ketone or toluene in many formulations. Moreover, IBAc is widely used in coatings, adhesives, printing inks, fragrances, and cosmetics. The global consumption of IBAc was 187 million pounds in 2005[49]. Another target ester, isoamyl acetate (IAAc), has one more carbon than IBAc. Due to its unique banana flavor, it is used as flavoring additives in foods and beverages[50]. Similar to IBAc, IAAc can also be used as a green solvent in surface coatings and pharmaceuticals.

Another potential application of these esters is biofuel. For example, several valerate esters (C6-C10) have been proved to be fully compatible with transportation fuels[51]. These medium-chain esters contain high energy content that is compatible with existing infrastructures[51]. Moreover, they all have very low solubility in water which is beneficial for separation process[52]. Medium-chain esters are not hygroscopic like ethanol, which are suitable for cold starting and will prevent corrosion. Currently, ethanol[53] and biodiesels[9, 54] are the primary targets for biofuel production. However, ethanol has low energy content and is highly hygroscopic. Although biodiesel contains higher energy density, it gels under cold weather[55] and is not efficient for extracellular secretion due to

the high molecular weights[9]. Therefore, medium-chain esters have the potential to address these significant challenges in current biofuel industry.

Several methods have been developed for the production of medium-chain esters. Currently, they are mainly manufactured via Fischer esterification, but this process may raise environmental concerns since the reactants are often derived from crude oil and harsh acids are used to catalyze esterification reactions. Extraction from plant materials has low yields and results in high processing costs[56]. Direct esterification or trans-esterification reactions can be catalyzed by enzymes such as lipases. However, to shift the reaction equilibrium towards ester synthesis, a significant amount of organic solvent such as *n*-hexane has to be used making the process environmentally unfriendly[56]. Naturally, several sake yeasts are able to produce IBAc and IAAc in low levels[57, 58]. Recently, there are several studies on the production of IAAc using externally supplemented 3-methyl-1-butanol (3MB) and intracellular acetyl-CoA[50, 59, 60]. Both pathway and cofactor manipulations were implemented to enhance IAAc production. Since 3MB was fed to fermentation culture, this process is not completely renewable. However, the enzyme alcohol acyltransferase (AAT) used in these previous studies condenses an alcohol and an acyl-CoA to form esters. The energy stored in the thioester bond therefore drives the equilibrium towards ester production[61]. Based on AAT, I designed and engineered metabolic pathways by expanding 2-keto acid synthetic pathways for the direct biosynthesis of IBAc and IAAc in *E. coli*.

The production of higher alcohols[8, 21] and carboxylic acids[62, 63] exploiting amino acid precursors has proven to be successful. These amino acid pathways generate 2-keto

acids that can be converted into desired products. Since these pathways are commonly found in different organisms, a variety of hosts can be explored. Here the metabolic platform for IBAc and IAAc production was constructed by expanding native valine and leucine biosynthetic pathways in *E. coli* (**Fig. 2.1**). Acetyl-CoA is a key metabolite and is ubiquitous in *E. coli*. For the production of both IBAc and IAAc, a common intermediate is 2-ketoisovalerate (KIV). KIV is a precursor for valine biosynthesis and its production was improved by overexpressing three enzymes including acetolactate synthase AlsS[64], 2,3-dihydroxy isovalerate oxidoreductase IlvC, and 2,3-dihydroxy isovalerate dehydratase IlvD[65]. Followed by the last two steps in the Ehrlich pathway[66], KIV can first be converted into isobutyraldehyde by a 2-keto-acid decarboxylase (Kivd from *Lactobacillus lactis*) and then to isobutanol by an alcohol dehydrogenases YqhD[67]. For IAAc production, to elongate the carbon chain of KIV, the leucine pathway which overexpresses 2-isopropylmalate synthase LeuA, isopropylmalate isomerase complex LeuC and leuD, and 3-isopropylmalate dehydrogenase LeuB was introduced. KIV is converted to 2-keto-4-methyl-pentanoate and then to 3-methyl-1-butanol[68] by the last two steps in the Ehrlich pathway. The final step for the production of our target compounds IBAc and IAAc was achieved by an AAT that catalyzes the reactions: condensing isobutanol or 3-methyl-1-butanol with acetyl-CoA to form IBAc or IAAc, respectively.

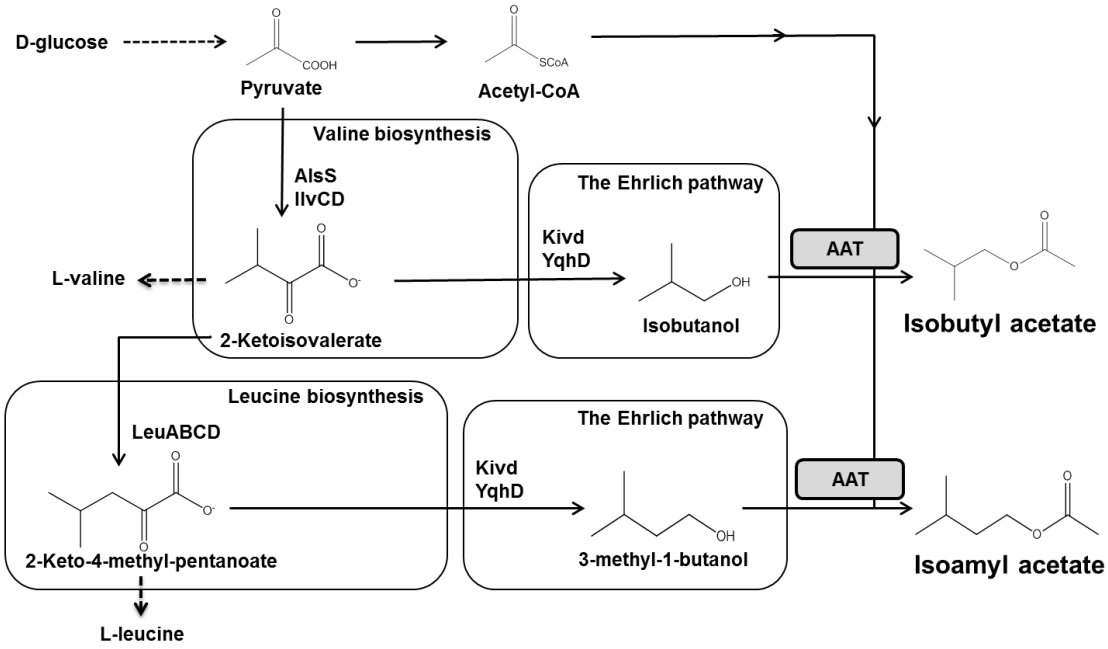

Figure 2.1| Metabolic pathway from glucose to isobutyl acetate (IBAc) and isoamyl acetate (IAAc). Abbreviation: AAT (Alcohol acyltransferase).

To further enhance the production of these medium-chain esters, the acetate production pathway (*poxB-pta*) and the lactate production pathway (*ldh*) were inactivated to increase intracellular levels of both acetyl-CoA and targeted alcohols. In this work, the production of two medium-chain esters, IBAc and IAAc directly from glucose was demonstrated. Particularly, IBAc biosynthesis was successfully scaled up in a 1.3-L benchtop bioreactor and produced 36 g/l IBAc in 72 h.

2. Results and Discussion

2.1 Design and construction of the biosynthetic pathways for the production of IBAc and IAAc

To produce IBAc and IAAc in *E. coli*, pathways downstream from pyruvate to the desired compounds were overexpressed. Genes were expressed from plasmids under the regulation of $P_{LlacO-1}$ promoter[69]. To produce IBAc, the two synthetic operons applied are shown in **Fig. 2.2A**. The first operon (pIBAc4—pIBAc8) was composed of three genes on a medium copy plasmid in the transcriptional order *ilvD-alsS-AAT*. Five candidate AATs were investigated in this work. The second operon (pYT2) was used to overexpress 2-keto-acid decarboxylase and alcohol dehydrogenase as the last two steps in the Ehrlich pathway. These two genes were cloned on a high copy plasmid (pYT2) in a transcriptional order *kivd-yqhD*. For the synthesis of IAAc, the other two similar synthetic operons used are shown in **Fig. 2.2B**. In order to elongate carbon chain by the leucine pathway for the production of isoamyl alcohol, the first operon (pIAAc2—pIAAc6) overexpresses four more genes. Genes *leuA*, *leuB*, *leuC*, and *leuD* involved in leucine biosynthesis were introduced in the first medium copy plasmid between *alsS* and *AAT* which had a transcription order of *ilvD-alsS-leuA-leuB-leuC-leuD-AAT*. The same second high copy plasmid pYT2 was used for alcohol synthesis. More details of the plasmids used are provided in **Table 2.1**. The primers used are shown in **Table 2.S1** in supporting information. The wild type *E. coli* strain was transformed with these synthetic operons for initial production experiments.

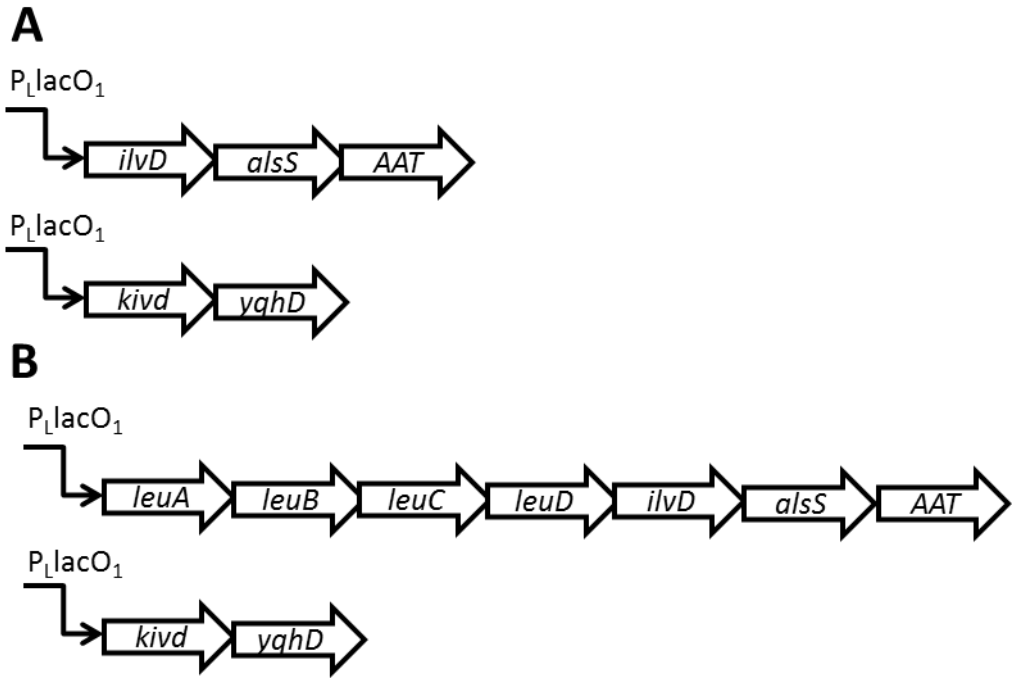

Figure 2.2| Synthetic operons for (A) isobutyl acetate (IBAc) production and (B) isoamyl acetate (IAAc) production. Abbreviation: AAT (Alcohol acyltransferase).

Table 2.1| Strains and plasmids used in this study.

Strain/plasmid	Relevant genotype[a]	Reference
Strains		
BW25113	*rrnB*$_{T14}$Δ*lac*ZWJ16 *hsd*R514 Δ*ara*BAD$_{AH33}$Δ*rhaBAD*$_{LD78}$	[70]
BL21	*E. coli*B F- *dcmompThsdS*(r_B- m_B-) gal [malB$^+$]$_{K-12}$(λ^S)	[71]
XL10-Gold	Tet^{R}Δ (*mcrA*)183 Δ (*mcrCB-hsaSMR-mrr*)173 *endA1supE*44 *thi-1 recA1*	Stratagene
XL-1 Blue	*recA1endA1gyrA96thi-1 hsd*R*17 supE44 relA1lac* [F′*proABlac1*^{q}ZΔM15 Tn*10* (Tet^R)]	Stratagene
IBA3	BW25113 F′Δ*ldhA*Δ*poxB*Δ*pta*	This study
Plasmids		
pIPA4	ColE1 ori; Amp^r; P$_L$lacO$_1$: *kivd* (LL)-*PadA* (EC)	[72]
pIBA1	p15A ori; Kan^r; P$_L$lacO$_1$: *ilvD* (EC)-*alsS* (BS)	[62]
pIVC1	p15A ori; Kan^r; P$_L$lacO$_1$: *leu*ABCD (EC)-*ilvD* (EC)-*alsS* (BS)	[72]
pIBAc4	p15A ori; Kan^r; P$_L$lacO$_1$: *ilvD* (EC)-*alsS* (BS)-*luxE* (CB)	This study
pIBAc5	p15A ori; Kan^r; P$_L$lacO$_1$: *ilvD* (EC)-*alsS* (BS)-*ATF1*	This study

	(SC)	
pIBAc6	p15A ori; Kan^r; $P_L lacO_1$: *ilvD* (EC)-*alsS* (BS)-*ATF2* (SC)	This study
pIBAc7	p15A ori; Kan^r; $P_L lacO_1$: *ilvD* (EC)-*alsS* (BS)-*BPBT* (PH)	This study
pIBAc8	p15A ori; Kan^r; $P_L lacO_1$: *ilvD* (EC)-*alsS* (BS)-*SAAT* (STR)	This study
pIAAc2	p15A ori; Kan^r; $P_L lacO_1$: *leu*ABCD (EC)-*ilvD* (EC)-*alsS* (BS)-*luxE* (CB)	This study
pIAAc3	p15A ori; Kan^r; $P_L lacO_1$: *leu*ABCD (EC)-*ilvD* (EC)-*alsS* (BS)- *ATF1* (SC)	This study
pIAAc4	p15A ori; Kan^r; $P_L lacO_1$: *leu*ABCD (EC)-*ilvD* (EC)-*alsS* (BS)- *ATF2* (SC)	This study
pIAAc5	p15A ori; Kan^r; $P_L lacO_1$: *leu*ABCD (EC)-*ilvD* (EC)-*alsS* (BS)- *BPBT* (PH)	This study
pIAAc6	p15A ori; Kan^r; $P_L lacO_1$: *leu*ABCD (EC)-*ilvD* (EC)-*alsS* (BS)- *SAAT* (STR)	This study
pYT2	ColE1 ori; Amp^r; $P_L lacO_1$: *kivd* (LL)-*yqhD* (EC)	This study
pYT3	ColE1 ori; Amp^r; $P_L lacO_1$: 6xhis-*luxE* (CB)	This study
pYT4	ColE1 ori; Amp^r; $P_L lacO_1$: 6xhis-*ATF1* (SC)	This study
pYT5	ColE1 ori; Amp^r; $P_L lacO_1$: 6xhis-*ATF2* (SC)	This study
pYT6	ColE1 ori; Amp^r; $P_L lacO_1$: 6xhis-BPBT (PH)	This study
pYT7	ColE1 ori; Amp^r; $P_L lacO_1$: 6xhis-SAAT (STR)	This study

[a] EC, *Escherichia coli*; BS, *Bacillus subtilis*; LL, *Lactococcus lactis*; CB, *Clarkia breweri*; SC, *S. cerevisiae*; PH, *Petunia x hybrid*; STR, Strawberry (*Fragaria x ananassa)*

2.2 Screening of AATs for IBAc and IAAc production

Various AATs showed capability of catalyzing the esterification reaction in various organisms. Thus, five candidate AATs including benzyl alcohol O-benzoyltransferase encoded by *luxE*[73], alcohol acetyltransferase I encoded by *ATF1*[74, 75], alcohol acetyltransferase II encoded by *ATF2*[76], benzyl alcohol O-benzoyltransferase encoded by *BPBT*[77], and strawberry alcohol acyltransferase encoded by *SAAT*[78] were cloned and examined in this study. These five enzymes were selected from KEGG database[79] based on their reported activity to catalyze different esterification reactions.

The effect of the five candidate AATs on production titers of IBAc and IAAc was examined. Recombinant strains were constructed with the synthetic operons as shown in **Fig. 2.2** and **Table 2.1**. Shake flask fermentations and product analysis were carried out as described in materials and methods section. Except AAT, all other enzymes were the same for each producing strain. Therefore, under the same fermentation condition from 20 g/l glucose, the strain with the highest production titer was expected to have the most active AAT. The activity here represented the synergetic effect of kinetic parameters and protein expression level. For IBAc production (**Fig. 2.3A**), the highest titer was achieved at 2.14 g/l with the introduction of ATF1. The strain containing ATF2 could produce 1.69 g/l. However, for LuxE, BPBT, and SAAT strains, only less than 0.5 g/l IBAc was produced. Please note that IAAc production (**Fig. 2.3B**) had a similar trend with IBAc production though the overall titers were lower. The ATF1 overexpression strain could produce 0.39 g/l, while ATF2 enabled 0.25 g/l IAAc production. The other three enzymes LuxE, BPBT, and SAAT were only able to produce around 0.1 g/l of IAAc. ATF1 was therefore identified to be the most active AAT for both IBAc and IAAc production.

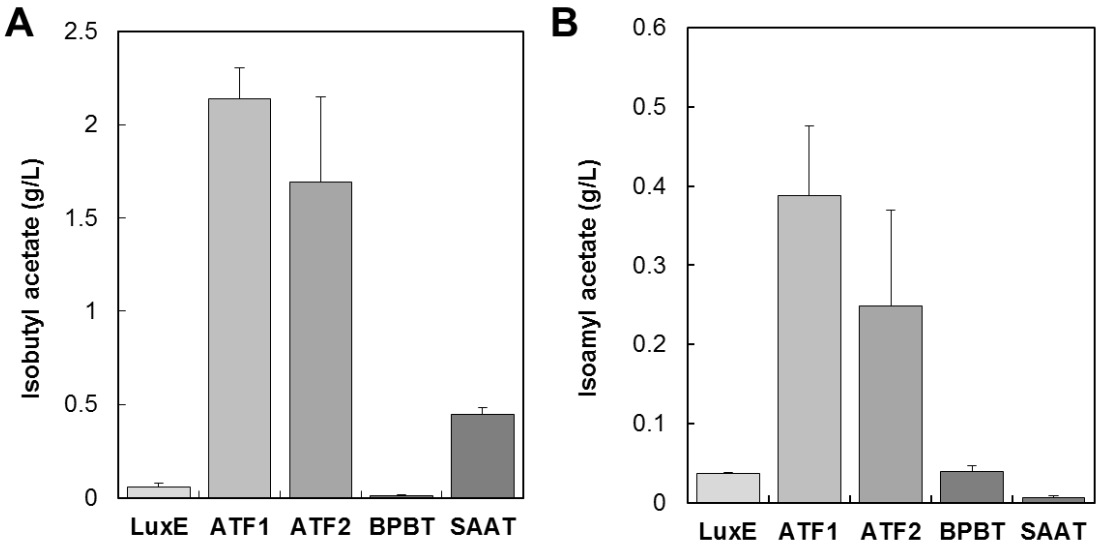

Figure 2.3| Summary of production results with overexpressing different alcohol acyltransferases (AATs). (A) Isobutyl acetate production in WT cells. Strains carrying *alsS*, *ilvD*, and different AATs along with *kivd* and *yqhD* were tested for ester production. (B) Isoamyl acetate production in WT cells. Strains carrying *alsS*, *ilvD*, *leuABCD* and different AATs along with *kivd* and *yqhD* were assayed for ester production. Error bars are ±SD for n=3 independent shake flask fermentation experiments from three independent colonies.

2.3 AAT enzyme characterization

In vitro enzymatic assays were carried out to compare the kinetic parameters of the five candidate AATs towards respective substrates. The method is based on the reaction of free CoA with 5,5′-dithiobis-(2-nitrobenzoic acid) (DTNB). If the AAT catalyzed the reaction combing alcohols and acetyl-CoAs, free CoAs will be released and coupled with DTNB to form a yellow 5-thio-2-nitrobenzoate anion product, whose absorbance at 412 nm can be measured[21]. The kinetic parameters, k_{cat} and K_M, for isobutanol and 3MB, were then determined individually by fitting the initial reaction rates with Michaelis-Menten kinetics. The values of the catalytic rate constant (k_{cat}) and Michaelis-Menton

constant (K_M) of the five enzymes are shown in **Table 2.2**. The *in vivo* expression levels of these AATs were also compared by SDS-PAGE (**Fig. 2.S1** in supporting information). Samples were prepared by normalizing cell density OD_{600} to 5.0. In the soluble part, there were 2.6 mg/l LuxE, 6.4 mg/l ATF1, 12 mg/l ATF2, 9.2 mg/l BPBT, and 1.6 mg/l SAAT, respectively for strains overexpressing these AATs. Considering IBAc production, ATF1 and ATF2 not only have higher expression levels than other AATs but also have higher k_{cat} values (1.83 and 1.54 s^{-1}, respectively) than those of the other three enzymes. Therefore, higher titers of IBAc (2.14 and 1.69 g/l) were achieved by ATF1 and ATF2. For the production of IAAc, although BPBT has a low k_{cat} (0.18 s^{-1}) towards 3MB, its high expression level (9.2 mg/l) with a 58.4 $s^{-1}M^{-1}$ specific constant (k_{cat}/K_M) resulted in the 0.04 g/l IAAc production by overexpressing BPBT. ATF1 and ATF2 again have overall higher expression levels and k_{cat} values for 3MB (2.94 and 1.59 s^{-1}, respectively) than the remaining three enzymes. Overexpression of ATF1 and ATF2 resulted in 0.39 and 0.25 g/l of IAAc production respectively during the fermentation process. These enzymatic data confirmed the desired enzyme activities. Based on the kinetic parameters and *in vivo* protein expression, to optimize the production of these esters, I may improve the solubility of AATs or further engineer ATF1 by directed evolution to improve its *in vitro* activities.

Table 2.2| Kinetic parameters of the five alcohol acyltransferases[a]

Enzyme	Substrate	K_M (mM)	k_{cat} (s^{-1})	k_{cat}/K_M ($s^{-1}M^{-1}$)
LuxE	Isobutanol	15.14 ± 2.43	0.042± 0.01	2.77
ATF1	Isobutanol	20.19 ± 1.06	1.83± 0.15	90.6
ATF2	Isobutanol	27.66± 5.67	1.54± 0.35	55.7
BPBT	Isobutanol	4.05 ± 0.49	0.10 ± 0.02	24.7
SAAT	Isobutanol	28.39 ± 3.91	0.016± 0.007	0.56
LuxE	3-methyl-1-butanol	17.6 ± 3.67	0.053± 0.006	3.01
ATF1	3-methyl-1-butanol	25.97 ± 4.39	2.94± 0.11	113.2
ATF2	3-methyl-1-butanol	21.51 ± 1.56	1.59± 0.23	73.9
BPBT	3-methyl-1-butanol	3.08 ± 0.68	0.18± 0.06	58.4
SAAT	3-methyl-1-butanol	30.45 ± 4.83	0.018± 0.004	0.59

[a]Error bars indicate the standard deviations from three independent experiments.

2.4 Deletion of competitive pathways to improve ester production

Acetate accumulations are often problematic in many bioprocesses. Competition for glucose between the product-synthesizing pathway and acetate-producing pathways would cause a waste of substrate and thus a serious economic sink[80]. In addition, acetate is also detrimental to the recombinant protein productivity since cell growth may be inhibited at high levels of this byproduct[80, 81]. It was reported that inactivating the acetate production pathway also decreased byproduct ethanol production[82]. In order to analyze byproduct formations quantitatively, HPLC was used to identify the byproducts produced (**Table 2.3**). Shake flask fermentations have shown the accumulation of acetate especially for better IBAc and IAAc producing strains such as strains overexpressing *ATF1* and *ATF2* (pIBAc5, pIBAc6, pIAAc3, and pIAAc4).

Table 2.3| Metabolite concentrations of IBAC and IAAc producing strains

Host Strain	Plasmids	Final metabolite concentration (g/l)[a]			% of the theoretical maximum
		Acetate	Isobutanol	IBAc or IAAc[b]	
BW25113	pIBAc4, pYT2	0.63 ± 0.25	2.95 ± 0.24	0.056 ± 0.024	0.65
BW25113	pIBAc5, pYT2	1.41 ± 0.36	1.81 ± 0.17	2.137 ± 0.169	24.9
BW25113	pIBAc6, pYT2	1.76 ± 0.56	2.64 ± 0.42	1.691 ± 0.458	19.7
BW25113	pIBAc7, pYT2	0.37 ± 0.15	2.96 ± 0.29	0.011 ± 0.008	0.13
BW25113	pIBAc8, pYT2	1.00 ± 0.09	2.14 ± 0.06	0.447 ± 0.034	5.20
IBA3	pIBAc5, pYT2	0.81 ± 0.09	1.29 ± 0.04	2.481 ± 0.081	28.8
BW25113	pIAAc2, pYT2	0.89 ± 0.19	0.68 ± 0.29	0.036 ± 0.002	0.50
BW25113	pIAAc3, pYT2	1.96 ± 0.37	0.21 ± 0.08	0.386 ± 0.088	5.38
BW25113	pIAAc4, pYT2	1.88 ± 0.41	0.36 ± 0.15	0.249 ± 0.120	3.45
BW25113	pIAAc5, pYT2	1.25 ± 0.35	0.75 ± 0.12	0.040 ± 0.006	0.55
BW25113	pIAAc6, pYT2	0.96 ± 0.12	1.09 ± 0.06	0.006 ± 0.002	0.08
IBA3	pIAAc3, pYT2	1.38 ± 0.03	0.16 ± 0.05	0.781 ± 0.045	10.8

[a]Errors indicate the standard deviations from three independent experiments. Concentrations were measured at 48 h of fermentation.
[b]IBAc for the first six strains and IAAc for the rest six strains.

It was expected that blocking acetate-producing pathways could improve production. Pyruvate oxidase (*poxB*) and phophotransacetylase (*pta*) were characterized as the two major acetate-producing enzymes[80]. For the production of IBAc and IAAc, both acetate-producing pathways compete directly for the precursors, pyruvate and acetyl-CoA. Therefore, the strategy here was to knock out genes involved in acetate production. It was previously reported that inactivating acetate production pathway could channel more carbon flux to acetyl-CoA, resulting in higher IAAc production[60]. In this work, three genes involved in both acetate and lactate production, *ldh*, *poxB*, and *pta*, were thus knocked out. This triple knockout strain is named IBA3. IBA3 strain was then transformed with the synthetic operons for IBAc and IAAc production. Under the same fermentation condition with 20 g/l glucose supplemented, IBAc production titer

increased to 2.48 g/l (**Fig. 2.4A**) by the introduction of *ATF1* in IBA3 strain. The improvement for IAAc production (**Fig. 2.4B**) is more significant (p-value = 0.0022). The production titer doubled from 0.39 g/l (WT) to 0.78 g/l (IBA3). Although the concentrations were lower, acetate production was still detected during the fermentation of IBA3 strain (**Table 2.3**). Besides the two deleted pathways, alternative pathways to acetate such as citrate lyase activation pathway[83] or ornithine biosynthesis pathway[84] may contribute to the acetate produced. These results demonstrate that the deletion of byproducts producing genes would improve the productions of the desired products IBAc and IAAc.

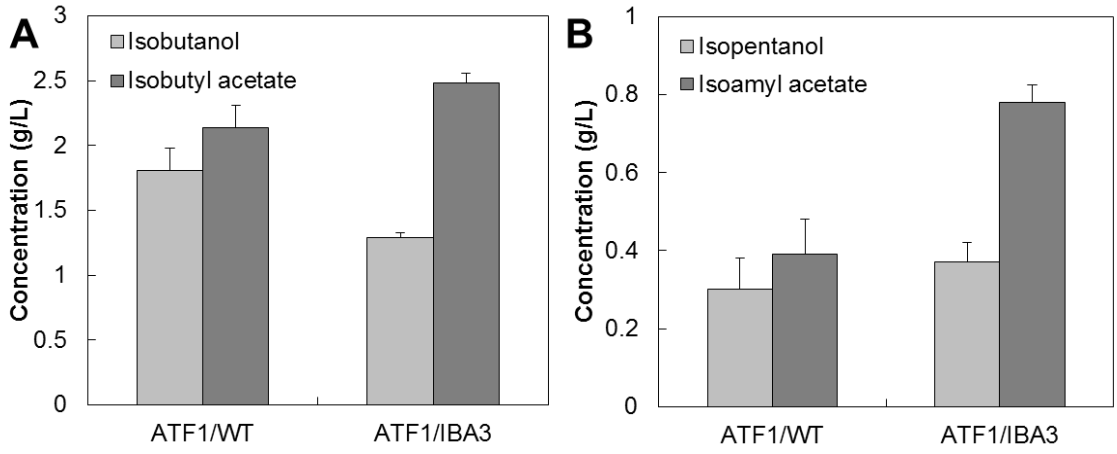

Figure 2.4| Fermentation results of ester production in WT strain and IBA3 (Δ*ldh*Δ*poxB*Δ*pta*) strain. (A) IBAc production. WT and IBA3 Strains containing alsS, ilvD, *kivd*, *yqhD*, and *ATF1* were assayed for IBAc prodcution. (B) IAAc production. WT and IBA3 Strains containg*alsS*, *ilvD*, *leuABCD*, *kivd*, yqhD, and *ATF1* were tested for IBAc production. Error bars are ±SD for n=3 shake flask fermentation experiments from three independent colonies.

2.5 Time-course profiles of the engineered IBAc and IAAc strains

After successful improvement of both IBAc and IAAc production by deleting competing routes, shake flask fermentations were conducted with the improved strains and the production time-courses for the final IBAc and IAAc producing strains are shown in **Fig. 2.5** and **Fig. 2.6**, respectively. For IBAc, **Fig. 2.5A** shows the cell density measured by OD_{600}. It increased exponentially during the first 12 h and leveled off at later stage. IBAc (**Fig. 2.5D**) was constantly produced in 48 h when the cells were consuming glucose (**Fig. 2.5B**). The IBAc production curve (**Fig. 2.5D**) is inversely correlated with glucose concentration curve (**Fig. 2.5B**). For IBAc production experiments, main byproducts were isobutanol and acetate, with final concentrations at 1.30 g/l and 0.81 g/l, respectively (**Fig. 2.5C**). The production profile of isobutanol (**Fig. 2.5C**) was closely correlated with the production profile of IBAc (**Fig. 2.5D**). At later stages, cells stopped growing and consuming glucose. For the production of IAAc, cell density profile (**Fig. 2.6A**) was similar to IBAc production (**Fig. 5A**). It increased exponentially for the first 12 h and tapered off later. IAAc was produced constantly during the 48 h and the production curve (**Fig. 2.6D**) was inversely correlated to glucose concentration profile (**Fig. 2.6B**). At the end of IAAc production experiment, final byproducts concentrations detected were 1.38 g/l, 0.38g/l, and 0.16 g/l of acetate, 3MB, and isobutanol, respectively (**Fig. 2.6C**). 3MB and isobutanol plateaued after 20 h, yet acetate concentration kept increasing until the end of fermentation (**Fig. 2.6C**). At the end of IBAc production experiment, 19.7 g/l of glucose was consumed the OD_{600} reached 8.0. On the other hand, at the end of IAAc production experiment, 19.3 g/l of glucose was

consumed and the final OD_{600} reached 5.9. For both production experiments, acetate accumulation is believed to lead to subsequent decrease in cell growth and production rate at later stages. The maximum theoretical yields of IBAc and IAAc of the designed pathways are 0.43 g IBAc/g glucose and 0.36 g IAAc/g glucose respectively. For the most active strains achieved in this study, 2.48 g/l of IBAC and 0.78 g/l of IAAc were produced with 20 g/l glucose supplemented. These accounted for 28.8% and 10.8% of their maximum theoretical yields, respectively.

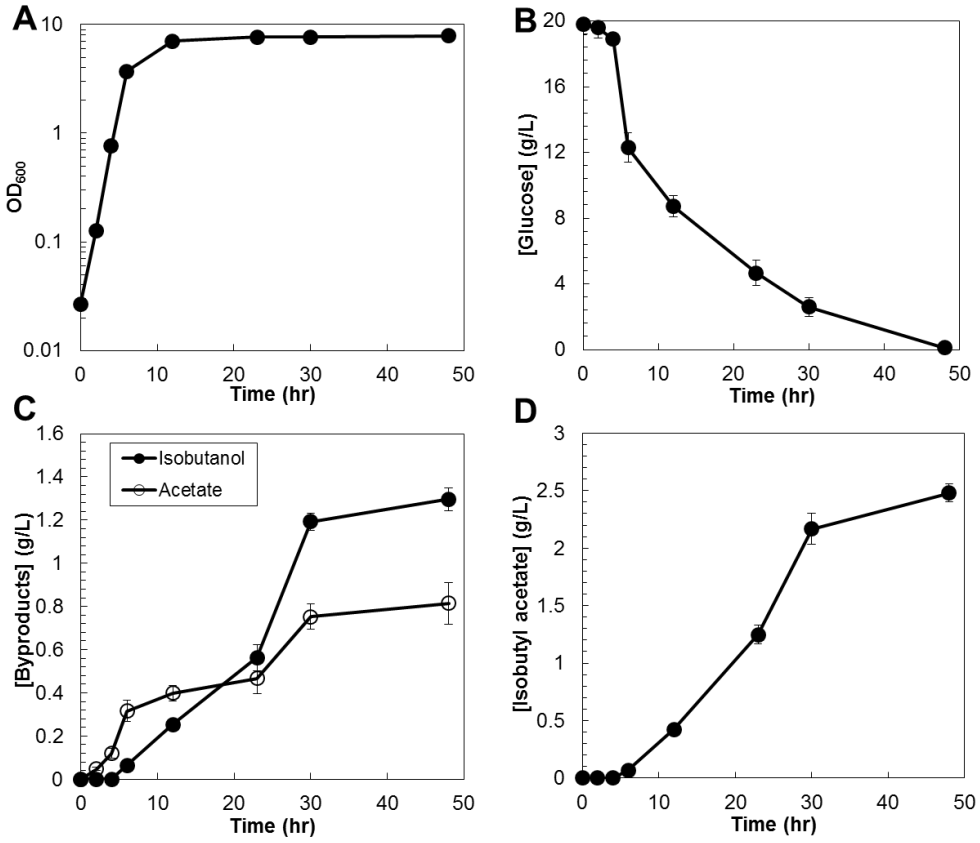

Figure 2.5| Detailed isobutyl acetate production time course of IBA3 (Δ*ldh*Δ*poxB*Δ*pta*) strain containing the two production plasmids pIBAc5 and pYT2. Cultures in flasks were shaken vigorously at 30°C with initial glucose concentration 20 g/l. Samples were taken at 0, 2, 4, 6, 12, 23, 30, 48 h of fermentation time. Abbreviations: OD_{600} (optical density at 600 nm). Error bars are ±SD for n=3 shake flask fermentation experiments from three independent colonies.

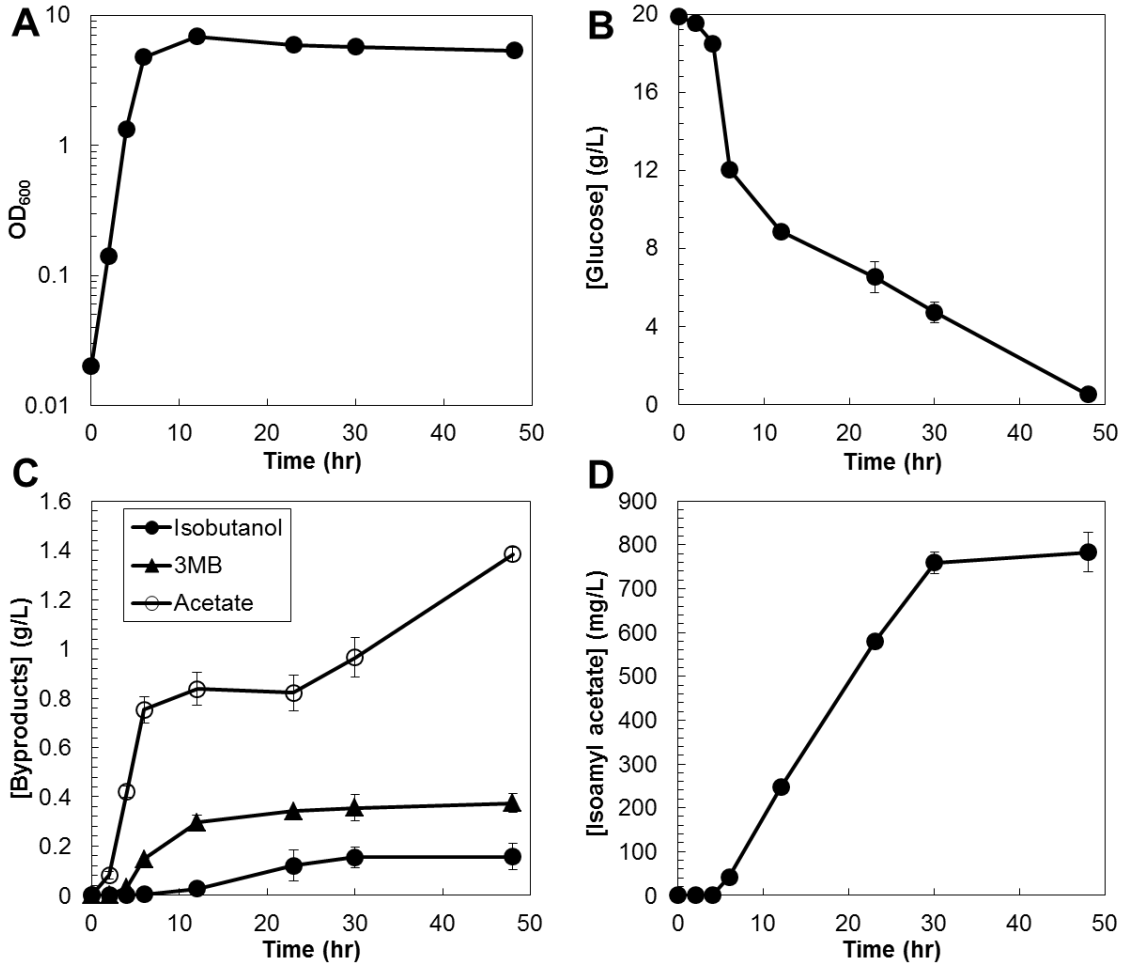

Figure 2.6| Detailed isamyl acetate production time course of IBA3 (Δ*ldh*Δ*poxB*Δ*pta*) strain containing the two production plasmids pIAAc3 and pYT2. Cultures in flasks were shaken vigorously at 30°C with initial glucose concentration 20 g/l. Samples were taken at 0, 2, 4, 6, 12, 23, 30, 48 h of fermentation time. Abbreviations: OD_{600} (optical density at 600 nm), 3MB (3-methyl-1-butanol). Error bars are ±SD for n=3 shake flask fermentation experiments from three independent colonies.

2.6 IBAc production scale-up in benchtop bioreactors

The IBA3 strain harboring plasmids pIBAc5/pYT2 was used for scale-up fermentation in a 1.3-L bench-top bioreactor. The fermentation experiments were performed by controlling pH at 6.8, dissolved oxygen (DO) above 10%, and temperature at 30 °C. 0.3

mM IPTG was used to induce protein expression when OD_{600} reached 6.0. The induction time represents the beginning of the fermentation in **Fig. 2.7**. IBAc is a volatile chemical with a relative volatility 1.7 times of that of n-butyl acetate. Thus, a medium aeration rate (0.5 vvm) was used to *in situ* remove the produced IBAc from culture broth. The time profile of IBAc, isobutanol, acetate production and OD_{600} are shown in **Fig. 2.7**. Initial glucose concentration was 10 g/l and manual additions of 600 g/l glucose feeding solution were applied to meet metabolic demands of the fermentation cultures. This strategy enabled strain IBA3 to accumulate 36 g/l (**Fig. 2.7**) of IBAc at a yield of 42% of the theoretical maximum in 72 h. In this fermentation condition, isobutanol concentration was maintained at a low level (< 6 g/l). No lactate, formate, or ethanol was detected. Acetate is the main by-product which started to accumulate after 24 h and reached 7.3 g/l at the end. In the shake flasks (**Fig. 2.5**), acetate production was about one thirds of IBAc production. While in the bioreactor, acetate production was only about one fifths of IBAc production. The decrease in acetate/IBAc ratio in the bioreactor may result from more oxygen supplied in the bioreactor than in shake flasks.

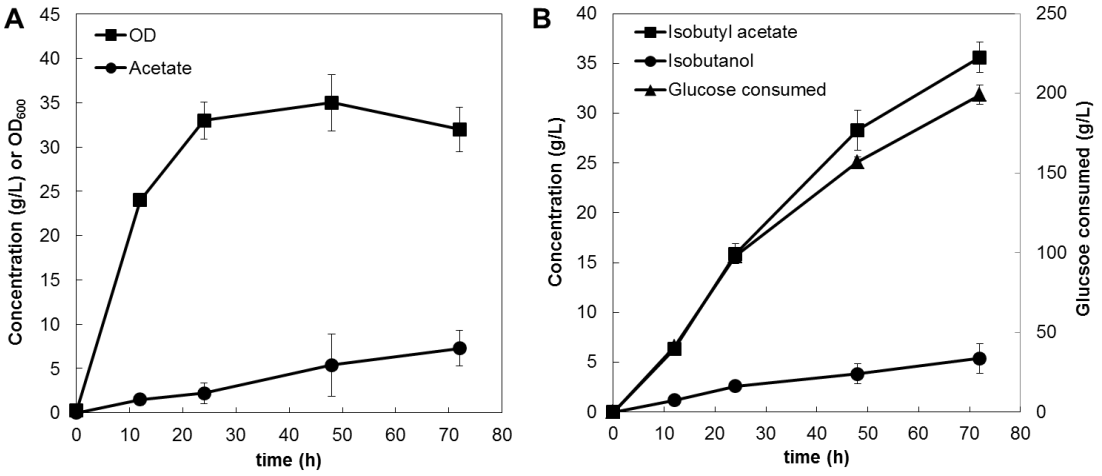

Figure 2.7| Isobutyl acetate production time profile of IBA3 strain harboring pIBAc5/pYT2 in a 1.3-L bench-top bioreactor. (A)OD_{600} and acetate concentration time curves (B)Isobutanol and IBAc production curves and glucose consumption curve. IBAc and isobutanol concentrations were calculated as sum of the quantities determined in three receivers and broth culture considering a working volume of 0.5 l. Error bars are ±SD for n=3 independent bioreactor fermentation experiments.

3. Conclusions

Medium-chain esters are not only important flavor and solvent components but also potential fuel alternatives. This is one of the earliest reports on biosynthesis of these compounds directly from glucose by *E. coli*[61, 85, 86]. The production of IBAc and IAAc were chosen for demonstration and this production platform and be easily expanded to various esters. Native valine and leucine biosynthetic pathways in *E. coli* were successfully expanded for the production of IBAc and IAAc, respectively. Five candidate AATs were introduced for the condensation of alcohol and acetyl-CoA. After successfully producing these desired compounds, the production was further improved by deleting competing metabolic routes producing lactate and acetate. The best producing strains enabled production of 2.48 g/l IBAc with overexpressing ATF1 and 0.78 g/l of IAAc with

overexpressing ATF1. These values correspond to 28.8% and 10.8% of the theoretical maxima for IBAc and IAAc, respectively. IBAc fermentation process was scaled up the in a 1.3-L bench-top bioreactor and enabled 36 g/l IBAc after 72 h. This demonstrates the feasibility and potential for scale-up production of this valuable chemical. To further improve the production and yield, it is important to enlarge the pools of isobutanol or 3MB and therefore high yield strains of isobutanol or 3MB should be tested for in the future. Besides, further works will be dedicated to design metabolic pathways for higher medium-chain esters which contain higher energy density.

4. Materials and Methods

4.1 Bacterial strains

All strains and plasmids are listed in **Table 2.1**. Oligonucleotides used are listed in **Table 2.S1** in supporting information. *E. coli* strain BW25113 (*rrnB*$_{T14}$Δ*lac*ZWJ16 *hsd*R514 Δ*ara*BAD$_{AH33}$ Δ*rhaBAD*$_{LD78}$) was used as the wild-type host (WT)[70] for this study. XL1-Blue and XL10-Gold competent cells from Stratagene were used to construct plasmids. BL21 strain was used to express proteins for enzyme assays. Strain IBA3 was constructed by knocking out genes *pta*, *poxB*, and *ldhA* from the chromosome. P1 transduction with Keio collection strains[87] enabled the gene deletion. The removal of each gene segment was confirmed by colony polymerase chain reaction (colony PCR) using the appropriate primers.

4.2 Reagents, media, and cultivation

FastDigest restriction enzymes were purchased from Thermo Scientific. Quick ligation™ kit and Phusion high-fidelity® PCR kit were supplied by New England Biolabs. Oligonucleotides were ordered from Eurofins MWG Operon. For production experiments, three independent colonies were picked from plates with freshly transformed *E. coli* strains and cultured overnight at 37 °C in 2 ml 2×YT medium containing 100 mg/l ampicillin and 50 mg/l kanamycin. 200 μl of overnight cultures were transferred into 125-ml screw cap conical flasks containing 10 ml M9 medium[88] supplied with 20 g/l glucose, 5 g/l yeast extract, 10 mg/l thiamine. Antibiotics were added as necessary for plasmid maintenance (100 μg/ml ampicillin, and 50 μg/ml kanamycin). All antibiotics and reagents were purchased from Sigma-Aldrich or Fisher Scientific. Protein expression was induced at the beginning of fermentation by adding 0.1 mM isopropyl β-D-1-thiogalactopyranoside (IPTG). 0.3 g $CaCO_3$ was added into the flask for neutralization of acetic acid or other acids produced. Caps were sealed with Parafilm (Pechiney Plastic Packaging Inc.). After incubation for 48 h at 30 °C, fermentation samples were harvested and analyzed.

4.3 DNA techniques

The plasmids pIPA4, pIVC1[72], and pIBA1[62] were designed and constructed as previously described. Vectors expressing various alcohol acyltransferases (AAT) genes for isobutyl acetate production (pIBAc4—pIBAc8) were constructed based on pIBA1. For the construction of pIBAc4, pIBAc7, and pIBAc8, genes *luxE*, *BPBT* and *SAAT* were

artificially synthesized by PCR assembly of oligonucleotides[89] because the genomic DNA of *Clarkia breweri*, *Petunia × hybrida*, and *Fragaria × ananassa* were not available. The protocols of plasmid construction are summarized in supporting information.

4.4 Protein expression and purification

Transformed cells (BL21 with pYT3, pYT4, pYT5, pYT6, or pYT7) were inoculated from an overnight pre-culture at 1/100 dilution and grown in 200 ml of 2×YT medium containing 100 mg/l ampicillin. When the OD_{600} reached 0.6-1.0, 0.5 mM IPTG was added to induce protein expression, followed by incubation at 30°C for 3 h. Then the cells were pelleted by centrifuging at 3,220 rcf for 15 minutes. The supernatants were discarded and the pellets were stored at -80°C. All the following steps were carried out at 4 °C to prevent protein degradation. For lysis, the cell pellets were first thawed on ice-water mixture and re-suspended in 15 ml lysis buffer. The lysis buffer (pH=7.6) contained 50 mM Tris-HCl, 100 mM NaCl, 10mM imidazole, 5% glycerol, 1 mM DTT. Cell lysis was performed by sonication using the Heat Systems Ultrasonics W-225 Sonicator in a continuous mode set at 50% duty cycle and output control 5. Each sample was sonicated for 6 cycles of one-minute sonication with intermittent one-minute cooling on ice-water mixture. The cell lysates were centrifuged at 10,733 rcf for 15 minutes. For protein purification, 4 ml of HisPur Ni-NTA resin solution purchased from Thermo Scientific was loaded in each column and the storage buffer was allowed to pass through by gravity to get a 2 ml final resin bed volume. The resin was equilibrated with 10 ml of lysis buffer and drained. All 15 ml of soluble cell lysate was loaded in the

column and allowed to pass through by gravity. The column was then washed twice with 20 ml of wash buffer (50 mM Tris-HCl, 100 mM NaCl, and 25mM imidazole, pH=7.6). The bound protein was eluted with 15 ml of elution buffer (pH=8.0) which contained 50 mM Tris-HCl, 250 mM NaCl, and 250 mM imidazole. The final protein sample was then buffer-exchanged using Amicon Ultra centrifugal filters (Millipore) with the storage buffer (50 μM Tris-HCl, 2mM $MgSO_4$ 20% glycerol, pH=8). The concentrated protein were aliquoted (100 μl) into PCR tubes, flash frozen with dry ice and methanol mixture and stored at -80°C. Purified protein concentrations were determined by Quick Start Bradford protein assay kit purchased from Bio-Rad Laboratories.

4.5 Enzymatic assays

The assay mixture was composed of100 mM KCl, 2 mM$MgCl_2$, 1 mM acetyl-CoA, 50 mM Tris-HCl (pH=8.0) with a total volume of 100 μl. ATF1, ATF2 (each 100 nM) and BPBT (1.2 μM) were reacted with isobutanol or 3-methyl-1-butanol in a concentration range from 1 mM to 100 mM for 30 min at 30 °C. SAAT (150 nM) and LuxE (120 nM) were reacted with isobutanol or 3-methyl-1-butanol in a concentration range from 1 mM to 100 mM for 90 min at 30 °C. The reactions were stopped by adding 0.06g NaCl. 0.2 ml of a freshly prepared 1 mM solution of 5,5′-dithiobis-(2-nitrobenzoic acid) in 100 mM Tris-HCl buffer (pH=8.0) was added. Then the yellow 5-thio-2-nitrobenzoate anion product was quantified by measurement at 412 nm. The values obtained were adjusted for unspecific hydrolysis by deducting the absorbance of controlled samples without addition of alcohols. A molar extinction coefficient of 13,600 $M^{-1}cm^{-1}$ was appliedfor the

final calculation[21]. K_M and k_{cat} values were obtained by nonlinear least-squares regression. The analyses were done using the *nlinfit* function of the Matlab software program.

4.6 Metabolite detection

Byproduct analysis was performed on an Agilent 1260 Infinity HPLC equipped with an Aminex HPX 87H column and a refractive index detector. The mobile phase was 5 mM H_2SO_4 at a flow rate of 0.6 ml/min. The column temperature was at 35 °C and the detection temperature was at 50 °C. The data were presented as mean values with error bars indicating the standard deviation. The ester products were quantified by a Hewlett Packard (HP) 6890 gas chromatograph (GC) equipped with a flame ionization detector (FID). The separation of ester and alcohol compounds was carried out using a DB-WAX capillary column (30 m, 0.32 mm-inside diameter, 0.50-μm film thickness) from Agilent Technologies. GC oven temperature was initially held at 70°C for 2 min and raised to 120°C with a gradient of 30 °C/min. The temperature was then raised to 140°C with a gradient of 10°C/min. Finally, the temperature was then raised with a gradient of 30°C/min to 200 °C and held for 5 min to clean any remaining chemicals in the column. Helium was used as the carrier gas with 10.35 psi inlet pressure. A mixture of hydrogen, air, and helium was fed to the FID. The temperature of injector and detector was maintained at 250 °C. The column was injected with 2 μl of the hexane-extract solution from the culture broth and *n*-butanol was used as the internal standard.

4.7 Bioreactor culture condition

Medium recipe for bioreactor fermentations is specified in supporting information. Fermentations were performed in 1.3-L bench-top bioreactor (New Brunswick Bioflo® 115) with a working volume of 0.5 l. A shake flask with 50 ml LB medium was inoculated with 1% of overnight pre-culture and appropriate antibiotics at 37 °C. After the inoculum grew to OD_{600} at 1.0, 50 ml inoculum was used to inoculate a bioreactor and brought the initial tank volume to 0.5 l. Cells were first grown at 37 °C. Until OD_{600} reached 6.0, 0.3 mM of IPTG was added and the temperature was decreased to 30 °C to start IBAc production. The induction time corresponds to the beginning of fermentation in **Fig. 2.7**. The pH was controlled by 26% NH_4OH solution. Dissolved oxygen (DO) level was maintained above 10% by adjusting agitation rate (from 300 to 800 rpm). Air flow rate was maintained at 0.5 vvm in order to provide oxygen for cells and to strip IBAc out from the culture broth. The exhaust gases from the bioreactor were bubbled in a trap containing 1800 ml of water cooled with ice-salt mixture. After that, gases entered into a second trap which was the same as the first one and then were finally bubbled into a third trap containing 500 ml of oleyl alcohol (Sigma-Aldrich) cooled with tap water. Fermentation was run in batch mode until the glucose was consumed by the culture, and then the glucose feeding solution was manually fed to meet metabolic demands.

5. Supporting Information

5.1 Cloning procedure

Primers used in this work are listed in **Table 2.S1**. Primers luxEalsS-F and luxEvec-R were used to amplify gene *luxE*. Primers BPBTalsS-F and BPBTvec-R were used to amplify gene *BPBT* and primers SAATalsS-F and SAATvec-R were used to amplify gene *SAAT*. For the construction of plasmids pIBAc5 and pIBAc6, genes *ATF1* and *ATF2* were amplified based on *S. cerevisiae* genomic DNA. ATF1alsS-F and ATF1vec-R were used for *ATF1*. Primers ATF2alsS-F and ATF2vec-R were designed to amplify *ATF2*. All these fragments (*luxE, ATF1, ATF2*, *BPBT, and SAAT*) have *Blp*I cutting sites at either end. Then pIBA1 was digested with *Blp*I and the digested backbone (the large portion) was gel purified and then ligated to these five fragments respectively to form vectors pIBAc4-pIBAc8. To construct vectors with various alcohol acyltransferases for the production of isoamyl acetate (pIAAc2- pIAAc6), a similar procedure was followed. The only difference is pIVC1 was digested and used as the backbone. The five alcohol acyltransferases fragments were amplified with appropriate primers.

Vectors pYT2 and pYT3 were built based on plasmid pIPA4. ColE1 *ori* from pIPA4 was removed by digestion with *Acc*65I and *Xba*I and used as the backbone for these vectors. Primers veckivd-F and kivd-R were used to amplify *kivd* from *Lactococcus lactis* genomic DNA. Gene *yqhD* was amplified from *E. coli* K12 genomic DNA using primers yqhDkivd-F and yqhDvec-R. These two fragments (*kivd* and *yqhD*) were then joined by splice overlap extension (SOE) and ligated with the backbone to create pYT2. To characterize enzyme activity, hexahistidine (His6)-tagged *luxE, ATF1*, *ATF2*, *BPBT*,

and *SAAT* was amplified frompIBAc4, pIBAc5, pIBAc6, pIBAc7, and pIBAc8using primers: hisluxE-F and hisluxE-R; hisATF1-F and hisATF1-R; hisATF2-F and hisATF2-R; hisBPBT-F and hisBPBT-R; and hisSAAT-F and hisSAAT-R. These fragments were then ligated with the ColE1 *ori* backbone to create pYT3, pYT4, pYT5, pYT6, and pYT7. All plasmids in this work were sequenced using appropriate primers to confirm sequence fidelity.

Table 2.S1| Primers used in this study

Primers	Relevant genotype
luxEalsS-F	5′-GAAAACGAAAGCTCTCTAA**GCTGAGC**AGGAGAAATTAACTATGGCGCATGATCAGAGCCT-3 ′
luxEvec-R	5′-AGCCTTTCGTTTTATTTGATGCCTCTAGA**GCTCAGC**TTACAGGCTGCTCTGGGTGAAATG-3′
ATF1alsS-F	5′-CGAAAGCTCTCTAA**GCTGAGC**AGGAGAAATTAACTATGAATGAAATCGATGAGAAAAATC-3′
ATF1vec-R	5′-AGCCTTTCGTTTTATTTGATGCCTCTAGA**GCTCAGC**TTAAGGGCCTAAAAGGAGAGCTTT-3′
ATF2alsS-F	5′-CGAAAGCTCTCTAA**GCTGAGC**AGGAGAAATTAACTATGGAAGATATAGAAGGATACGAAC-3′
ATF2vec-R	5′-CCTTTCGTTTTATTTGATGCCTCTAGA**GCTCAGC**TTAAAGCGACGCAAATTCGCCGATGG-3′
BPBTalsS-F	5′-AAACGAAAGCTCTCTAA**GCTGAGC**AGGAGAAATTAACTATGGACAGCAAACAGAGCAGCG-3′
BPBTvec-R	5′-CCTTTCGTTTTATTTGATGCCTCTAGA**GCTCAGC**TTAAAGCGCTGGGGTGATGAACGCAT-3′
SAATalsS-F	5′-AAACGAAAGCTCTCTAA**GCTGAGC**AGGAGAAATTAACTATGGAGAAAATAGAAGTGAGCA-3′
SAATvec-R	5′-

	CCTTTCGTTTTATTTGATGCCTCTAGAGCTCAGCTTAGATCA GCGTCTTTGGACTCGCCA-3′
veckivd-F	5′-ACTGACCGAATTCATTAAAGAGGAGAAAGGTACCATGTATAC AGTAGGAGATTACCTATT-3′
kivd-R	5′-TTAGCGGGCGGCTTCGTATATACGGC-3′
yqhDkivd-F	5′-CTGAACAAAATAAATCATAAAGGAGAAATTAACTATGAACAA CTTTAATCTGCACACCCC-3′
yqhDvec-R	5′-GACTGAGCCTTTCGTTTTATTTGATGCC**TCTAGA**TTAGCGGG CGGCTTCGTATATACGGC-3′
hisluxE-F	5′-GGGCCC**GGATCC**ATGGCGCATGATCAGAGCCTGTCGTT-3′
hisluxE-R	5′-GGGCCC**TCTAGA**TTACAGGCTGCTCTGGGTGAAATGTT-3′
hisATF1-F	5′-GAGAGGATCGCATCACCATCACCATCAC**GGATCC**ATGAATG AAATCGATGAGAAAAATCA-3′
hisATF1-R	5′-GACTGAGCCTTTCGTTTTATTTGATGCC**TCTAGA**TTAAGGGC CTAAAAGGAGAGCTTTGT-3′
hisATF2-F	5′-GGGCCC**GGATCC**ATGGAAGATATAGAAGGATACGAACC-3′
hisATF2-R	5′-GGGCCC**TCTAGA**TTAAAGCGACGCAAATTCGCCGATGG-3′
hisBPBT-F	5′-GGGCCC**GGATCC**ATGGACAGCAAACAGAGCAGCGAATT-3′
hisBPBT-R	5′-GGGCCC**TCTAGA**TTAAAGCGCTGGGGTGATGAACGCAT-3′
hisSAAT-F	5′-GGGCCC**GGATCC**ATGGAGAAAATAGAAGTGAGCATTAA-3′
hisSAAT-R	5′-GGGCCC**TCTAGA**TTAGATCAGCGTCTTTGGACTCGCCA-3′

5.2 Bioreactor culture medium composition

Culture media for bioreactor fermentations contained, per liter: glucose, 10 g; K_2HPO_4, 7.5 g; $MgSO_4*7H_2O$, 2 g; citric acid monohydrate, 2 g; ferric ammonium citrate, 0.3 g; yeast extract, 20 g; 98% sulfuric acid, 0.8 ml; ampicillin, 0.1 g; kanamycin, 0.05 g; 1000X Modified Trace Metal Solution, 1 ml; and Vitamin Solution, 1ml. 1000X Modified Trace Metal Solution contained, in grams per liter: NaCl, 10; citric acid, 40; $ZnSO_4*7H_2O$, 1.0; $MnSO_4*H_2O$, 30; $CuSO_4*5H_2O$, 0.1; H_3BO_3, 0.1; $Na_2MoO_4*2H_2O$, 0.1; $FeSO_4*7H_2O$, 1.0; $CoCl_2*6H_2O$, 1.0. Vitamin Solution contained, in grams per liter: thiamine hydrochloride, 1.0; D-(+)-biotin, 1.0; nicotinic acid, 1.0; pyridoxine hydrochloride, 4.0. The feeding solution contained, in grams per liter: glucose, 600; K_2HPO_4, 7.4; ampicillin, 0.1; kanamycin, 0.05; 0.3 mM IPTG; Modified Trace Metal Solution, 1 ml; and Vitamin Solution, 8 ml.

5.3 *In vivo* protein expression

WT strain was transformed with his-tagged plasmids (pYT3, pYT4, pYT5, pYT6, and pYT7) overexpressing five candidate AATs. The protein expression process was described in Methods and Materials section 2.4. For SDS-PAGE analysis, whole cell extracts and soluble protein fractions were examined. Cells expressing each AAT were collected and normalized according to its OD_{600}. For whole cell extract part, 1ml of cells were taken and dissolved in 8M urea. 50 μl samples were taken and mixed with 50 μl Laemmli Sample Buffer (Bio-Rad) as the whole cell extract samples. Rest cells were sonicated and centrifuged at 4°C with 12000 rcf for 3 min. Then 50 μl of the supernatant

was taken from each sample and mixed with 50 μl Laemmli Sample Buffer (Bio-Rad) as the soluble protein samples. Untransformed WT strain was used as negative control. All the samples were then heated at 95°C for 5 min and 20 μl of sample was applied for each AAT. Precision PlusProtein™ Prestained Standards (Bio-Rad) were used as shown in **Fig. 2.S1**. A 0.5 mg/ml BSA standard (Bio-Rad) was applied to both gels (data not shown) as internal standards to quantify the protein expression levels. The results were calculated by the software ImageJ [90]. All the samples were prepared by normalizing the cell density OD_{600} to 5.0. Under this cell density, for the whole cell extract part, there were 30 mg/l LuxE, 36 mg/l ATF1, 43 mg/l ATF2, 46 mg/l BPBT, and 5.5 mg/l SAAT; for the soluble protein part, there were 2.6 mg/l LuxE, 6.4 mg/l ATF1, 12 mg/l ATF2, 9.2 mg/l BPBT, and 1.6 mg/l SAAT.

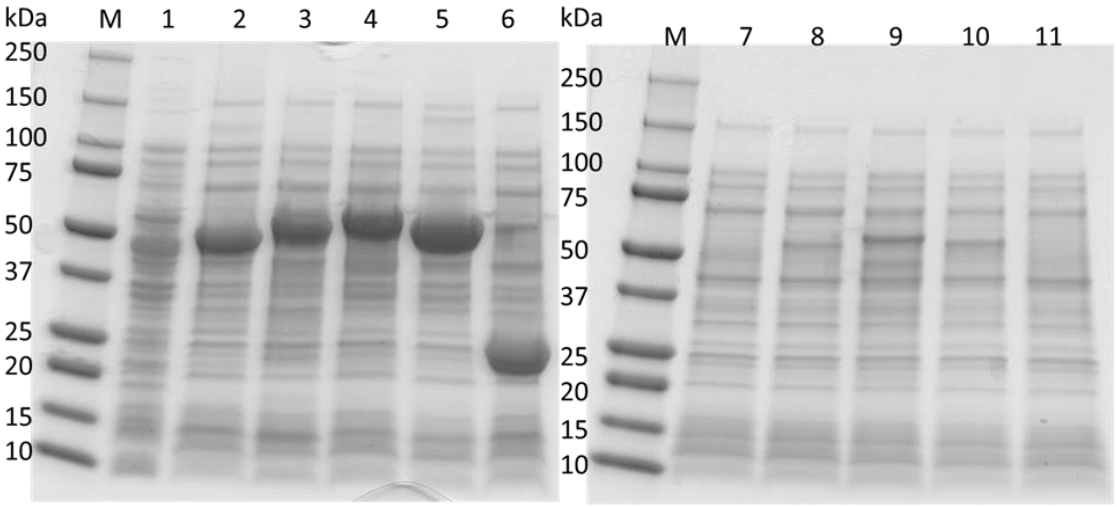

Figure 2.S1| Whole cell extracts and soluble protein fractions of various AAT-overexpressing strains. Lanes M are protein molecular weight markers. Molecular weights are labeled in kDa. Lanes 1 to 6 are whole cell extracts of cells overexpressing different AAT as 1: The negative control without overexpression of AAT, 2: LuxE, 3: ATF1, 4: ATF2, 5: BPBT, 6: SAAT. Lanes 7 to 11 are soluble fractions of cells as 7: LuxE, 8: ATF1, 9: ATF2, 10: BPBT, 11: SAAT.

Chapter 3. Engineering a Nonphosphorylative Metabolism for 1,4-Butanediol Production from Lignocellulosic Feedstock

Summary

Conversion of lignocellulosic biomass into value-added products provides significant environmental and economic benefits. Here we report the engineering of an unconventional metabolism for the production of TCA cycle derivatives from biomass sugars D-xylose, L-arabinose, and D-galacturonate. A growth-based selection platform was designed to identify gene clusters functional in *E. coli* that can perform this nonphosphorylative assimilation of sugars into the TCA cycle in less than 6 steps. To demonstrate the application of this new metabolic platform, we built artificial biosynthetic pathways to 1,4-butanediol (BDO) with a theoretical molar yield of 100%. By screening and engineering downstream pathway enzymes, 2-ketoacid decarboxylases and alcohol dehydrogenases, we constructed *E. coli* strains capable of producing BDO from D-xylose, L-arabinose, and D-galacturonate in 1.3-l bioreactors. The titers, rates, and yields are higher than those previously reported utilizing conventional pathways. This work demonstrates the potential of the nonphosphorylative metabolism for biomanufacturing with improved biosynthetic efficiencies.

1. Introduction

The use of edible biomass such as corn or sugarcane for biomanufacturing has affected food supply on a global scale and elevated food prices[91]. In an effort to circumvent the contention of resources for "food versus chemical" purposes, lignocellulosic feedstock

presents a promising solution. Lignocellulosic feedstock is the most abundant inedible biomass with an annual output of around 2×10^{11} metric tons[92]. Common sources of lignocellulose include corn stover, switchgrass, sugar beet pulp, and citrus peel. Utilization of D-xylose, L-arabinose, and D-galacturonate is critical for the economic viability of lignocellulosic fermentation, as they constitute more than 1/3 of the sugars in lignocellulose[93, 94]. Over the past several years, there has been remarkable progress in lignocellulosic ethanol production[95, 96, 97, 98]. However, the low price of ethanol has led other studies to focus on producing more valuable compounds, such as xylitol and biodiesel[9, 99, 100]. The development of new metabolic platforms with an expanded chemical repertoire will promote the applications of cellulosic processes.

As the metabolic hub of the cell, the TCA cycle leads to a variety of high value bioproducts, including amino acids and industrial chemicals (**Fig. 3.1**). The conventional metabolic routes for carbon feedstocks to enter the TCA cycle are glycolysis and pentose phosphate pathways (PPP). These traditional metabolisms, however, involve lengthy reaction steps (>10 steps to TCA cycle) and complex regulations that limit the production yield and rate. For example, one reported pathway to produce 1,4-butanediol (BDO) requires 21 reaction steps, imposing significant difficulty on feasible metabolic engineering[101]. Moreover, after several decades of industrial practices, the fermentation yields of amino acids are still much lower than their theoretical maxima[102].

An attractive alternative exists in an unconventional metabolism that converts lignocellulosic materials directly into 2-ketoglutarate (2-KG) in less than 6 steps (**Fig. 3.1**). In this proposed mechanism, D-xylose is first converted into D-xylonolactone by

D-xylose dehydrogenase (XDH), followed by hydrolysis to D-xylonate by D-xylonolactonase (XL). D-xylonate is subsequently dehydrated to 2-keto-3-deoxy-D-xylonate by D-xylonate dehydratase (XD), which is then converted to 2,5-dioxopentanoate (DOP) by 2-keto-3-deoxy-D-xylonate dehydratase (KdxD). This D-xylose oxidation pathway was first discovered in 1960[103] and the xylose-inducible *xylXABCD* operon (CC0823—CC0819) was later annotated in *Caulobacter crescentus*[104]. Through a similar metabolism, L-arabinose can be converted to DOP by L-arabinose dehydrogenase (ADH), L-arabinolactonase (AL), L-arabonate dehydratase (AD), and 2-keto-3-deoxy-L-arabonate dehydratase (KdaD). The intermediate, DOP, produced from D-xylose and L-arabinose can be further oxidized to 2-KG, a key intermediate of the TCA cycle, by 2-ketoglutarate semialdehyde dehydrogenase (KGSADH)[105]. This L-arabinose degradation pathway has been discovered in *Pseudomonas fragi*[103], and later demonstrated in *Azospirillum brasilense*[106].

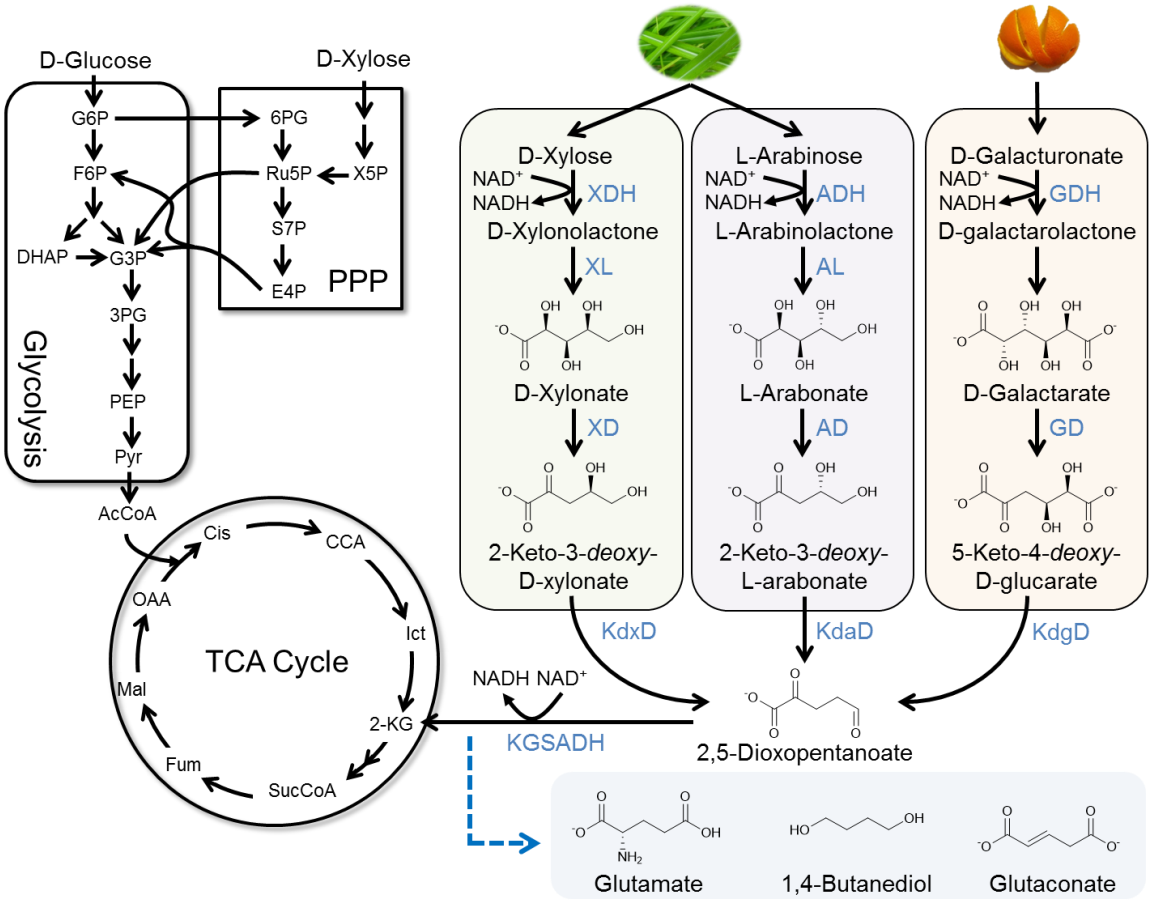

Figure 3.1| Assimilation pathways of lignocellulosic sugars through the nonphosphorylative metabolism. The pathway for D-xylose metabolism consists of D-xylose dehydrogenase (XDH), D-xylonolactonase (XL), D-xylonate dehydratase (XD), and 2-keto-3-deoxy-D-xylonate dehydratase (KdxD). The L-arabinose assimilation pathway is comprised of L-arabinose dehydrogenase (ADH), L-arabinolactonase (AL), L-arabonate dehydratase (AD), and 2-keto-3-deoxy-L-arabonate dehydratase (KdaD). The pathway for D-galacturonate metabolism was designed by using uronate dehydrogenase (UDH), D-galactarate dehydratase (GD), and 5-keto-4-deoxy-D-glucarate dehydratase (KdgD). The DOP produced from these feedstocks is then converted into 2-KG by 2-ketoglutarate semialdehyde dehydrogenase (KGSADH) which is a key intermediate of the TCA cycle.

A comparable metabolism for the assimilation of uronic acids, such as D-galacturonate, has also been identified. Uronate dehydrogenase (UDH) can catalyze the transformation of D-galacturonate into D-galactaro-1,4-lactone[107]; the lactone ring is

then hydrolyzed either spontaneously or with the aid of a lactonase to form D-galactarate[108]. D-Galactarate can be converted to 5-keto-4-deoxy-D-glucarate by D-galactarate dehydratase (GD) and then to DOP by 5-keto-4-deoxy-D-glucarate dehydratase (KdgD)[109] . The DOP produced can again be further oxidized to 2-KG using a KGSADH described earlier. This alternative metabolism does not involve any phosphorylating reactions, making it more energy-efficient than the conventional pathways such as glycolysis and PPP. This nonphosphorylative pathway can be utilized as a shortcut to the TCA cycle, potentially accelerating the production of TCA cycle derivatives. In addition, the theoretical yield of 2-KG from these pentoses and uronic acids is 100 mol% through this metabolism, which is notably higher than that from pentose phosphate pathway (83 mol%).

Nonphosphorylative metabolism has been known for over fifty years[103]; however, the full reconstitution of this pathway from sugars to 2-KG has not been demonstrated in the workhorse microorganism, *E. coli*. Recently, several reports have partially reconstituted and applied the nonphosphorylative pathway from D-xylose[110, 111, 112, 113], but the utilization of L-arabinose and D-galacturonate for chemical synthesis via this pathway has not been explored. Here we describe our selection platform to discover nonphosphorylative gene clusters that are functional in *E. coli*. We first tested the platform using a previously identified gene cluster from *C. crescentus*[104, 105], and then subsequently used the platform for gene mining to assemble novel, putative gene clusters from various microorganisms that allow the nonphosphorylative assimilation of D-xylose, L-arabinose, and D-galacturonate. We purified the corresponding enzymes and

determined their kinetic parameters to validate the *in vivo* activities. The establishment of this alternative metabolism in *E. coli* provides a novel metabolic platform for biosynthesis of a variety of chemicals such as succinate, glutaconate, and the "glutamate family" of amino acids. Furthermore, it enables biotransformation of pharmaceutically important natural products catalyzed by 2-ketoglutarate-dependent dioxygenases[114, 115].

In particular, we designed a new synthetic pathway to 1,4-butanediol (BDO)[116], a raw material for many commercial products such as Spandex. This pathway uses a 2-ketoacid decarboxylase (KDC) to convert DOP into butanedial. Butanedial is then transformed into BDO by an alcohol dehydrogenase (ADH). The total biosynthetic pathway starting from the pentoses to BDO requires only 6 steps, which is less than 1/3 of the previously reported pathway[101]. Additionally, we utilized protein engineering techniques to reduce the accumulation of the byproduct, 1,2,4-butanetriol (BTO), by improving the selectivity of KDC towards DOP. The engineered KDC improved BDO titer from 1.83 to 3.8 g/l at a yield of 63% of the theoretical maximum.

Based on this nonphosphorylative platform, we also expanded the sugar repertoire to produce 5.6 g/l BDO from L-arabinose and 2.3 g/l BDO from D-galacturonate, which has not been reported before. We then examined the scale-up feasibility for each substrate in 1.3 L bioreactors, where engineered strains were able to produce 12 g/l of BDO from D-xylose in 30 h, 15.6 g/l BDO from L-arabinose in 75 h, and 16.5 g/l of BDO from D-galacturonate in 90 h.

2. Results

2.1 Establishing the nonphosphorylative metabolism in *E. coli*

To facilitate the discovery and engineering of nonphosphorylative gene clusters, we developed a selection platform based on cell growth (**Fig. 3.2a**). Here, we knocked out the *E. coli* isocitrate dehydrogenase gene, *icd*, so the oxidation of isocitrate to 2-KG was interrupted. Thus, the cells required an exogenous supply of 2-KG to grow. Since the alternate nonphosphorylative pathway can convert pentoses (such as D-xylose and L-arabinose) and uronic acids (such as D-galacturonate) to 2-KG, the activity of the pathway was coupled to cell growth. This platform can thus be used to screen for active gene clusters in *E. coli*. Gene clusters can also be further optimized by using directed evolution on the introduced pathway and identifying cells with improved growth.

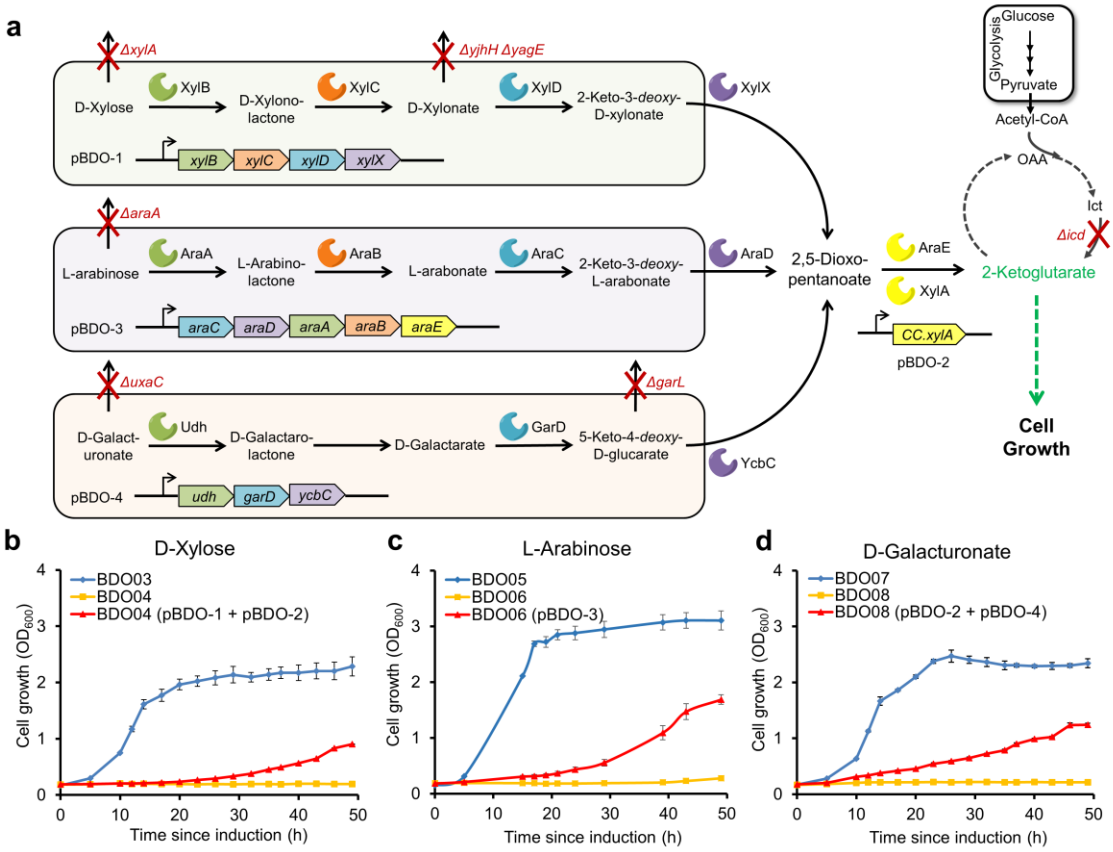

Figure 3.2| The growth platform to test functional nonphosphorylative gene clusters in *E. coli*. (a) The growth assay was designed based on the supply of 2-KG, a TCA cycle intermediate. Isocitrate dehydrogenase gene (*icd*) was knocked out to cut off 2-KG production through glycolysis/TCA cycle. The nonphosphorylative pathway plasmids (pBDO-1 and pBDO-2 for the D-xylose pathway, pBDO-3 for the L-arabinose pathway, pBDO-4 (a synthetic operon) and pBDO-2 for the D-galacturonate pathway) were then transformed into cells to compensate the production of 2-KG. (b) Strains BDO03 (BW25113 Δ*xylA* Δ*yjhH* Δ*yagE*), BDO04 (BW25113 Δ*xylA* Δ*yjhH* Δ*yagE* Δ*icd*), and BDO04 transformed with plasmids pBDO-1 and pBDO-2 were grown in M9 minimum media supplemented with 5 g/l glucose and 5 g/l D-xylose. (c) Strains BDO05 (BW25113), BDO06 (BW25113 Δ*icd*), and BDO06 transformed with plasmid pBDO-3 were grown in M9 minimum media supplemented with 5 g/l glucose and 5 g/l L-arabinose. (d) Strains BDO07 (BW25113 ⊿*uxaC* ⊿*garL*), BDO08 (BW25113 ⊿*uxaC* ⊿*garL* Δ*icd*), and BDO08 transformed with plasmids pBDO-4 and pBDO-2 were grown in M9 minimum media supplemented with 5 g/l glucose and 5 g/l D-galacturonate. All error bars shown in (b), (c), and (d) represent SD (n=3).

To build the selection platform, we cloned the gene cluster *xylBCDX* (**Fig. 3.2a**) from *C. crescentus* into plasmid pBDO-1 (Supporting informaion, **Table 3.S1**) where *xylB*

encodes the XDH; *xylC* encodes the XL; *xylD* encodes the XD and *xylX* encodes the KdxD (**Fig. 3.1**). We cloned the gene *xylA* of the *C. crescentus* xylose operon, annotated as the KGSADH, into a separate plasmid pBDO-2 (**Table 3.S1**). Furthermore, to maximize the flux of D-xylose through the nonphosphorylative pathway, we knocked out the endogenous D-xylose (*xylA*) and D-xylonate (*yagE*, *yjhH*) consuming pathways in *E. coli*, generating strain BDO03 (**Table 3.S1**). We also deleted *icd* gene to generate strain BDO04, a 2-KG auxotroph that is incapable of producing 2-KG (**Table 3.S1**). While strain BDO03 showed exponential growth in minimal media containing glucose and D-xylose, strain BDO04 showed almost no growth due to the disruption of the TCA cycle. We then transformed BDO04 with plasmids pBDO-1 and pBDO-2, and the resulting strain showed growth on mixed sugars with OD reaching ~1.0 after 50 h (**Fig. 3.2b**). This could be attributed to the 2-KG produced from D-xylose via the nonphosphorylative pathway (pBDO-1 and pBDO-2).

Similar gene clusters encoding the L-arabinose assimilation pathway have been identified in several species of soil bacteria including *Burkholderia spp.*[117], *Pseudomonas saccharophilia*[118] and *Rhizobium spp*[119]. In this work, we discovered a novel L-arabinose assimilation gene cluster from *Burkholderia multivorans* using BLAST based on the previously identified L-arabinose gene cluster of *Burkholderia thailandensis*[105]. To demonstrate the platform, we cloned this putative L-arabinose gene cluster from *B. multivorans araCDABE* (*BmulJ 5323-5321-5320-5316-5314*), responsible for L-arabinose degradation to 2-KG, into plasmid pBDO-3 (**Table 3.S1**). The gene *araA* encodes the ADH; *araB* codes the AL; *araC* codes the AD; *araD* was annotated as the KdaD and

araE encodes the KGSADH (**Fig. 3.1**). To eliminate the L-arabinose consumption pathways in *E. coli*, we used strain BDO05 with *araA* gene knocked out, which served as the positive control for the growth assay (**Table 3.S1**). Strain BDO05 showed exponential growth in media containing both glucose and L-arabinose, but when *icd* gene was knocked out (strain BDO06), cells could not grow in the same media due to the disruption of the TCA cycle. When BDO06 strain was transformed with plasmid pBDO-3 containing the L-arabinose assimilation gene cluster, growth on glucose and L-arabinose media was restored due to the supplementation of 2-KG through the nonphosphorylative pathway. The BDO06 strain transformed with pBDO-3 grew to an OD of ~1.7 in 50 h (**Fig. 3.2c**), thus establishing the *in vivo* activity of the novel *B. multivorans* L-arabinose gene cluster in *E. coli*.

Gene clusters with an analogous function for the hexuronic acid degradation have been found in *Bacillus* species[109] and *Pseudomonas putida*[120]. To establish D-galacturonate pathway, we designed a synthetic operon consisting of the following genes: *udh* from *P. putida* encoding the GDH, *garD* from *E. coli* encoding the GD, and *ycbC* from *B. subtilis* encoding the putative KdgD (**Fig. 3.1**). We cloned this operon into plasmid pBDO-4 (**Table 3.S1**). We used the plasmid pBDO-2 with *xylA* gene of *C. crescentus* to convert DOP to 2-KG. In order to maximize the flux of galacturonate via the heterologous pathway, we knocked out the genes encoding the pathways involved in consumption of either the substrate (Δ*uxaC*) or intermediates (Δ*garL*) resulting in strain BDO07 (**Table 3.S1**). BDO07 grew exponentially after induction in the media containing both glucose and D-galacturonate. Similar to the D-xylose and L-arabinose

pathways, when *icd* was knocked out (strain BDO08), cells could not grow since the strain is a 2-KG auxotroph. When we transformed strain BDO08 with plasmids pBDO-2 and pBDO-4, 2-KG was produced from D-galacturonate using the nonphosphorylative pathway, thus allowing cells to grow to an OD of ~1.25 in 50 h (**Fig. 3.2d**).

2.2 Validating the enzymatic activities by *in vitro* assays

After demonstrating that the putative gene clusters could function *in vivo* using a growth-based selection platform, we sought to further confirm key enzymatic functions and identify *in vitro* activities of the nonphosphorylative pathways. All the kinetic parameters are shown in **Table 3.1**. In the D-xylose pathway from *C. crescentus*, D-xylose dehydrogenase (XylB) and xylonate dehydratase (XylD) have k_{cat} values of 12.1 s^{-1} and 7.6 s^{-1}, respectively. However, the enzyme 2-keto-3-deoxy-D-xylonate dehydratase (XylX) has a relatively low k_{cat} of 0.53 s^{-1}. Since XylX is also the enzyme with the highest K_M (1.9 mM) in the pathway, its specific constant (k_{cat}/K_M) is therefore the lowest (0.26 $s^{-1}mM^{-1}$) among the three enzymes. This indicates that XylX is the bottleneck enzyme in the D-xylose degradation pathway.

Table 3.1| Kinetic parameters of key pathway enzymes. Data is presented as mean±SD (n=3).

Enzyme	Substrate	K_M (mM)	k_{cat} (s^{-1})	K_M/k_{cat} (mM^{-1} s^{-1})
XylB	D-Xylose	0.85±0.08	12.1±2.2	14
XylD	D-Xylonate	1.18±0.05	7.60±1.1	6.4
XylX[a]	2-Keto-3-deoxy-D-xylonate	1.90±0.08	0.53±0.1	0.26
AraA	L-Arabinose	3.14±0.12	101.4±5.2	32.3
AraC	L-Arabonate	2.05±0.05	0.17±0.01	0.083
AraD[a]	2-Keto-3-deoxy-L-arabonate	9.69±0.2	0.2±0.02	0.023
Udh	D-Galacturonate	0.15±0.05	24.1±3.6	160
GarD	D-Galactarate	0.76±0.02	18.9±0.8	25
YcbC[a]	5-Keto-4-deoxy-D-glucarate	0.43±0.06	2.17±0.2	5.1
Kivd[a]	2,5-Dioxopentanoate	2.8±0.6	4.8±0.4	1.7
Kivd(V461I)[a]	2,5-Dioxopentanoate	2.2±0.4	5.6±0.7	2.5
Kivd[a]	2-Keto-3-deoxy-D-xylonate	1.6±0.7	12.3±3.5	7.7
Kivd(V461I)[a]	2-Keto-3-deoxy-D-xylonate	4.7±1.3	2.4±0.5	0.51
YqhD[a]	Butanedial	1.9±0.1	45.0±6.2	23

[a]Enzyme activity was determined using a coupled assay

In the L-arabinose pathway from *B. multivorans*, the first enzyme, L-arabinose dehydrogenase (AraA), has the highest k_{cat} value of 101.4 s^{-1} while the downstream enzymes, L-arabonate dehydratase (AraC) and 2-keto-3-deoxy-L-arabonate dehydratase (AraD) have relatively low k_{cat} values of 0.17 s^{-1} and 0.23 s^{-1}, respectively. The enzyme AraD has the highest K_M (9.7 mM) and a low k_{cat}, making it the rate-limiting step of the L-arabinose pathway.

For the D-galacturonate pathway, uronate dehydrogenase (Udh) from *P. putida* has the highest k_{cat} (24.1 s^{-1}) and lowest K_M (0.15 mM) among the three enzymes. Galactarate dehydratase (GarD) from *E. coli* has the highest K_M (0.76 mM) in the pathway but a much higher k_{cat} (18.9 s^{-1}) than the 5-keto-4-deoxy-D-glucarate dehydratase (YcbC) from *B. subtilis*. Similar to D-xylose and L-arabinose pathway, the last enzyme (YcbC) in

the D-galacturonate pathway that produces DOP has the lowest specific constant and is considered the bottleneck enzyme in the D-galacturonate degradation. These bottleneck enzymes from the three substrates could explain why transformants harboring these nonphosphorylative pathways did not grow as well as the wild type cells.

2.3 Identification of enzymes to convert DOP into BDO

With the establishment of the nonphosphorylative metabolism, we explored its biosynthetic applications by designing new synthetic pathways to BDO. We hypothesized that DOP can be converted to BDO by a 2-ketoacid decarboxylase (KDC) and an alcohol dehydrogenase (ADH) (**Fig. 3.3a**). We designed the BDO producing pathways using the following steps: (1) introducing the nonphosphorylative metabolism to convert the pentoses and hexuronic acid into a pool of DOP, (2) screening for the best KDC that can convert DOP to butanedial, and (3) screening for the best ADH that can reduce butanedial into BDO.

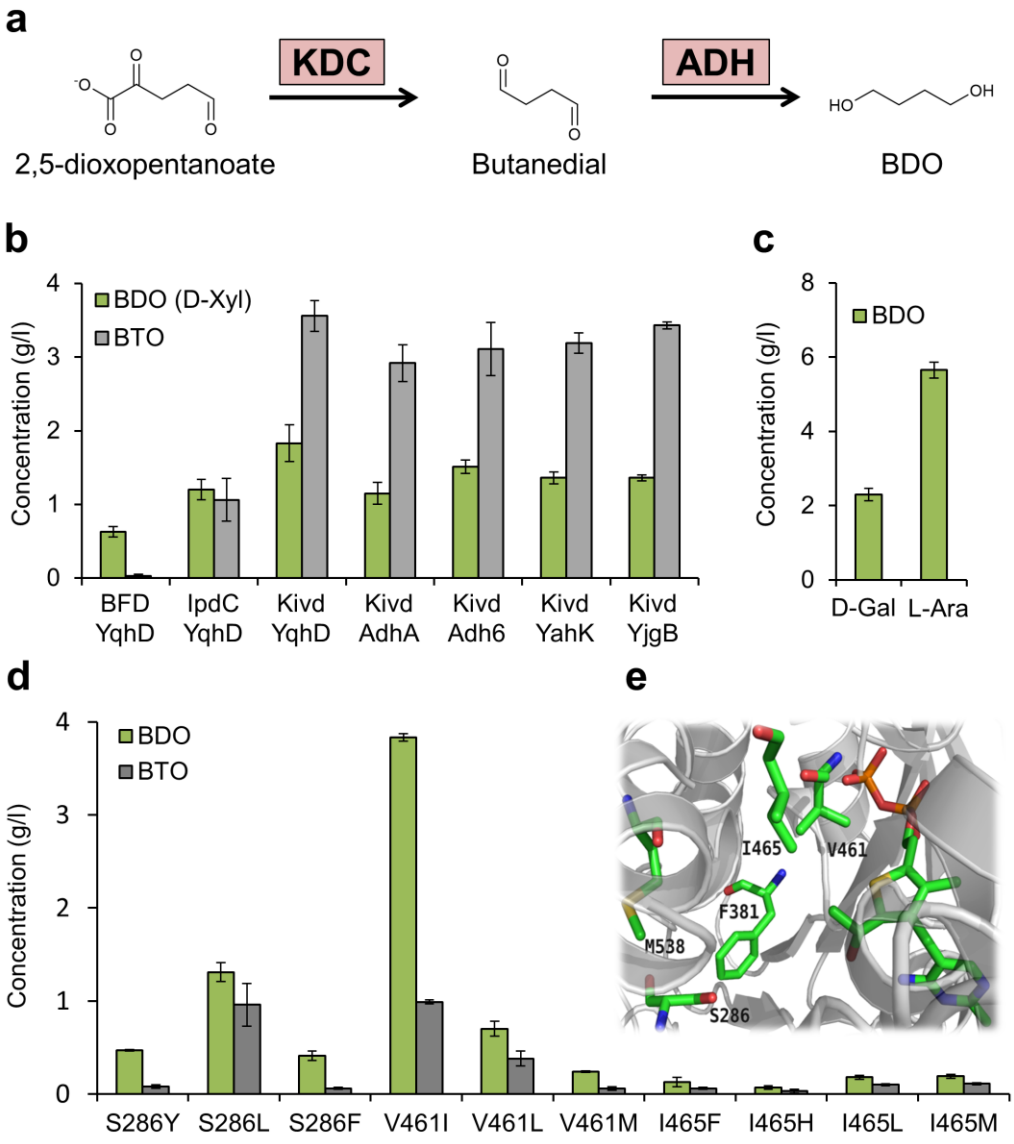

Figure 3.3| BDO production using different combinations of 2-ketoacid decarboxylase (KDC) and alcohol dehydrogenase (ADH) and different Kivd mutants. (a) BDO production pathway from DOP catalyzed by KDC and ADH. (b) Shake-flask production of BDO from D-xylose. Three KDC (Kivd, IpdC, and BFD) and five ADH (YqhD, AdhA, Adh6, YahK, and Yjgb) were examined. (c) Shake-flask production of BDO from L-arabinose and D-galacturonate using Kivd+YqhD. There was no BTO production using these substrates. (d) Shake-flask production of BDO using Kivd mutants from D-xylose. Ten Kivd mutants, S286Y, S286L, S286F, V461I, V461L, V461M, I465F, I465H, I465L, and I465M, were tested for BDO production. (e) The binding pocket of Kivd (PDB ID: 2VBG). Residues S286, V461, and I465 were mutated to larger residues to improve the substrate specificity. Error bars in (b), (c) and (d) represent SD (n=3).

Since the D-xylose pathway of *C. crescentus* has been partially established in *E. coli*[110], we selected it for enzyme screening. First, to convert DOP to butanedial, we screened three KDCs, 2-ketoacid decarboxylase (Kivd) from *Lactococcus lactis*[121], indolepyruvate decarboxylase (IpdC) from *Salmonella typhimurium*[24], and benzoylformate decarboxylase (BFD) from *P. putida*[122] and cloned them into plasmids pBDO-5, pBDO-6, pBDO-7, respectively (**Table 3.S1**). These plasmids also carried a promiscuous alcohol dehydrogenase YqhD from *E. coli*, for screening based on BDO production. To maximize the carbon flux towards the desired pathway, we transformed strain BDO03 with these plasmids individually along with the DOP producing plasmid, pBDO-1. It is important to note that all the strains used for BDO production do not have *icd* inactivation, and can thus utilize glucose for growth. In the shake flask experiment, we used 20 g/l of D-xylose and the strains carrying Kivd, IpdC and BFD produced 1.83, 1.20 and 0.63 g/l BDO, along with 3.56, 1.06 and 0.03 g/l BTO, respectively (**Fig. 3.3b**). It is notable that all of these enzymes are promiscuous enough to catalyze the decarboxylation of DOP to BDO. Overall, the data (**Fig. 3.3b**) indicated that Kivd, amongst the three set of investigated enzymes, was the best KDC towards DOP.

Besides KDC, we also investigated ADHs from different organisms to see which combination would produce maximal titer of BDO. Other than YqhD, we chose the following ADHs as candidate enzymes: *L. lactis* alcohol dehydrogenase AdhA[123]; *S. cerevisiae* alcohol dehydrogenase Adh6[124]; *E. coli* putative alcohol dehydrogenase YahK (PDB ID: 1UUF); and *E. coli* putative alcohol dehydrogenase YgjB[125]. We cloned these

enzymes individually after Kivd to build an expression cassette on a high copy plasmid as pBDO-8, pBDO-9, pBDO-10, and pBDO-11, respectively (**Table 3.S1**). Strains carrying AdhA, Adh6, YahK, and YgjB could produce 1.15, 1.51, 1.36 and 1.36 g/l BDO together with 3.11, 2.92, 3.19 and 3.43 g/l BTO, respectively (**Fig. 3.3b**). Overall, the best combination was Kivd with YqhD allowing a yield of 0.15 g/g, which is only 25% of the theoretical maximum. However, the byproduct BTO yield from D-xylose was 0.28 g/g, which was around two times higher than BDO. The apparent K_m and k_{cat} of Kivd towards DOP is 4.8 mM and 4.8 s^{-1}, respectively, and the apparent kinetic parameters of YqhD towards butanedial is 1.9 mM (K_M) and 45.0 s^{-1} (k_{cat}) (**Table 3.1**).

Based on the screening results of the D-xylose pathway, we applied Kivd and YqhD (pBDO-5) for the L-arabinose and D-galacturonate pathways. For L-arabinose, we cloned the putative *B. multivorans* cluster *araCDAB* (*BmulJ 5323-5321-5320-5316*) that can convert L-arabinose to DOP, into plasmid pBDO-12. The strain BDO05 transformed with plasmids pBDO-12 and pBDO-5, was able to produce 5.65 g/l of BDO from 20 g/l L-arabinose in production experiments. For D-galacturonate, we transformed strain BDO07 with plasmids pBDO-4 and pBDO-5 and the engineered strain was capable of producing 2.34 g/l of BDO from 20 g/l D-galacturonate (**Fig. 3.3c**). Both L-arabinose and D-galacturonate pathways did not result in BTO production.

2.4 Optimization of BDO production by protein engineering

While the discovery of Kivd and YqhD allowed for the production of BDO, the promiscuous nature of Kivd did not provide a good selectivity for the decarboxylation step in the D-xylose pathway. BTO is produced by decarboxylation of the D-xylose intermediate, 2-keto-3-deoxy-D-xylonate (**Fig. 3.S7**). This suggests that compared to DOP, Kivd prefers to bind to the intermediate 2-keto-3-deoxy-D-xylonate as a substrate leading to a much higher titer of BTO than our target product. Conversely, there was no accumulation of BTO using L-arabinose as the substrate, indicating that Kivd is not active on the stereoisomer, 2-keto-3-deoxy-L-arabonate. To increase the production of BDO, we examined the effect of protein engineering on improving Kivd selectivity towards DOP. According to the crystal structure[126] (PDB ID: 2VBG), amino acid residues S286, V461 and I465, in combination with the cofactor thiamine diphosphate (ThDP), delineate the active site of Kivd (**Fig. 3.3d&e**) . Since 2-keto-3-deoxy-D-xylonate, with its extra hydroxyl group, is a bulkier substrate than DOP, we attempted to shrink the binding site of Kivd to enhance its selectivity towards the smaller substrate. We constructed ten mutants of Kivd, including S286Y, S286L, S286F, V461I, V461L, V461M, I465F, I465H, I465L and I465M, and tested them in shake flask experiments.

The fermentation results indicated that the best mutant, V461I, produced 3.83 g/l BDO with only 0.99 g/l BTO, which represents a yield of 0.37 g/g D-xylose which is 63% of the theoretical maximum. Compared with wild type Kivd, BDO production titer with V461I mutant increased over 2-fold. This can be attributed to the extra methyl group in isoleucine compared to valine, which shrinks the Kivd binding pocket, making

it more selective towards DOP. Enzymatic assays also showed that the mutant V461I on Kivd notably reduces the specific constant (k_{cat}/K_M) towards BTO substrate, 2-keto-3-deoxy-D-xylonate, from 7.7 to 0.5 $mM^{-1}s^{-1}$ (**Table 3.1**), while improving the activity towards BDO substrate (DOP) from 1.7 to 2.5 $mM^{-1}s^{-1}$. Therefore, the enzyme characterization data was consistent with the fermentation results (**Fig. 3.3d**).

2.5 Fermentation scale-up

We tested the scale-up feasibility of these BDO biosynthetic pathways by fed-batch fermentations in 1.3-L bioreactors. For the D-xylose pathway, we used the recombinant strain BDO03 transformed with plasmids pBDO-1 and pBDO-16 and fed a mixture of glucose and D-xylose as substrates during the fermentation process. The engineered strain produced 9.21 g/l BDO in 36 h and consumed 42.1 g/l of D-xylose (**Fig. 3.4a**). Glucose was fed to support cell growth. To further exploit glucose for the production of value-added chemicals, we introduced another plasmid pMEV-1[127] into the engineered strain for the co-production of BDO and mevalonate (MEV). MEV is an important intermediate in the production of the branched lactone, β-methyl-δ-valerolactone, which could be used as building blocks for high-performing biobased polymers[127]. We used the BDO03 strain transformed with pBDO-1, pBDO-16, and pMEV-1 for the fed-batch fermentation and the engineered strain produced 12.0 g/l BDO by consuming 46 g/l of D-xylose in 30 h after induction (**Fig. 3.4b**). Not only was glucose efficiently utilized (20.2 mol% of glucose was converted into MEV), but the yield of BDO from D-xylose was also improved from 36% to 43% of the theoretical maximum by introducing MEV

production pathway. Acetate started to accumulate to a final concentration of 11 g/l when cells entered stationary phase and inhibited further production of both BDO and MEV.

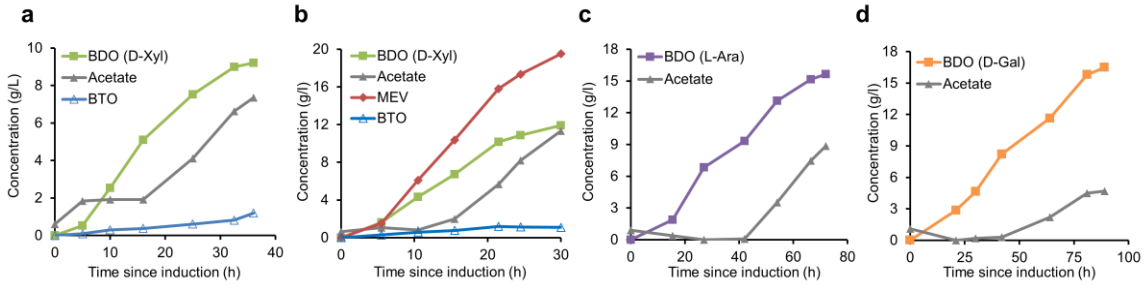

Figure 3.4| Production of BDO from D-xylose, L-arabinose, and D-galacturonate in 1.3-l bioreactors. (a) Production of BDO from D-xylose. (b) Co-production of BDO and mevalonate from D-xylose and glucose. (c) Production of BDO from L-arabinose. (d) Production of BDO from D-galacturonate. Abbreviations: D-Xyl, D-xylose; MEV, mevalonate; L-Ara, L-arabinose; D-Gal, D-galacturonate. Bioreactor experiments were performed in at least triplicates for each substrate and results for one representative experiment are shown.

We used the L-arabinose recombinant strain, BDO05 transformed with pBDO-5 and pBDO-12, in the fed-batch fermentation with a mixture of glucose and L-arabinose as the feed. The engineered strain produced 15.6 g/l BDO in 72 h and consumed 70.5 g/l of L-arabinose which resulted in a yield of 37% of the theoretical maximum. The final acetate concentration was 8.9 g/l, inhibiting further production of BDO (**Fig. 3.4c**). Similarly, we tested the D-galacturonate strain BDO07 transformed with pBDO-4 and pBDO-5 in a 1.3-L bioreactor. We fed a mixture of glucose and D-galacturonate to the bioreactor and the engineered strain produced 16.5 g/l of BDO from 50.5 g/l of D-galacturonate (70% of the theoretical maximum) in 90 h (**Fig. 3.4d**).

2.6 Identification of new gene clusters

After successfully demonstrating the use of the nonphosphorylative metabolism of D-xylose, L-arabinose, and D-galacturonate for BDO production, we wanted to identify putative nonphosphorylative operons from other organisms that may show higher activities in *E. coli*. Therefore, we used the growth based selection platform that employs a 2-KG auxotroph to perform gene mining. Using BLAST, we identified a putative operon from *Burkholderia xenovorans* LB400 (DR64_8447—DR64_8450, DR64_8452) for nonphosphorylative assimilation of D-xylose to 2-KG. (**Fig. 3.S8**). We cloned genes for converting D-xylose to DOP (DR64_8447—DR64_8450) into plasmid pBDO-23 and cloned DR64_8452 to convert DOP to 2-KG into plasmid pBDO-24. To test the *in vivo* activity of this gene cluster in *E. coli*, we transformed the 2-KG auxotroph BDO04 with plasmids pBDO-23 and pBDO-24. The *B. xenovorans* D-xylose gene cluster rescued the growth of *E. coli* with OD reaching ~1.8 in 50 h (**Fig. 3.5a**). We further investigated the production of BDO using the newly identified *B. xenovorans* operon. The recombinant strain, BDO03 transformed with plasmids pBDO-23 and pBDO-5, was able to produce 2.73 g/l BDO with no BTO accumulation (**Fig. 3.5b**). To further corroborate this production profile, we characterized the *in vitro* enzyme activities of the new operon (**Table 3.S2**). The 2-keto-3-deoxy-D-xylonate dehydratase of *B. xenovorans* (DR64_8450) has a 9-fold higher k_{cat} (4.7 s^{-1}) compared to the corresponding dehydratase (XylX) of *C. crescentus* (0.53 s^{-1}). This can explain why there was no BTO accumulation using *B. xenovorans* operon. Thus the selection strategy could be used to discover highly active

enzymes from different microorganisms. These enzymes could be combinatorially assembled into synthetic operons for potential biosynthesis.

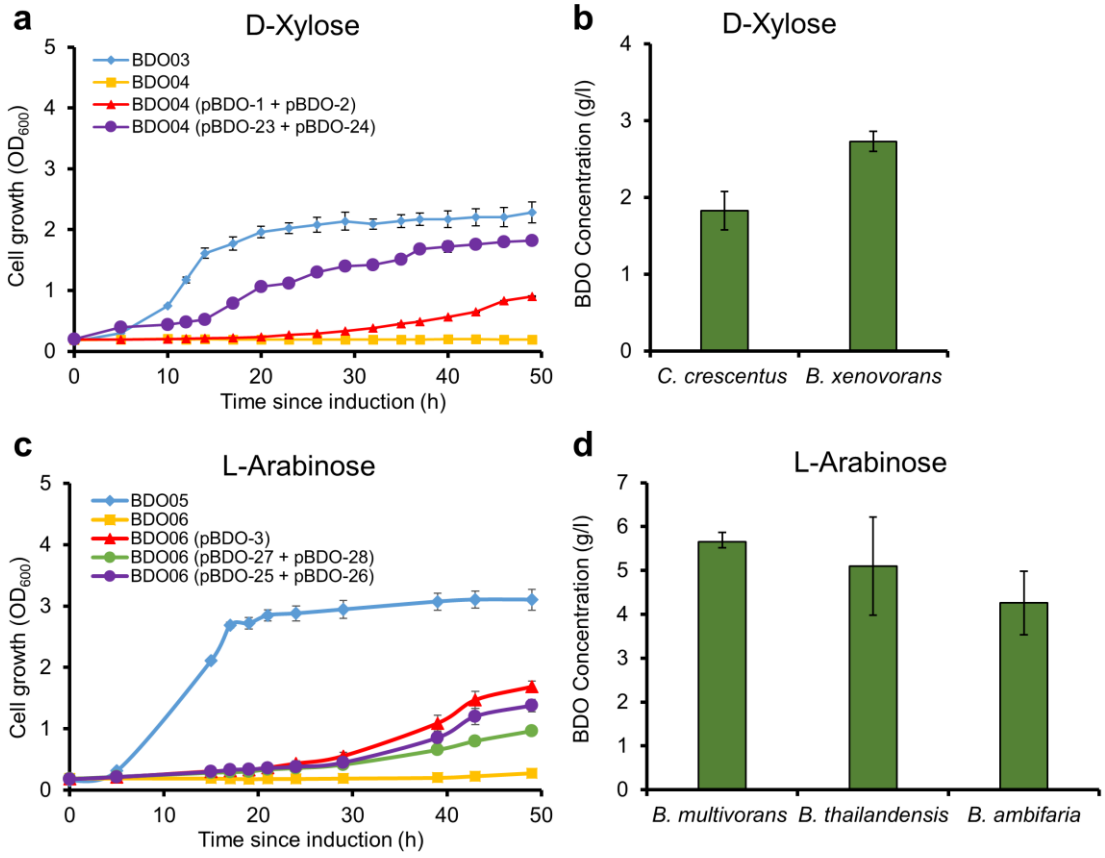

Figure 3.5| Growth platform to mine putative nonphosphorylative clusters in *E. coli* and BDO production using these novel operons. (a) Strains BDO03 (BW25113 Δ*xylA* Δ*yjhH* Δ*yagE*), BDO04 (BW25113 Δ*xylA* Δ*yjhH* Δ*yagE* Δ*icd*), BDO04 transformed with *C. crescentus* operon (pBDO-1 and pBDO-2) and BDO04 transformed with *B. xenovorans* operon (pBDO-23 and pBDO-24) were grown in M9 minimum media supplemented with 5 g/l glucose and 5 g/l D-xylose. (b) BDO production using newly identified *B. xenovorans* D-xylose operon and previous *C. crescentus* operon with Kivd and YqhD as downstream enzymes. (c) Strains BDO05 (BW25113), BDO06 (BW25113 Δ*icd*), BDO06 transformed with *B. multivorans* operon (pBDO-3), BDO06 transformed with *B. ambifaria* operon (pBDO-25 and pBDO-26) and BDO06 transformed with *B. thailandensis* operon (pBDO-27 and pBDO-28) were grown in M9 minimum media supplemented with 5 g/l glucose and 5 g/l L-arabinose. (d) BDO production using previously identified *B. thailandensis* and novel *B. multivorans* and *B. ambifaria* L-arabinose operons with Kivd and YqhD as downstream enzymes. All error bars shown in (b) and (d) represent SD (n=3).

For L-arabinose, we tested operons from two other *Burkholderia* species—an uncharacterized, putative *B. ambifaria* gene cluster (Bamb_4925—4918, Bamb_4915) and a previously identified, uncharacterized *B. thailandensis* gene cluster (BTH_II1632—1625)[105], both of which had high sequence similarity (**Fig. 3.S8**) to *B. multivorans* L-arabinose operon. We cloned the putative *B. ambifaria* genes Bamb_4918, Bamb_4922, Bamb_4923, and Bamb_4925 converting L-arabinose to DOP into plasmid pBDO-25. We cloned gene Bamb_4915 that converts DOP to 2-KG into plasmid pBDO-26. Similarly, we cloned the *B. thailandensis* genes responsible for DOP production—BTH_II1625, BTH_II1629, BTH_II1630, and BTH_II1632—into plasmid pBDO-27, and BTH_II1631, that converts DOP to 2-KG, into plasmid pBDO-28. Both gene clusters rescued the growth of the 2-KG auxotroph, BDO06, to an OD of ~1.5 in 50 h (**Fig. 3.5c**) via the nonphosphorylative pathway. After establishing the *in vivo* activities of both L-arabinose gene clusters, we used both clusters for BDO production. The strain carrying *B. ambifaria* genes (BDO05 with plasmids pBDO-25 and pBDO-5) produced 4.3 g/l BDO; and the *B. thailandensis* gene overexpression strain (BDO05 with plasmids pBDO-27 and pBDO-5) produced 5.0 g/l BDO in production experiments (**Fig. 3.5d**). Similar to *B. multivorans* operon, both *B. ambifaria* and *B. thailandensis* gene clusters did not produce any BTO.

3. Discussion

The nonphosphorylative metabolism allows assimilation of lignocellulosic sugars or sugar acids into the important TCA cycle intermediate, 2-KG, in fewer than 6 steps. This

work is the first to demonstrate the complete nonphosphorylative metabolism of D-xylose, L-arabinose, and D-galacturonate to 2-KG in the workhorse microorganism, *E. coli*. To discover gene clusters that are functional in *E. coli*, we developed a selection platform utilizing a 2-KG auxotroph. In particular, we applied the platform to identify a new nonphosphorylative D-xylose operon from *B. xenovorans* that has a more active 2-keto-3-deoxy-D-xylonate dehydratase than the previously reported one from *C. crescentus*. The discovery of more active enzymes/operons will enable further optimization of these pathways. The establishment of these pathways can serve as a new biosynthetic platform for TCA cycle derivatives which have extensive applications. Here BDO production is used as an example.

To establish the downstream pathway to BDO, we screened several different decarboxylases and dehydrogenases. The best enzyme combination for BDO production was the 2-ketoacid decarboxylase (Kivd) from *L. lactis* and the endogenous alcohol dehydrogenase (YqhD). We identified a Kivd mutant V461I by protein engineering which successfully improved BDO titer from D-xylose by more than 100% and reduced BTO accumulation. In a previous report, a different Kivd mutant V461A has been shown to improve 3-methyl-1-pentanol production[21] by expanding the binding pocket to accommodate a bulkier substrate. Conversely, in this work we shrank the binding pocket of Kivd to decrease the selectivity towards the bulkier and undesired substrate, 2-keto-3-deoxy-D-xylonate. In the future, directed evolution strategy can be combined with this rational design to further improve the selectivity. In a recent report, the nonphosphorylative D-xylose operon from *C. crescentus* has been used to produce 0.44

g/l BDO, utilizing a different downstream pathway[110]. We validated the distinction and efficacy of our pathway by extensive enzymatic assays (**Table 3.1**) and *in vitro* production experiments (**Fig. 3.S1**). In addition, the higher production titer and yield (3.88 g/l BDO with a yield of 0.37 g/g D-xylose) indicates that our pathway has a higher *in vivo* efficiency.

Furthermore, we tested the *C. crescentus* D-xylose gene cluster, *B. multivorans* L-arabinose operon and D-galacturonate synthetic operon, in a 1.3-l bioreactor to study the scale-up feasibility. Acetate accumulation and inefficient co-utilization of sugars caused by carbon catabolite repression[128, 129] were two important limiting factors in the processes. The strains could thus be further improved by knocking out acetate producing pathways or relieving carbon catabolite repression with the overexpression of D-xylose, L-arabinose, or D-galacturonate transporters[129]. Fermentation process engineering or strain evolution can also be applied for optimization.

While the results reported in this work demonstrate the production of a commodity chemical, BDO, the nonphosphorylative platform can also be extended to produce several TCA cycle derivatives including glutamate, glutaconate and 1-butanol, among others. The growth selection platform provides an effective and robust tool to screen better enzymes or identify nonphosphorylative pathways for other substrates. Compared to conventional metabolism such as glycolysis and PPP, these fewer-step and higher theoretical yield nonphosphorylative pathways are of critical importance to make lignocellulosic bioproducts more economically feasible.

4. Materials and Methods

4.1 Bacterial strains and growth conditions

The *E. coli* strains used in this study are listed in **Table 3.S1**. XL10-Gold was used for cloning and BL21 was used for protein expression and purification. Most of the other strains were derived from the wild-type *E. coli* K-12 strain BW25113[70]. P1 phages of *xylA*, *yjhH*, *yagE*, *icd*, *uxaC*, and *garL* were obtained from the Keio collection. The phages were used to transfect the corresponding strain for the construction of targeted knockout strains. All the knockout strains were then transformed with pCP20 plasmid to remove the kanamycin marker. The correct knockouts were verified by colony PCR. Unless otherwise stated, these *E. coli* strains were grown in test tubes at 37 °C in 2×YT rich medium (16 g/l Bacto-tryptone, 10 g/l yeast extract and 5 g/l NaCl) supplemented with appropriate antibiotics (ampicillin 100 mg/l and kanamycin 50 mg/l).

4.2 Plasmids construction

All the primers used in this study were ordered from Eurofins MWG Operon and are listed in **Table 3.S3**. in supporting information. PCR reactions were carried out with Phusion High-Fidelity DNA polymerase (New England Biolabs) according to the manufacturer's instructions. The sequences of all the plasmids produced were verified by restriction mapping and DNA sequencing.

To construct plasmid pBDO-1, five fragments of *xylB*, *xylC*, *xylD*, and *xylX* were amplified from *C. crescentus* genomic DNA by using primer pairs of xylBAcc-F/xylBBamHI-R, xylCBamHI-F/xylCNhe-R, xylDNheI-F/xylDHind-R, xylXHind-

F/xylXBlpRem-R and xylXBlpRem-F/xylXBlpI-R, and then the fragment of *xylX* was amplified with primer pairs of xylXHind-F/xylXBlpI-R by using xylX-1 and xylX-2 as template. The four fragments of *xylB*, *xylC*, *xylD*, and *xylX* were digested with Acc65I/BamHI, BamHI/NheI, NheI/HindIII and HindIII/BlpI, and then ligated with linearized pZAlac vector[23] digested with Acc65I and BlpI to form the plasmid, pBDO-1. To make the plasmid pBDO-2, the coding region of *xylA* was PCR amplified by oligos of CC0822Acc-F and CC0822Xba-R using genomic DNA of *C. crescentus* as template, and then this coding region was inserted into the site between Acc65I and XbaI of vector pZElac[23] after digestion. To construct the plasmids pBDO-3 and pBDO-12, the gene fragments of *araC (BmulJ 5323), araD (BmulJ 5321), araA (BmulJ 5320), araB (BmulJ 5316)* and *araE (BmulJ 5314)* were amplified from *Burkholderia multivorans* genomic DNA using primer pairs of araC-Acc65I-F/araC-NheI-R, araD-NheI-F/araD-remBlpI-R, araD-remBlpI-F/araA-HindIII-R, araA-HindIII-F/araB-NdeI-R and araB-NdeI-F/araE-BlpI-R respectively. The two fragments of araD-araA were then used as templates for overlap PCR using primer pair araD-NheI-F/araA-HindIII-R. The fragments *araC*, *araD-araA*, *araB* and *araE* were double-digested with enzymes Acc65I/NheI, NheI/HindIII, HindIII/NdeI and NdeI/BlpI respectively and these were ligated with linearized pZA-lac vector digested with Acc65I/BlpI to form the plasmid pBDO-3. To construct pBDO-12, fragment *araB* was amplified from *B. multivorans* genomic DNA using different primer pair araB-HindIII-F/araB-BlpI-R and the resulting PCR product was digested with HindIII/BlpI. The fragments *araC* Acc65I/NheI digest, *araD-araA* NheI/HindIII digest and *araB* HindIII/BlpI digest were ligated with

linearized pZA-lac vector digested with Acc65I and BlpI to construct pBDO-12. To make plasmid pBDO-4, one fragment of vector from pBDO-1 plasmid, one fragment of *ycbC* from *B. subtilis*, two fragments of garD-1 and garD-2 from *E. coli*, and two more fragments from *P. putida KT2440*, were amplified using primer pairs of pZA-F/pZAAcc-R, KdaBS-F/KdaBS-R, GarD-F/GarD-Acc-R, GarD-Acc-F/GarD-R, udh-F/udh-Bsa-R, and udh-Bsa-F/udh-R, respectively. These six fragments were assembled by the golden gate method[130] to form plasmid pBDO-4. Four fragments of *BFD*, *kivd*, *ipdC* and *yqhD* were amplified from genomic DNA of *P. putida*, *L. lactis*, *S. typhimurium* and *E. coli*, respectively, by using primer pairs of BFDAcc-F/BFDSphI-R, KIVDAcc-F/KIVDSphI-R, IPDCAcc-F/IPDCSphI-R and YqhDSphI-F/YqhDXbaI-R, respectively. Kivd and yqhD were digested with Acc65I/SphI and SphI/XbaI, and then inserted into the corresponding site of pZElac to form plasmid pBDO-5. *Kivd* in pBDO-5 was replaced by *ipdC* and *BFD* to build plasmids, pBDO-6 and pBDO-7. Two fragments of *adhA* and *adh6* were amplified from *L. lactis* and *S. cerevisiae* genomic DNA, respectively by using primer pairs adhA-SphI-F/adhA-XbaI-R and Adh6-SphI-F/Adh6-XbaI-R, another two fragments of *yahK* and *yjgB* were amplified from *E. coli* genomic DNA with primer pairs of yahK-SphI-F/yahK-XbaI-R and yjgB-SphI-F/yjgB-XbaI-R. These four fragments were used to replace *yqhD* in plasmid pBDO-5 to make plasmids of pBDO-8, pBDO-9, pBDO-10 and pBDO-11.

Twenty Kivd mutant fragments of S286Y-1, S286Y-2, S286L-1, S286L-2, S286F-1, S286F-2, V461I-1, V461I-2, V461L-1, V461L-2, V461M-1, V461M-2, I465F-1, I465F-2, I465H-1, I465H-2, I465L-1, I465L-2, I465M-1 and I465M-2 were amplified from

plasmid pBDO-5 by using primer pairs of KIVDAcc-F/S286Y-R, S286Y-F/KIVDSphI-R, KIVDAcc-F/S286L-R, S286L-F/KIVDSphI-R, KIVDAcc-F/S286F-R, S286F-F/KIVDSphI-R, KIVDAcc-F/V461I-R, V461I-F/KIVDSphI-R, KIVDAcc-F/V461L-R, V461L-F/KIVDSphI-R, KIVDAcc-F/V461M-R, V461M-F/KIVDSphI-R, KIVDAcc-F/I465F-R, I465F-F/KIVDSphI-R, KIVDAcc-F/I465H-R, I465H-F/KIVDSphI-R, KIVDAcc-F/I465L-R, I465L-F/KIVDSphI-R, KIVDAcc-F/I465M-R and I465M-F/KIVDSphI-R, respectively. Ten fragments of S286Y, S286L, S286F, V461I, V461L, V461M, I465F, I465H, I465L and I465M amplified with primers KIVDAcc-F, KIVDSphI-R by using PCR templates of S286Y-1 and S286Y-2; S286L-1 and S286L-2; S286F-1, and S286F-2; V461I-1 and V461I-2; V461L-1 and V461L-2; V461M-1 and V461M-2; I465F-1 and I465F-2; I465H-1 and I465H-2; I465L-1 and I465L-2; and I465M-1 and I465M-2; replaced the wild type *kivd* of pBDO-5 to form plasmids of pBDO-13, pBDO-14, pBDO-15, pBDO-16, pBDO-17, pBDO-18, pBDO-19, pBDO-20, pBDO-21, and pBDO-22.

To construct the plasmid pBDO-23, the gene fragments of *DR64-8447, DR64-8448, DR64-8449 and DR64-8450* were amplified from *B. xenovorans* LB400 genomic DNA using primer pairs of DR64-8447-F/DR64-8447-R, DR64-8448-F/DR64-8448-R, DR64-8449-F/DR64-8449-R and DR64-8450-F/DR64-8450-R respectively. The fragments *DR64-8447, DR64-8448, DR64-8449* and *DR64-8450* were double-digested with enzymes Acc65I/NheI, NheI/HindIII, HindIII/NdeI and NdeI/BlpI respectively and these were ligated with linearized pZA-lac vector digested with Acc65I/BlpI to form the plasmid pBDO-23. To make the plasmid pBDO-24, the *DR64-8452* gene was PCR

amplified by oligos DR64-8452-F and DR64-8452-R using genomic DNA of *B. xenovorans* as template, and then this coding region was inserted into the site between Acc65I and XbaI of vector pZElac[23] after digestion. To construct the plasmid pBDO-25, the gene fragments of *Bamb4925, Bamb4923, Bamb4922* and *Bamb4918* were amplified from *B. ambifaria* genomic DNA using primer pairs of Bamb4925-Acc-F/Bamb4925-Nhe-R, Bamb4923-Nhe-F/Bamb4922-HindR, and Bamb4918-Hind-F/Bamb4918-Nde-R, respectively. The fragments *Bamb4925, Bamb4923-4922* and *Bamb4918* were double-digested with enzymes Acc65I/NheI, NheI/HindIII and HindIII/NdeI respectively and these were ligated with linearized pZA-lac vector digested with Acc65I/NdeI to form the plasmid pBDO-25. To make the plasmid pBDO-26, the *Bamb4915* gene was PCR amplified by oligos Bamb4915-Acc-F/Bamb4915-Xba-R using genomic DNA of *B. ambifaria* as template, and then this coding region was inserted into the site between Acc65I and XbaI of vector pZElac[23] after digestion. To construct the plasmid pBDO-27, the gene fragments of *BTH_II1632, BTH_II1630, BTH_II1629* and *BTH_II1625* were amplified from *B. thailandensis* genomic DNA using primer pairs of BTH1632-Acc-F/BTH1632-BamHR, BTH1630BamHF/BTH1629-Hind-R, and BTH1625-Hind-F/BTH1625-Blp-R respectively. The fragments *BTH_II1632, BTH_II1630-1629* and *BTH_II1625* were double-digested with enzymes Acc65I/BamHI, BamHI/HindIII and HindIII/BlpI respectively and these were ligated with linearized pZA-lac vector digested with Acc65I/BlpI to form the plasmid pBDO-27. To make the plasmid pBDO-28, the *BTH_II1631* gene was PCR amplified by oligos BTH1631-Acc-F/BTH1631-Xba-R

using genomic DNA of *B. thailandensis* as template, and then this coding region was inserted into the site between Acc65I and XbaI of vector pZElac[23] after digestion.

To characterize enzyme activities, hexahistidine (His6)-tagged xylB, xylD, xylX, araA, araC, araD, udh, garD, ycbC, DR64_8447, DR64_8449, and DR64_8450 were amplified from pBDO-1, pBDO-3, pBDO-4, and pBDO-23 using primers His-xylB-F and His-xylB-R; His-xylD-F and His-xylD-R; His-xylX-F and His-xylX-R; His-araA-F and His-araA-R; His-araC-F and His-araC-R; His-araD-F and His-araD-R; His-udh-F and His-udh-R; His-garD-F and His-garD-R; His-ycbC-F and His-ycbC-R; His-DR64_8447-F and His-DR64_8447-R; His-DR64_8449-F and His-DR64_8449-R; and His-DR64_8450-F and His-DR64_8450-R, respectively. These fragments were then ligated with the ColE1 *ori* backbone to create pBDO-29, pBDO-30, pBDO-31, pBDO-32, pBDO-33, pBDO-34, pBDO-35, pBDO-36, pBDO-37, pBDO-38, pBDO-39, and pBDO-40. All plasmids in this work were sequenced using appropriate primers to confirm sequence fidelity.

4.3 Growth assay

For the D-xylose, L-arabinose and D-galacturonate growth assays, the Δ*icd* strains (BDO04 for D-xylose, BDO06 for L-arabinose and BDO08 for galacturonate) were transformed with 2-ketoglutarate producing plasmids (pBDO-1 and pBDO-2 for *C. crescentus* D-xylose; pBDO-3 for *B. multivorans* L-arabinose; pBDO-2 and pBDO-4 for D-galacturonate, pBDO-23 and pBDO-24 for *B. xenovorans* D-xylose, pBDO-25 and pBDO-26 for *B. ambifaria* L-arabinose; and pBDO-27 and pBDO-28 for *B. thailandensis*

L-arabinose). Three freshly transformed colonies were inoculated overnight in 2 ml 2×YT containing appropriate antibiotics. The optical density (OD) of all strains were measured using a spectrophotometer at 600 nm and the cell densities were normalized before starting the assays. M9 minimal media containing 5 g/l of each carbon source (glucose and D-xylose/L-arabinose/D-galacturonate), appropriate antibiotics and 0.2 mM IPTG was used for all assays. Optical density was measured every few h using a spectrophotometer.

4.4 Protein expression and purification

His-tagged proteins were transformed into BL21 strain. The transformed cells were inoculated from an overnight pre-culture at 1/100 dilution and grown in 200 ml of 2×YT medium containing 100 mg/l ampicillin. When the OD_{600} reached 0.6, 0.5 mM IPTG was added to induce protein expression, followed by incubation at 30°C overnight. Then the cells were pelleted by centrifuging at 3,220 rcf for 15 minutes. The supernatants were discarded and the pellets were stored at -80 °C. All the following steps were carried out at 4 °C to prevent protein degradation. For lysis, the cell pellets were first thawed on ice-water mixture and re-suspended in 15 ml lysis buffer. The lysis buffer (pH=7.6) contained 50 mM Tris-HCl, 100 mM NaCl, 10 mM imidazole, 5% glycerol, 1 mM DTT. Cell lysis was performed by sonication using the Heat Systems Ultrasonics W-225 Sonicator in a continuous mode set at 50% duty cycle and output control 5. Each sample was sonicated for 6 cycles of one-minute sonication with intermittent one-minute cooling on ice-water mixture. The cell lysates were centrifuged at 10,733 rcf for 15

minutes. The supernatant was collected for purification. 4 ml of HisPur Ni-NTA resin solution (Thermo Scientific) was loaded in a column and the storage buffer was allowed to pass through by gravity to get a 2 ml final resin bed volume. The resin was equilibrated with 10 ml of lysis buffer and drained. The supernatant was then loaded in the column and allowed to pass through by gravity. The column was then washed twice with 10 ml of wash buffer (50 mM Tris-HCl, 100 mM NaCl, and 25mM imidazole, pH=7.6). The bound protein was eluted with 15 ml of elution buffer (pH=8.0) which contained 50 mM Tris-HCl, 250 mMNaCl, and 250 mM imidazole. The final protein sample was then buffer-exchanged using Amicon Ultra centrifugal filters (Millipore) with the storage buffer (50M Tris-HCl, 2mM $MgSO_4$, 20% glycerol, pH=8.0). The concentrated protein were aliquoted (50 µl) into PCR tubes, flash frozen with dry ice and ethanol mixture and stored at -80°C. Purified protein concentration was determined by Quick Start Bradford protein assay kit purchased from Bio-Rad Laboratories.

4.5 Enzymatic assays

D-Xylose dehydrogenase (XylB/DR64-8447), L-arabinose dehydrogenase (AraA), and uronate dehydrogenase (Udh): Enzyme activities of XylB/DR64-8447, AraA and Udh were assayed by monitoring initial NADH generation at 340 nm at 30 °C using D-xylose, L-arabinose, and D-galacturonate as substrates, respectively[120]. Kinetic assays were carried out using 0 to 10 mM D-xylose/L-arabinose/D-galacturonate and 1 mM NAD^+ in 100 mM Tris-HCl and 5 mM $MgCl_2$, pH 7.5. A series of enzymatic assays were

conducted to estimate the initial activity as a function of starting substrate concentration. This data was used to fit the parameters of the Michaelis-Menten kinetic model, k_{cat} and K_M, by nonlinear least-squares regression using the intrinsic *nlinfit* function of the Matlab software program. Kinetic constants (k_{cat}/K_M) for following enzymes were calculated with the same method.

Xylonate dehydratase (XylD/DR64-8449), L-arabonate dehydratase (AraC), and D-galactarate dehydratase (GarD): Enzymatic activities of the three dehydratases were assayed according to a modified procedure of MacGee and Doudoroff using the semicarbazide method[131]. Kinetic assays were carried out using 100 nM of D-xylonate dehydratase/L-arabonate dehydratase/D-galactarate dehydratase in 100 mM Tris-HCl and 5 mM $MgSO_4$, pH 7.5. The reaction was initiated by the addition of D-xylonate/L-arabonate/D-galactarate and stopped after 0, 1, 2, 3, 5, and 10 min with 2% (v/v) trifluoroacetic acid. The samples were then mixed with 100 μl of 0.1 M semicarbazide hydrochloride (containing 1.5% sodium acetate trihydrate) and incubated at room temperature for 30 min. Finally, the 2-ketoacids produced were quantified by detection of their semicarbazone absorbance at 250 nm.

2-Keto-3-deoxy-D-xylonate dehydratase (XylX/DR64-8450), 2-keto-3-deoxy-L-arabonate dehydratase (AraD), and 5-keto-4-deoxy-D-glucarate dehydratase (YcbC): Enzymatic activities of XylX, DR64-8450, AraD, and YcbC were assayed spectrophotometrically in a coupled assay with the corresponding previous dehydratase and 2-ketoglutaric semialdehyde dehydrogenase (KGSADH)[131]. The assay was performed in 100 mM Tris-HCl buffer (pH=7.5) with 5mM $MgSO_4$ containing 0-20 mM

D-xylonate/L-arabonate/D-galactarate and 1mM NAD^+. After the addition of 100 nM D-xylonate dehydratase (XylD/DR64-8449)/L-arabonate dehydratase (AraC)/D-galactarate dehydratase (GarD) and 100 nM of the KGSADH, the mixture was incubated at 25 °C for 15 min. No change in absorbance at 340 nm was observed in this stage. The reaction was initiated by the addition of an appropriate amount of 2-keto-3-deoxy-D-xylonate dehydratase (XylX/DR64-8450)/2-keto-3-deoxy-L-arabonate dehydratase (AraD)/5-keto-4-deoxy-D-glucarate dehydratase (YcbC), and the increasing absorbance at 340 nm caused by NADH produced in the reaction was monitored.

2-Ketoacid decarboxylase (Kivd) and alcohol dehydrogenase (YqhD): The decarboxylase activity of Kivd was measured by a coupled enzymatic assay with AraC, AraD, and YqhD[132]. Excess AraC, AraD, and YqhD was used and the oxidation of NADPH was monitored at 340 nm. The assay mixture contained 1 mM NADPH, 1 μM AraC, 1 μM AraD, and 100 nM YqhD and 0.1-10 mM L-arabonate in assay buffer (100 mM Tris-HCl buffer, pH=7.5, 5 mM $MgSO_4$, 0.5 mM ThDP) with a total volume of 0.1 ml. The mixture was incubated at 30 °C for 1 h and 10 nM Kivd was added. The dehydrogenase activity of YqhD was assayed according to NADPH initial consumption rates in a coupled assay. The assay mixture contained 1mM NADPH, 100 nM Kivd, 1 μM AraC, 1 μM AraD, and 0.1-10 mM L-arabonate in 100 μl of 100 mM Tris-HCl buffer (pH=7.5) with 5 mM $MgSO_4$. The mixture was first incubated at 30 °C for 1 h. Afterwards, 10 nM YqhD was added and the NADPH consumption rate was monitored.

4.6 Shake flask batch fermentation

125 ml conical flasks with 0.2 g $CaCO_3$ were autoclaved and dried to perform all small-scale fermentations. The flasks were filled with 5 ml M9 medium supplemented with 5 g/l yeast extract, 20 g/l glucose, 20 g/l D-xylose/L-arabinose/D-galacturonate and the corresponding antibiotics. 200 μl of overnight cultures incubated in 2×YT medium were transferred into the flasks and placed in a shaker at a speed of 250 rpm. After adding 0.1 mM isopropyl-β-D-thiogalactoside (IPTG), the flasks were screw-capped and sealed by parafilm and the fermentation was performed for 48 h at 30 °C. The fermentation products were measured by HPLC.

4.7 Fed-batch fermentation in bioreactors

Fermentation media for bioreactor cultures contained the following composition, in grams per liter: glucose, 10; yeast extract, 10; K_2HPO_4, 7.5; citric acid monohydrate, 2.0; $MgSO_4 \cdot 7H_2O$, 2.0, ferric ammonium citrate, 0.3; thiamine hydrochloride, 0.008; D-(+)-biotin, 0.008; nicotinic acid, 0.008; pyridoxine, 0.032; ampicillin, 0.1; kanamycin, 0.05; spectinomycin, 0.1 (for BDO and MEV co-production only); 95—98% H_2SO_4, 0.8 mL; and 1 ml trace metal solution. Trace metal solution contained, in grams per liter: NaCl, 10; citric acid, 40; $ZnSO_4 \cdot 7H_2O$, 1.0; $MnSO_4 \cdot H_2O$, 30; $CuSO_4 \cdot 5H_2O$, 0.1; H_3BO_3, 0.1; $Na_2MoO_4 \cdot 2H_2O$, 0.1; $FeSO_4 \cdot 7H_2O$, 1.0; $CoCl_2 \cdot 6H_2O$, 1.0. The feed solution contained, in grams per liter: glucose, 600; K_2HPO_4, 7.4; antifoam, 10 ml.

Fermentation experiments were performed in 1.3-l Bioflo 115 Bioreactors (Eppendorf) using an initial working volume of 0.5 l. The bioreactor was inoculated with

10% of overnight pre-culture with 2×YT medium. The culture condition was set at 37 °C, 20% dissolved oxygen level (DO), and pH 6.8. After OD_{600} reached 6.0, 0.2 mM IPTG and 20 g/l D-xylose/L-arabinose/D-galacturonate was added. Temperature was changed to 30 °C and DO was set to 10%. The pH was controlled at 6.8 by automatic addition of 26% ammonium hydroxide solution. Air flow rate was maintained at 1 vvm during the whole process and DO was controlled by the agitation rate (from 300 to 800 rpm). The feeding rate of glucose was manually adjusted according to the glucose consumption rate of cells to meet metabolic balance. D-Xylose, L-arabinose, or D-galacturonate was added in batches. Fermentation culture was sampled every few h to determine cell density and production level.

4.8 Metabolite analysis

Fermentation products were analyzed using an Agilent 1260 Infinity HPLC equipped with an Aminex HPX87H column and a refractive-index detector (RID). The mobile phase was 0.01 N H_2SO_4 with a flow rate of 0.6 ml/min. The column temperature and RID temperature were 35 °C and 50 °C, respectively.

5. Supporting Information

Table 3.S1| Strains and plasmids used in this study.

Name	Relevant genotype	Reference
Strains		
BW25113	*rrnB*$_{T14}$ ΔlacZ$_{WJ16}$*hsdR514* Δ*araBAD*$_{AH33}$ Δ*rhaBAD*$_{LD78}$	[70]
XL10-Gold	Tet^{R}Δ (*mcrA*)183 Δ (*mcrCB-hsaSMR-mrr*)173 *endA1supE*44 *thi-1 recA1*	Stratagene
BL21	*E. coli* B F- *dcmomptThsdS*(r_B- m_B-) gal [malB$^+$]$_{K-12}$(λ^S)	[71]
BDO01	BW25113 Δ*xylA*	This work
BDO02	BW25113 Δ*xylA*Δ*yjhH*	This work
BDO03	BW25113 Δ*xylA*Δ*yjhH*Δ*yagE*	This work
BDO04	BW25113 Δ*xylA*Δ*yjhH*Δ*yagE*Δ*icd*	This work
BDO05	BW25113	[70]
BDO06	BW25113 Δ*icd*	This work
BDO07	BW25113 Δ*garL*Δ*uxaC*	This work
BDO08	BW25113 Δ*garL*Δ*uxaC*Δ*icd*	This work
Plasmids		
pBDO-1	P15A origin,Kan^R, P$_L$*lacO*$_1$: *xylB-xylC-xylD-xylX*	This work
pBDO-2	ColE1 origin, Amp^R, P$_L$*lacO*$_1$:*xylA*(CC)	This work
pBDO-3	P15A origin, Kan^R, P$_L$*lacO*$_1$:*araC-araD-araA-araB-araE*	This work
pBDO-4	P15A origin, Kan^R, P$_L$*lacO*$_1$:*udh-garD-ycbC*	This work
pBDO-5	ColE1 origin, Amp^R, P$_L$*lacO*$_1$: *kivd -yqhD*	This work
pBDO-6	ColE1 origin, Amp^R, P$_L$*lacO*$_1$: *ipdC -yqhD*	This work
pBDO-7	ColE1 origin, Amp^R, P$_L$*lacO*$_1$: *BFD-yqhD*	This work
pBDO-8	ColE1 origin, Amp^R, P$_L$*lacO*$_1$:*kivd-adhA*	This work
pBDO-9	ColE1 origin, Amp^R, P$_L$*lacO*$_1$:*kivd-adh6*	This work
pBDO-10	ColE1 origin, Amp^R, P$_L$*lacO*$_1$:*kivd-yahK*	This work
pBDO-11	ColE1 origin, Amp^R, P$_L$*lacO*$_1$:*kivd-yjgB*	This work
pBDO-12	P15A origin, Kan^R, P$_L$*lacO*$_1$:*araC-araD-araA-araB*	This work
pBDO-13	ColE1 origin, Amp^R, P$_L$*lacO*$_1$:*kivd(S286Y)-yqhD*	This work
pBDO-14	ColE1 origin, Amp^R, P$_L$*lacO*$_1$:*kivd(S286L)-yqhD*	This work
pBDO-15	ColE1 origin, Amp^R, P$_L$*lacO*$_1$:*kivd(S286F)-yqhD*	This work
pBDO-16	ColE1 origin, Amp^R, P$_L$*lacO*$_1$:*kivd(V461I)-yqhD*	This work
pBDO-17	ColE1 origin, Amp^R, P$_L$*lacO*$_1$:*kivd(V461L)-yqhD*	This work
pBDO-18	ColE1 origin, Amp^R, P$_L$*lacO*$_1$:*kivd(V461M)-yqhD*	This work
pBDO-19	ColE1 origin, Amp^R, P$_L$*lacO*$_1$:*kivd(I465F)-yqhD*	This work
pBDO-20	ColE1 origin, Amp^R, P$_L$*lacO*$_1$:*kivd(I465H)-yqhD*	This work
pBDO-21	ColE1 origin, Amp^R, P$_L$*lacO*$_1$:*kivd(I465L)-yqhD*	This work
pBDO-22	ColE1 origin, Amp^R, P$_L$*lacO*$_1$:*kivd(I465M)-yqhD*	This work
pBDO-23	P15A origin,Kan^R, P$_L$*lacO*$_1$: *DR64_8447-8448-8449-8450*	This work
pBDO-24	ColE1 origin, Amp^R, P$_L$*lacO*$_1$: *DR64_8452*	This work
pBDO-25	P15A origin,Kan^R, P$_L$*lacO*$_1$: *Bamb_4925-4923-4922-4918*	This work

pBDO-26	ColE1 origin, Amp^R, P_L*lacO*$_1$: *Bamb_4915*	This work
pBDO-27	P15A origin,Kan^R, P_L*lacO*$_1$: *BTH_II1632-1630-1629-1625*	This work
pBDO-28	ColE1 origin, Amp^R, P_L*lacO*$_1$: *BTH_II1631*	This work
pBDO-29	ColE1 origin, Amp^R, P_L*lacO*$_1$: 6xhis-xylB	This work
pBDO-30	ColE1 origin, Amp^R, P_L*lacO*$_1$: 6xhis-xylD	This work
pBDO-31	ColE1 origin, Amp^R, P_L*lacO*$_1$: 6xhis-xylX	This work
pBDO-32	ColE1 origin, Amp^R, P_L*lacO*$_1$: 6xhis-araA	This work
pBDO-33	ColE1 origin, Amp^R, P_L*lacO*$_1$: 6xhis-araC	This work
pBDO-34	ColE1 origin, Amp^R, P_L*lacO*$_1$: 6xhis-araD	This work
pBDO-35	ColE1 origin, Amp^R, P_L*lacO*$_1$: 6xhis-udh	This work
pBDO-36	ColE1 origin, Amp^R, P_L*lacO*$_1$: 6xhis-garD	This work
pBDO-37	ColE1 origin, Amp^R, P_L*lacO*$_1$: 6xhis-ycbC	This work
pBDO-38	ColE1 origin, Amp^R, P_L*lacO*$_1$: 6xhis-DR64_8447	This work
pBDO-39	ColE1 origin, Amp^R, P_L*lacO*$_1$: 6xhis- DR64_8449	This work
pBDO-40	ColE1 origin, Amp^R, P_L*lacO*$_1$: 6xhis- DR64_8450	This work
pMEV-1	pUC origin, $Spec^R$, P_L*lacO*$_1$: *atoB-mvaS-mvaE*	127

Table 3.S2| *In vitro* enzymatic activities of *B. xenovorans* and *C. crescentus* D-xylose operons

Enzyme name	*B. xenovorans*			*C. crescentus*		
	K_m (mM)	k_{cat} (s^{-1})	k_{cat}/K_m (s^{-1} mM^{-1})	K_m (mM)	k_{cat} (s^{-1})	k_{cat}/K_m (s^{-1} mM^{-1})
D-xylose dehydrogenase	1.97±0.12	49.9±4.2	25.3	0.85±0.08	12.1±2.2	14
D-xylonate dehydratase	1.52±0.08	1.73±0.3	1.14	1.18±0.05	7.6±1.1	6.4
2-keto-3-deoxy-D-xylonate dehydratase[a]	8.96±0.2	4.72±0.5	0.53	1.9±0.08	0.53±0.1	0.26

[a] Enzyme activity was determined using a coupled assay

Table 3.S3| Primers used in this study

xylBAcc-F	GGGCCC GGTACC ATGTCCTCAGCCATCTATCCCAGCCT
xylBBamHI-R	GGGCCCGGATCC TTAACGCCAGCCGGCGTCGATCCAGT
xylCBamHI-F	GGGCCC GGATCC AGGAGAAATTAACTATGACCGCTCAAGTCACTTGCGT ATG

xylCNhe-R	GGGCCC GCTAGC TTAGACAAGGCGGACCTCATGCTGGG
xylDNheI-F	GGGCCC GCTAGC AGGAGAAATTAACTATGAGGTCCGCCTTGTCTAACCG CAC
xylDHind-R	GGGCCC AAGCTT TTAGTGGTTGTGGCGGGGCAGCTTGG
xylXHind-F	GGGCCC AAGCTT AGGAGAAATTAACTATGGTTTGTCGGCGGCTTCTAGC ATG
xylXBlpRem-R	GCGCAGCTGGCGTTGTTGTCCTTGGCCTTTCTGAGCA GCAGGGCCGAACGACCTTCGAA
xylXBlpRem-F	TTCGAAGGTCGTTCGGCCCTGCTGCTCAGAAAGGCCA AGGACAACAACGCCAGCTGCGC
xylXBlpI-R	GGGCCC GCTCAGC TTAGAGGAGGCCGCGGCCGGCCAGGT
CC0822Acc-F	GGGCCC GGTACC ATGACCGACACCCTGCGCCATTACAT
CC0822Xba-R	GGGCCC TCTAGA TTACGACCACGAGTAGGAGGTTTTGG
BFDAcc-F	GGGCCC GGTACC ATGGCTTCGGTACACGGCACCACATA
BFDSphI-R	GGGCCC GCATGC TTACTTCACCGGGCTTACGGTGCTTA
KIVDAcc-F	GGGCCC GGTACC ATGTATACAGTAGGAGATTACCTATT
KIVDSphI-R	GGGCCC GCATGC TTATGATTTATTTTGTTCAGCAAATA
IPDCAcc-F	GGGCCC GGTACC ATGCAAAACCCCTATACCGTGGCCGA
IPDCSphI-R	GGGCCC GCATGC TTATCCCCCGTTGCGGGCTTCCAGCG
YqhDSphI-F	GGGCCC GCATGC AGGAGAAATTAACTATGAACAACTTTAATCTGCACACC CC
YqhDXbaI-R	GGGCCC TCTAGA TTAGCGGGCGGCTTCGTATATACGGC
Adh6-SphI-F	GGGCCC GCATGC AGGAGATATACCATGTCTTATCCTGAGAAATTTGAAG

	G
Adh6-XbaI-R	GGGCCC TCTAGA CTAGTCTGAAAATTCTTTGTCGTAGC
yahK-SphI-F	GGGCCC GCATGC AAGGAGATATACC ATGAAGATCAAAGCTGTTGGTGCATA
yahK-XbaI-R	GGGCCC TCTAGA TTAGTCTGTTAGTGTGCGATTATCGA
yjgB-SphI-F	GGGCCC GCATGC AAGGAGATATACC ATGTCGATGATAAAAAGCTATGCCGC
yjgB-XbaI-R	GGGCCC TCTAGA TTAAAAATCGGCTTTCAACACCACGC
adhA-SphI-F	GGGCCC GCATGC AAGGAGATATACC ATGAAAGCAGCAGTAGTAAGACACAA
adhA-XbaI-R	GGGCCC TCTAGA TTATTTAGTAAAATCAATGACCATTC
pZAAcc-R	GGGCCC GGTCTCA ATAG TTTCTCCTCTTTAATGAATTCGGTCA
KdaBS-F	GGGCCC GGTCTCA CTAT GGTACC ATGAGCCGTATCAGAAAAGCACCCGC
KdaBS-R	GGGCCC GGTCTCA TTAC TTAAACCGTCGCGGCTTTTTTCGGAA
GarD-F	GGGCCC GGTCTCA GTAA GCTAGC AGGAGAAATTAACTATGGCCAACATCGAAATCAGACA
GarD-Acc-R	GGGCCC GGTCTCA ACCG CCATCAGGCCGTACGGCGTACC
GarD-Acc-F	GGGCCC GGTCTCA CGGT GCCCGTCATTAAAATGGCAACCCG
GarD-R	GGGCCC GGTCTCA CAGG TTAGGTCACCGGTGCCGGGTTAAACA
udh-F	GGGCCC GGTCTCA CCTG AAGCTT AGGAGAAATTAACTATGACCACTACCCCCTTCAATCG
udh-Bsa-R	GGGCCC GGTCTCA TGTC TCGATGCCGTAGCGGTCAAAGTAG
udh-Bsa-F	GGGCCC GGTCTCA GACA GTCAGCATTCGCATCGGCTCGTCG
udh-R	GGGCCC GGTCTCA GCGG TTAGTTGAACGGGCCGGCCACGGCGA
pZA-F	GGGCCC GGTCTCA CCGC GCTGAGCTCTAGAGGCATCAAATAAAACGAAAG
KivdS286Y-R	TTTAAATGATGAGTGAAGGCTCCTGTTGAGTAGTCTG TGAGTTTAACTCCAAGCATCA
KivdS286Y-F	TGATGCTTGGAGTTAAACTCACAGACTACTCAACAGG

	AGCCTTCACTCATCATTTAAA
KivdS286L-R	TAAATGATGAGTGAAGGCTCCTGTTGAGAGGTCTGT GAGTTTAACTCCAAGCATCAGG
KivdS286L-F	CCTGATGCTTGGAGTTAAACTCACAGACCTCTCAACAG GAGCCTTCACTCATCATTTA
KivdS286F-R	TTAAATGATGAGTGAAGGCTCCTGTTGAGAAGTCTGT GAGTTTAACTCCAAGCATCAG
KivdS286F-F	CTGATGCTTGGAGTTAAACTCACAGACTTCTCAACAG GAGCCTTCACTCATCATTTAA
KivdV461I-R	TTGATTTGGTCCATGAATTTCTCTTTCGATTGTATAAC CATCATTATTGATAATAAAGC
KivdV461I-F	GCTTTATTATCAATAATGATGGTTATACAATCGAAAGA GAAATTCATGGACCAAATCAA
KivdV461L-R	TTGATTTGGTCCATGAATTTCTCTTTCGAGTGTATAAC CATCATTATTGATAATAAAGC
KivdV461L-F	GCTTTATTATCAATAATGATGGTTATACACTCGAAAGA GAAATTCATGGACCAAATCAA
KivdV461M-R	TGATTTGGTCCATGAATTTCTCTTTCCATTGTATAACC ATCATTATTGATAATAA
KivdV461M-F	TTATTATCAATAATGATGGTTATACAATGGAAAGAGA AATTCATGGACCAAATCA
KivdI465F-R	TCATTGTAGCTTTGATTTGGTCCATGGAATTCTCTTTC GACTGTATAACCATCAT
KivdI465F-F	ATGATGGTTATACAGTCGAAAGAGAATTCCATGGACC AAATCAAAGCTACAATGA
KivdI465H-R	TCATTGTAGCTTTGATTTGGTCCATGGTGTTCTCTTTC GACTGTATAACCATCAT
KivdI465H-F	ATGATGGTTATACAGTCGAAAGAGAACACCATGGACC AAATCAAAGCTACAATGA
KivdI465L-R	TCATTGTAGCTTTGATTTGGTCCATGCAGTTCTCTTTC GACTGTATAACCATCAT
KivdI465L-F	ATGATGGTTATACAGTCGAAAGAGAACTGCATGGACC AAATCAAAGCTACAATGA
KivdI465M-R	TCATTGTAGCTTTGATTTGGTCCATGCATTTCTCTTTC GACTGTATAACCATCAT
KivdI465M-F	ATGATGGTTATACAGTCGAAAGAGAAATGCATGGACC AAATCAAAGCTACAATGA
Kivd-BamHI-R	GGGCCC GGATCC ATGTATACAGTAGGAGATTACCTATT
Kivd-Xba-R	GGGCCC TCTAGA TTATGATTTATTTTGTTCAGCAAATA
YqhD-BamHI-R	GGGCCC GGATCC

	ATGAACAACTTTAATCTGCACACCCC
YqhD-XbaI-R	GGGCCC TCTAGA TTAGCGGGCGGCTTCGTATATACGGC
XylA-BamHI-F	GGGCCC GGATCC ATGACCGACACCCTGCGCCATTACAT
XylA-XbaI-R	GGGCCC TCTAGA TTACGACCACGAGTAGGAGGTTTTGG
XylX-BamHI-F	GGGCCC GGATCC ATGGTTTGTCGGCGGCTTCTAGCATG
XylX-XbaI-R	GGGCCC TCTAGA TTAGAGGAGGCCGCGGCCGGCCAGGT
AraC-Acc65I-F	CCGAATTCATTAAAGAGGAGAAAGGTACCATGTCGGC AACGAAACCCAGGCTGCGCTCC
AraC-NheI-R	GATCCTGCGTCAGTCAAACGGCGGGCTAGCTCAGTGC GAGTGGCTCGGCACCTCCGCGCC
AraD-NheI-F	GAGGTGCCGAGCCACTCGCACTGAGCTAGCCCGCCGT TTGACTGACGCAGGATCCGAACC
AraD-remBlpI-R	GGCTCATCGTGCGCTCCTTGGTTCGTTGCTCACCGTG CCCAGCGCAGCACGAGCGGATCG
AraD-remBlpI-F	CGATCCGCTCGTGCTGCGCTGGGCACGGTGAGCAAC GAACCAAGGAGCGCACGATGAGCC
AraA-HindIII-R	TCGATGCTCAGGCGGCGCGCACGCAAGCTTTCAGCGG CCGAACGCTTCGGTGTCGACGCG
AraA-HindIII-F	GACACCGAAGCGTTCGGCCGCTGAAAGCTTGCGTGC GCGCCGCCTGAGCATCGATTATCG
AraB-NdeI-R	TTGCGCCGCGTCGCCGCCATATGTCAGGTTCCGACGC CGCGCTTCAGTGCGAATCGCGCG
AraB-NdeI-F	CTGAAGCGCGGCGTCGGAACCTGACATATGGCGGCG ACGCGGCGCAACCCGACCTGGGCC
AraE-BlpI-R	TCGTTTTATTTGATGCCTCTAGAGCTCAGCTCAGATCG GGTAATGCCGCGGCGCGGTCTG
AraB-BlpI-R	CCAGGTCGGGTTGCGCCGCGTCGCCGCGCTCAGCTCA GGTTCCGACGCCGCGCTTCAGTG
His-xylB-F	GGGCCCGGATCCATGTCCTCAGCCATCTATCCCAGCCT
His-xylB-R	GGGCCCTCTAGATTAACGCCAGCCGGCGTCGATCCAG T
His-xylD-F	GAGAGGATCGCATCACCATCACCATCACGGATCCATG AGGTCCGCCTTGTCTAACCGCAC
His-xylD-R	GACTGAGCCTTTCGTTTTATTTGATGCCTCTAGATTAG TGGTTGTGGCGGGGCAGCTTGG
His-xylX-F	GGGCCCGGATCCATGGTTTGTCGGCGGCTTCTAGCAT G

His-xylX-R	GGGCCCTCTAGATTAGAGGAGGCCGCGGCCGGCCAG GT
His-udh-F	GGGCCCGGATCCATGACCACTACCCCCTTCAATCGCCT
His-udh-R	GGGCCCTCTAGATTAGTTGAACGGGCCGGCCACGGC GA
His-garD-F	GGGCCCGGATCCATGGCCAACATCGAAATCAGACAAG A
His-garD-R	GGGCCCTCTAGATTAGGTCACCGGTGCCGGGTTAAAC A
His-ycbC-F	GGGCCCGGATCCATGAGCCGTATCAGAAAAGCACCCG C
His-ycbC-R	GGGCCCTCTAGATTAAACCGTCGCGGCTTTTTTCGGA A
His-araA-F	GGATCGCATCACCATCACCATCACGGATCCATGAGCC AAGTCGTTTCGCTGGGTGTCGTC
His-araA-R	GAGCCTTTCGTTTTATTTGATGCCTCTAGATTAGCGGC CGAACGCTTCGGTGTCGACGCG
His-araC-F	GGATCGCATCACCATCACCATCACGGATCCATGTCGG CAACGAAACCCAGGCTGCGCTCC
His-araC-R	GAGCCTTTCGTTTTATTTGATGCCTCTAGATTAGTGCG AGTGGCTCGGCACCTCCGCGCC
His-araD-F	GGATCGCATCACCATCACCATCACGGATCCATGACATC GAGCCGTACGCCGCGTTACCGC
His-araD-R	GAGCCTTTCGTTTTATTTGATGCCTCTAGATTAGCGTG CCCAGCGCAGCACGAGCGGATC
DR64-8447-F	AATTCATTAAAGAGGAGAAAGGTACCATGTCGTACGC AATCTATCCCAGCCT
DR64-8447-R	ACAGGGGGATGAATTTTCATAGTTAATTTCTCCTGGA TCCTTATTCTCCGTACCACCCGG
DR64-8448-F	CCGGGTGGTACGGAGAATAAGGATCCAGGAGAAATT AACTATGAAAATTCATCCCCCTGT
DR64-8448-R	CGCGGTGTGGATGCTGACATAGTTAATTTCTCCTGCT AGCTTATTGCGCGAAGCCCCATT
DR64-8449-F	AATGGGGCTTCGCGCAATAAGCTAGCAGGAGAAATTA ACTATGTCAGCATCCACACCGCG
DR64-8449-R	GATGGAGAAGTTGCGGACATAGTTAATTTCTCCTAAG CTTTTAGTGCGAATGCCTCGGAT
DR64-8450-F	ATCCGAGGCATTCGCACTAAAAGCTTAGGAGAAATTA ACTATGTCCGCAACTTCTCCATC
DR64-8450-R	CGTTTTATTTGATGCCTCTAGACATATGTTAGGCCGAC GCAAGCAGCCCGCGTGCG
DR64-8452-F	TTAAAGAGGAGAAAGGTACCATGAGCCAGTTTGCGA

	ACTA
DR64-8452-R	TTTTATTTGATGCCTCTAGATTAAACCGCGCCCGGACTCA
HisDR64-8447-F	GCATCACCATCACCATCACGGATCCATGTCGTACGCAATCTATCCCAGCC
HisDR64-8447-R	TTTCGTTTTATTTGATGCCTCTAGATTATTCTCCGTACCACCCGGCGTCG
HisDR64-8449-F	GCATCACCATCACCATCACGGATCCATGTCAGCATCCACACCGCGCCGGC
HisDR64-8449-R	TTTCGTTTTATTTGATGCCTCTAGATTAGTGCGAATGCCTCGGATTGCCG
HisDR64-8450-F	GCATCACCATCACCATCACGGATCCATGTCCGCAACTTCTCCATCCAGTT
HisDR64-8450-R	TTTCGTTTTATTTGATGCCTCTAGATTAGGCCGACGCAAGCAGCCCGCGT
Bamb4925-Acc-F	ACTGACCGAATTCATTAAAGAGGAGAAAGGTACCATGTCGGCAACAAAACCCAGGCTGCG
Bamb4925-Nhe-R	CTGCTCGATGTCATAGTTAATTTCTCCTGCTAGCTCAATGCGAATGGCTCGGCACGTCCG
Bamb4923-Nhe-F	GCCATTCGCATTGAGCTAGCAGGAGAAATTAACTATGACATCGAGCAGCACACCGCGCTA
Bamb4922-Hind-R	CAATCTGTTGCATGGGTTTTTTCTCCTGAAGCTTTCAGCGGCCGAACGCGTCGGTCCCGA
Bamb4918-Hind-F	GTTCGGCCGCTGAAAGCTTCAGGAGAAAAAACCCATGCAACAGATTGATCCGGCCGCGTC
Bamb4918-Nde-R	TCGTTTTATTTGATGCCTCTAGAGCTCACATATGTCAGCCGCGCGGCGCGCCCATGAATC
Bamb4915-Acc-F	ACTGACCGAATTCATTAAAGAGGAGAAAGGTACCATGACCGACAGACGGATGCTGATCGC
Bamb4915-Xba-R	GACTGAGCCTTTCGTTTTATTTGATGCCTCTAGATCATATCGGGTAATGCCGCGGCGTGG
BTH1632-Acc-F	ACCGAATTCATTAAAGAGGAGAAACCACGGTACCATGTCGGCATCGAAACCCAAGCTGCG
BTH1632-BamHR	GGCTCGTATTCATGGGTTTTTTCTCCTGGGATCCTCAGTGCGAATGCCGCGGCACCGCGG
BTH1630-BamHF	GCATTCGCACTGAGGATCCCAGGAGAAAAAACCCATGAATACGAGCCGTTCGCCGCGCTA
BTH1629-Hind-R	TTCGATGATTCCATAGTTAATTTCTCCTAAGCTTTCAGCGCTGAAACGGGTCGGCCGCGA
BTH1625-Hind-F	CGTTTCAGCGCTGAAAGCTTAGGAGAAATTAACTATGGAATCATCGAATCGGCCGGCGCG
BTH1625-Blp-R	GTTTTATTTGATGCCTCTAGAGCTCAGCCATATGTCAC

	GCGTTGCGCGCGAGCGCGAACC
BTH1631-Acc-F	ACTGACCGAATTCATTAAAGAGGAGAAAGGTACCATG AACGGGCCCACGGGCGAACTCCT
BTH1631-Xba-R	GACTGAGCCTTTCGTTTTATTTGATGCCTCTAGATCAC GTTCGCGCACCCGCGCTCGCCT

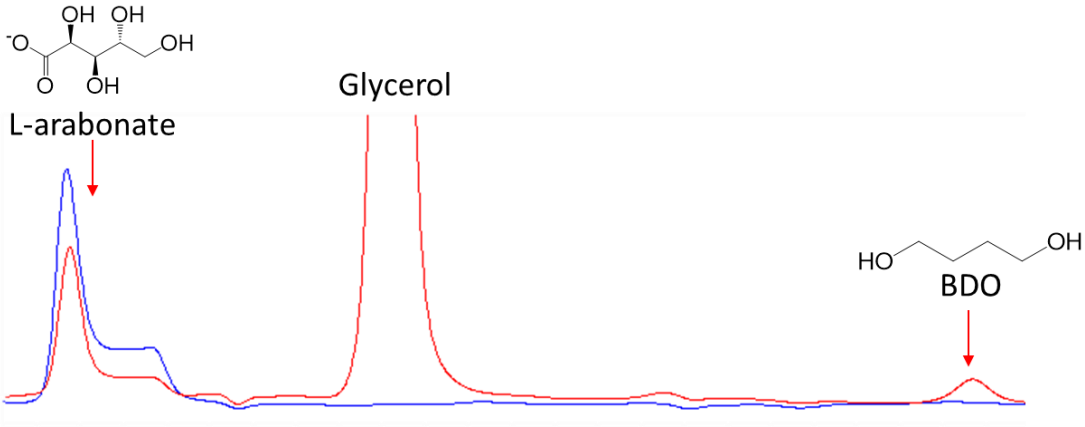

Fig. 3.S1| HPLC peak of *in vitro* BDO production using purified enzymes. Reaction was carried out in 100 mM Tris-HCl buffer (pH ~ 7.5) with 5 mM MgSO4 using 5 mM L-arabonate, 1 μM purified L-arabonate dehydratase (AraC), 1 μM purified L-KDA dehydratase (AraD), 1 μM purified Kivd, 1 μM purified YqhD, 5 mM thiamine diphosphate (ThDP) and 1 mM NADPH as co-factor. This reaction mixture was allowed to stand at room temperature for 30 mins and HPLC was performed on the resulting mixture. HPLC results showed that 2.5 mM L-arabonate was consumed and 1.7 mM BDO was produced after a half h. This validates the *in vitro* functionality of our proposed BDO pathway.

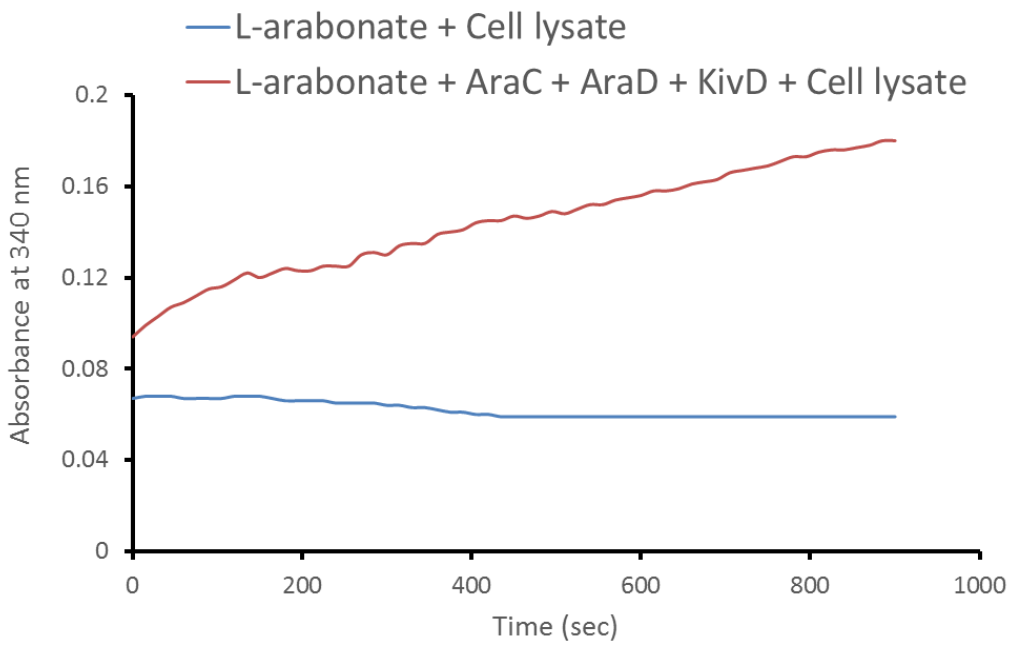

Fig. 3.S2| Butanedial oxidation by endogenous *E. coli* enzymes. In vitro enzyme assay was performed using cell extract. The reaction was carried out in 100 mM Tris-HCl buffer (pH ~ 7.5) with 5 mM MgSO4 containing 1 μM L-arabonate dehydratase (AraC), 1 μM L-KDA dehydratase (AraD), 1 μM Kivd with 5 mM thiamine diphosphate (ThDP) and 1mM NAD+ as co-factor. The reaction was initiated by adding 1 mM L-arabonate and 0.1 mg/ml of cell lysate and the absorbance was immediately measured at 340 nm using a spectrophotometer. A steady rise in absorbance was observed at 340 nm indicating oxidation of butanedial using NAD^+ by endogenous *E. coli* enzymes. A reaction mixture containing 1 mM L-arabonate, 0.1 mg/ml cell lysate and 1mM NAD^+ without purified AraC, AraD and Kivd was used as negative control. This sample did not show any increase in absorbance at 340 nm.

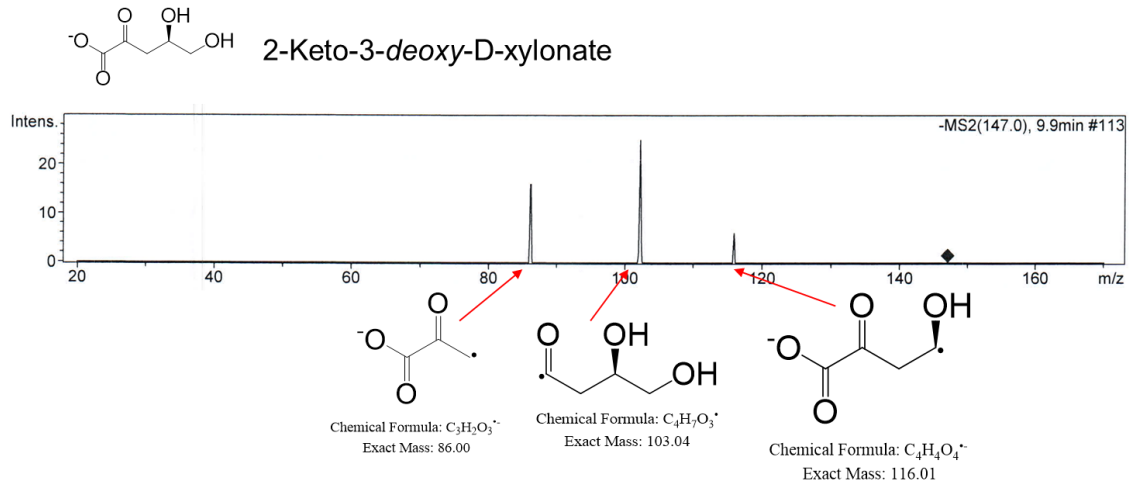

Fig. 3.S3| LC-MS data for 2-keto-3-deoxy-D-xylonate

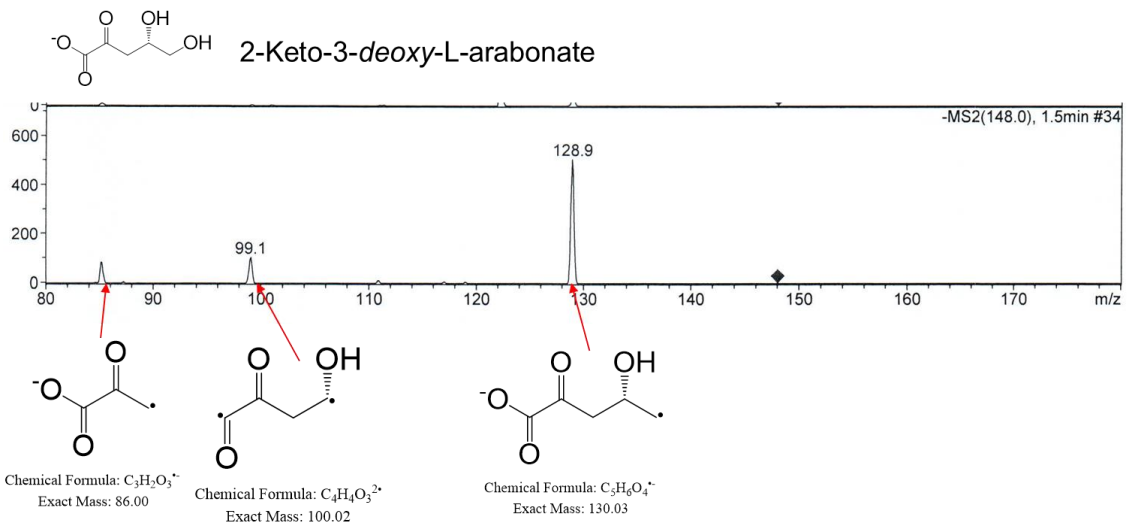

Fig. 3.S4| LC-MS data for 2-keto-3-deoxy-L-arabonate

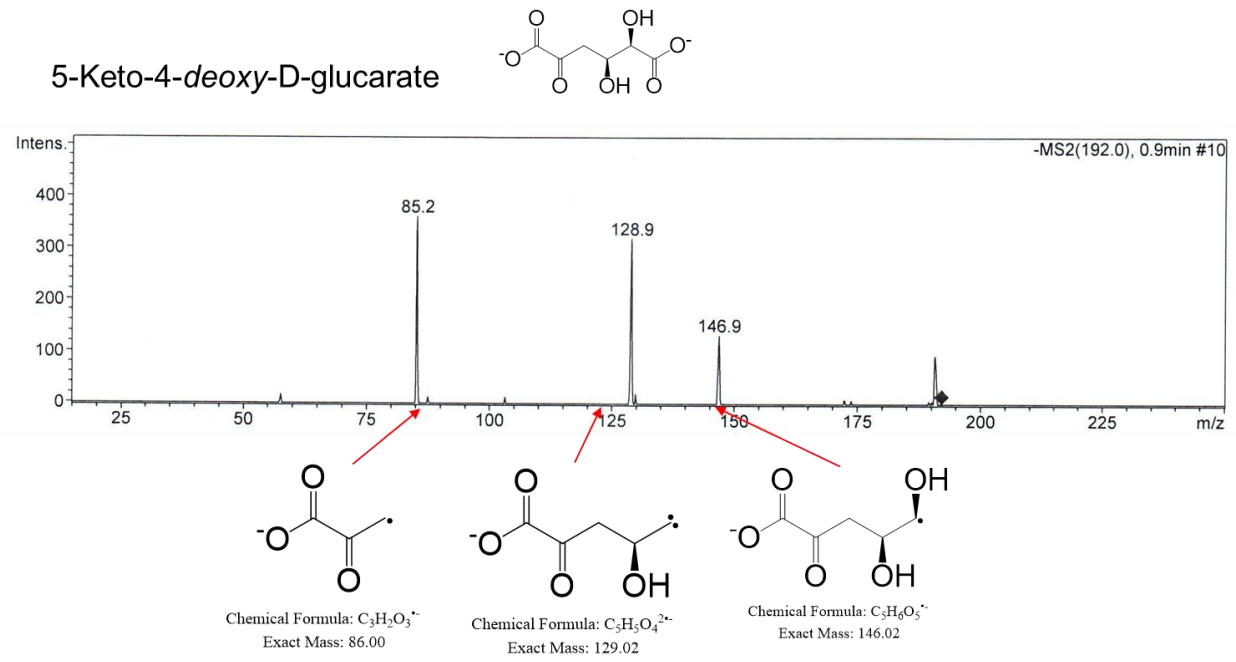

Fig. 3.5S| LC-MS data for 5-keto-4-deoxy-D-glucarate

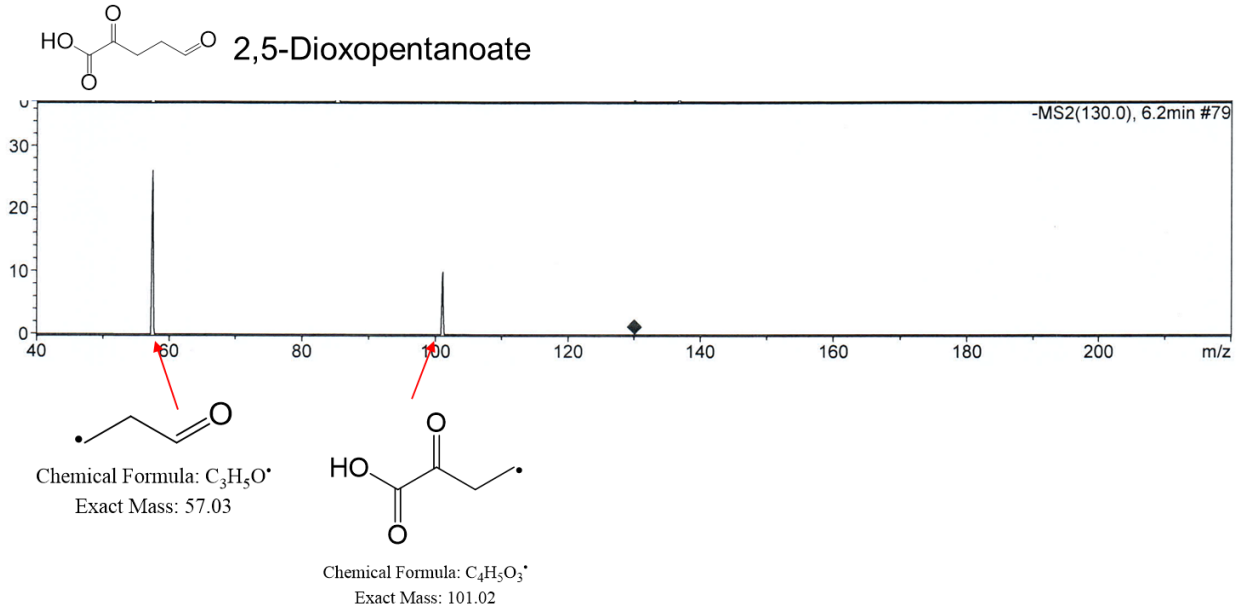

Fig. 3.6S| LC-MS data for 2,5-dioxopentanoate.

a)

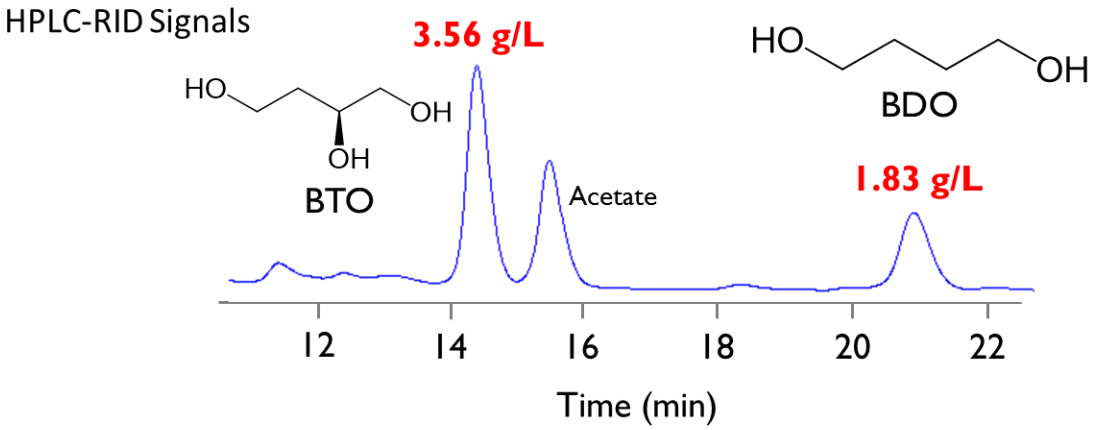

b)

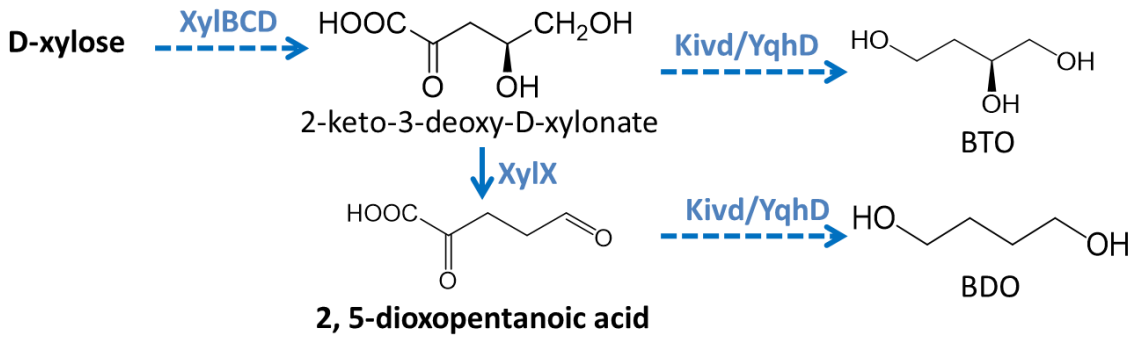

Fig. 3.S7| Accumulation of 1,2,4-butanedtriol (BTO). a) HPLC signal showing BTO accumulation with *C. crescentus* D-xylose operon. b) Mechanism showing BTO formation due to promiscous nature of 2-ketoacid decarboxylase (Kivd).

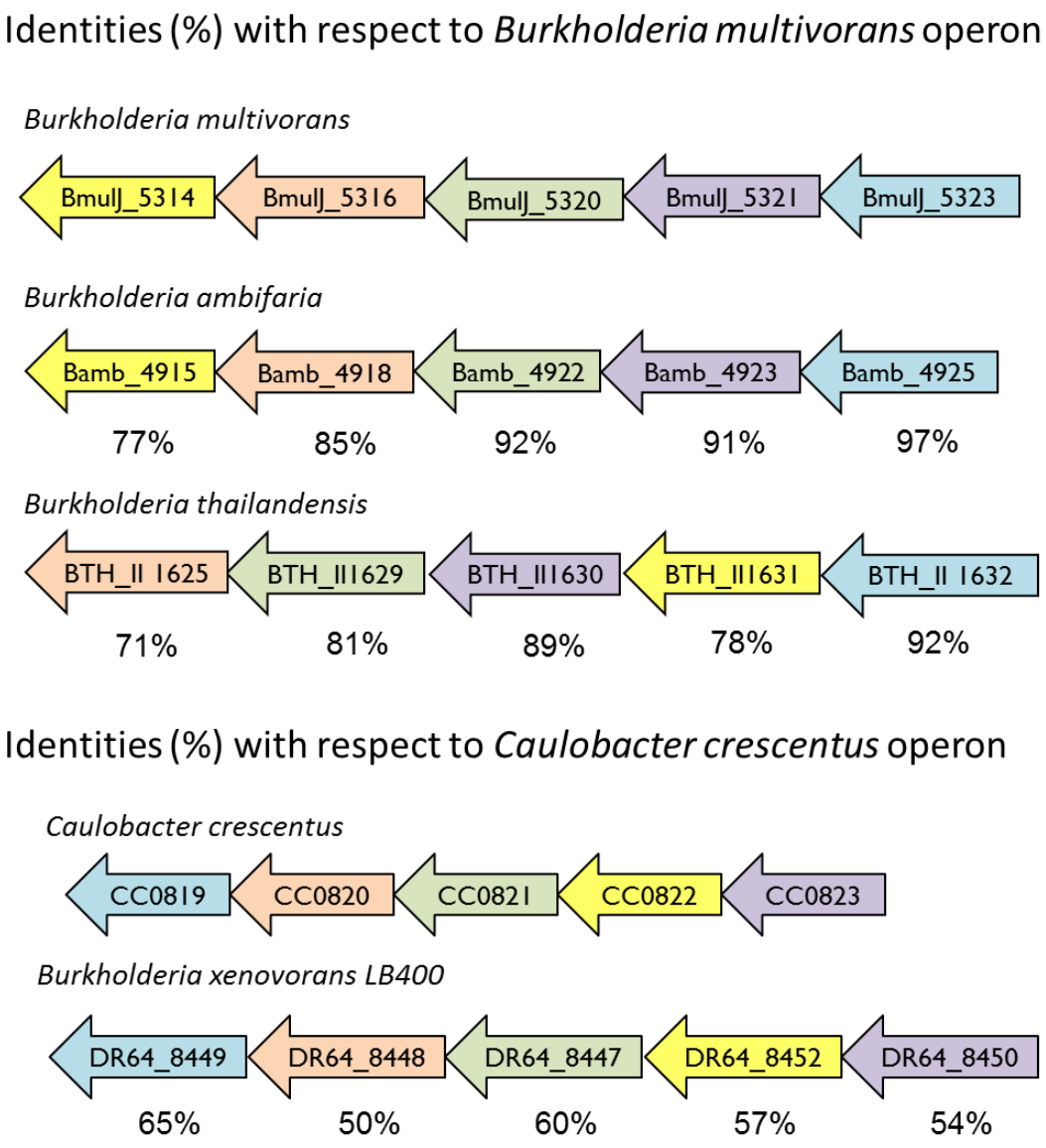

Fig. 3.S8| Sequence identities of different D-xylose and L-arabinose operons. Sequence identities of *B. ambifaria* and *B. thailandensis* L-arabinose operons with respect to *B. multivorans* L-arabinose operon. Sequence identity of *B. xenovorans* D-xylose operon with respect to *C. crescentus* D-xylose operon. Enzymes are color coded- green: D-xylose/L-arabinose dehydrogenase; orange: D-xylonolactonase/L-arabinolactonase; blue: D-xylonate/L-arabonate dehydratase; purple: 2-keto-3-deoxy-D-xylonate/2-keto-3-deoxy-L-arabonate dehydratase; yellow: 2-ketoglutarate semialdehyde dehydrogenase.

Chapter 4. Engineering Mesaconate Production from Pentoses via a Nonphosphorylative metabolism

Summary

Dicarboxylic acids are attractive biosynthetic targets due to their extensive applications and the challenging manufacturing process from fossil fuel feedstock. One specific target, mesaconate, is a branched unsaturated dicarboxylic acid that can be used as a co-monomer to produce hydrogels and flame retardant materials. In this study, we engineered a nonphosphorylative metabolism to produce mesaconate from D-xylose and L-arabinose. This nonphosphorylative metabolism is orthogonal to the intrinsic pentose metabolism in *E. coli* and has shorter enzymatic steps and a higher theoretical yield to TCA cycle intermediates. Therefore, mesaconate production pathways were built via this nonphosphorylative pathways from D-xylose and L-arabinose, respectively. To enhance the transportation of these pentoses, pentose transporters were examined. Further production optimization was achieved by operon screening and metabolic engineering. These efforts led to the engineered strains that enabled 11.6 g/l and 13.2 g/l mesaconate after 48 h from 20 g/l of D-xylose and L-arabinose, respectively. Finally, the engineered strain overexpressing both L-arabinose and D-xylose operons produced 14.7 g/l mesaconate from a D-xylose and L-arabinose mixture with a yield of 85% of the theoretical yield. This work demonstrates an effective system that convert pentoses into a value-added chemical mesaconate with promising titer, rate, and yield.

1. Introduction

Dicarboxylic acids have extensive applications in polymer industry in the preparation of copolymers such as polyesters and polyamide[133]. Moreover, dicarboxylic acids can also be hydrogenated to form the corresponding diols. For example, succinic acid can be hydrogenated to produce 1,4-butanediol[134]. However, most fossil feedstock-derived dicarboxylic acid manufacture processes are not only energy intensive and not sustainable but also environmentally unfriendly. For example, nitric acid oxidation is widely used to produce a dicarboxylic acid, adipic acid, and the emitted nitrous oxide (N_2O) during the process is considered to cause global warming and ozone depletion[135]. Due to these intrinsic disadvantages of fossil feedstock-derived processes, dicarboxylic acids are attractive targets for biosynthesis from bio-based feedstock[136].

Mesaconate is a branched and unsaturated dicarboxylic acid that was found in the organisms *Clostridium tetanomorphum*[137] and *B. xenovorans*[138]. It is an intermediate in a glutamate degradation pathway and can be further converted into pyruvate and acetyl-CoA. Mesaconate can be co-polymerized with acrylamide and crosslinked with ethylene glycol dimethacrylate or 1,4-butanediol dimethacrylate to form hydrogels[139]. These hydrogels had both high water absorbency and equilibrium water content which showed the biomedical potential. Dialkyl esters of mesaconate can undergo Diels-Alder reactions to give bicyclic compounds[140] and diallyl esters of mesaconate can be used to produce flame retardant materials[141]. Moreover, mesaconate can also be reduced by an oxygen-regulated periplasmic reductase (Mfr) from *Campylobacter jejuni* to form 2-methylsuccinate[142]. Overall, mesaconate is a versatile platform chemical that has broad

applications. Two pathways have been reported for mesaconate biosynthesis. The first one utilizes the intermediate mesaconyl-CoA generated from the ethylmalonyl-CoA pathway and expresses a heterologous thioesterase to convert it to mesaconate. The pathway was engineered in strain *Methylobacterium extorquens* AM1 and enabled 443 mg/l mesaconate production from methanol after optimization[143, 144]. The other pathway is a natural pathway which converts glutamate into mesaconate by glutamate mutase and 3-methylaspartate ammonia lyase (MAL). The first enzyme glutamate mutase catalyzes the conversion of glutamate into 3-methylaspartate and the second enzyme 3-methylaspartate ammonia lyase eliminated the ammonia group of 3-methylaspartate and generate mesaconate. The pathway has been identified in various *Clostridium* strains[145] and has been heterologously reconstructed in the industrial workhorse *E. coli*[146]. The engineered *E. coli* strain enabled 6.96 g/l of mesaconate from glucose after enhancement of glutamate mutase activity and intracellular coenzyme B12 regeneration[146]. In this study, we used the second pathway to produce mesaconate from glutamate and engineered the glutamate production via a nonphosphorylative metabolism from pentoses.

The simultaneous consumption of all biomass sugars is a major challenge in engineering *E. coli* for fermentation of lignocellulose-derived sugars[147]. Pentoses like D-xylose and L-arabinose are the most abundant sugars in hemicellulose which can make up to 30% of plant biomass[148]. Therefore, efficient utilization of pentoses is critical to an economically viable biosynthetic process. Wildtype *E. coli* can use pentoses as carbon source [149]. However, the utilization of D-xylose or L-arabinose is normally inhibited in the presence of glucose due to carbon catabolite repression (CCR)[150] since glucose can

effectively block the expression of pentose transporters and key enzymes needed for pentose metabolism. Previous research mainly focused on engineering phosphotransferase system (PTS) to alleviate CCR, but usually did not result in an effective strain. For example, an *E. coli* strain with a *ptsG* mutant could use D-xylose and glucose simultaneously to produce lactic acid, but it could not completely consume D-xylose and the yields of lactic acid decreased with increasing glucose feeding[151]. Moreover, the intrinsic metabolism for the pentoses (pentose phosphate pathway and glycolysis) requires at least 10 enzymatic steps to reach the TCA cycle and has a low theoretical yield at 83 mol% from pentoses to a key TCA cycle intermediate 2-ketoglutarate (2-KG). A promising alternative metabolism for pentoses has been found in some archaea or extremophiles strains[103]. This metabolism is nonphosphorylative and can effectively convert pentoses such as D-xylose and L-arabinose into 2-KG with only five enzymatic steps and a 100 mol% theoretical yield from pentoses to 2-KG. Besides, this nonphosphorylative metabolism is orthogonal to the intrinsic pentose metabolism and thus may serve as an attractive way to alleviate CCR and enhance co-utilization of glucose and pentoses. In a recent study, these nonphosphorylative pathways have been fully reconstituted in *E. coli* and successfully enabled the conversion of D-xylose and L-arabinose into 2-KG and 1,4-butanediol[152].

In this work, we first demonstrate mesaconate production from D-xylose and L-arabinose based on the nonphosphorylative biosynthetic platform. To enhance pentose uptake rates during the fermentation process, various pentose transporters were examined based on the improvement of final mesaconate production titers. Different

nonphosphorylative operons were also screened for D-xylose and L-arabinose, respectively. To further optimize mesaconate production from these pentoses, metabolic engineering strategies were applied by knocking out a competing pathway and enlarging the intracellular glutamate pool. The final engineered strains enabled 11.6 g/l and 13.2 g/l mesaconate production from D-xylose and L-arabinose after 48 h, respectively. Finally, we examined the co-utilization of glucose, D-xylose, and L-arabinose to biosynthesize mesaconate. The strain overexpressing D-xylose and L-arabinose operons simultaneously could produce 14.7 g/l mesaconate after 48 h with a yield of 0.74 g mesaconate/g of combined D-xylose and L-arabinose. This represents 85% of the theoretical yield. This study demonstrates the metabolic engineering efforts on systematically optimizing mesaconate production titer, rate, and yield from biomass sugars D-xylose and L-arabinose and shows a novel and promising mesaconate biosynthetic process.

2. Results and Discussion

2.1 Mesaconate production from a nonphosphorylative metabolism

To efficiently use pentoses (D-xylose and L-arabinose) as feedstocks for mesaconate production, biosynthetic pathways were designed by expanding a nonphosphorylative metabolism (**Fig. 4.1**). In the D-xylose pathway, D-xylose is converted into 2-ketoglutarate (2-KG) with five enzymatic steps including D-xylose dehydrogenase (XDH), D-xylonolactonase (XL), D-xylonate dehydratase (XD), 2-keto-3-deoxy-D-xylonate dehydratase (KdxD), and 2-ketoglutarate semialdehyde dehydrogenase

(KGSADH)[153]. Similarly, L-arabinose is transformed into 2-KG by L-arabinose dehydrogenase (ADH), L-arabinolactonase (AL), L-arabonate dehydratase (AD), 2-keto-3-deoxy-L-arabonate dehydratase (KdaD), and 2-ketoglutarate semialdehyde dehydrogenase (KGSADH). 2-KG produced from this nonphosphorylative metabolism is converted into glutamate. 3-methylaspartate is produced from glutamate by glutamate mutase and is then converted into mesaconate by MAL.

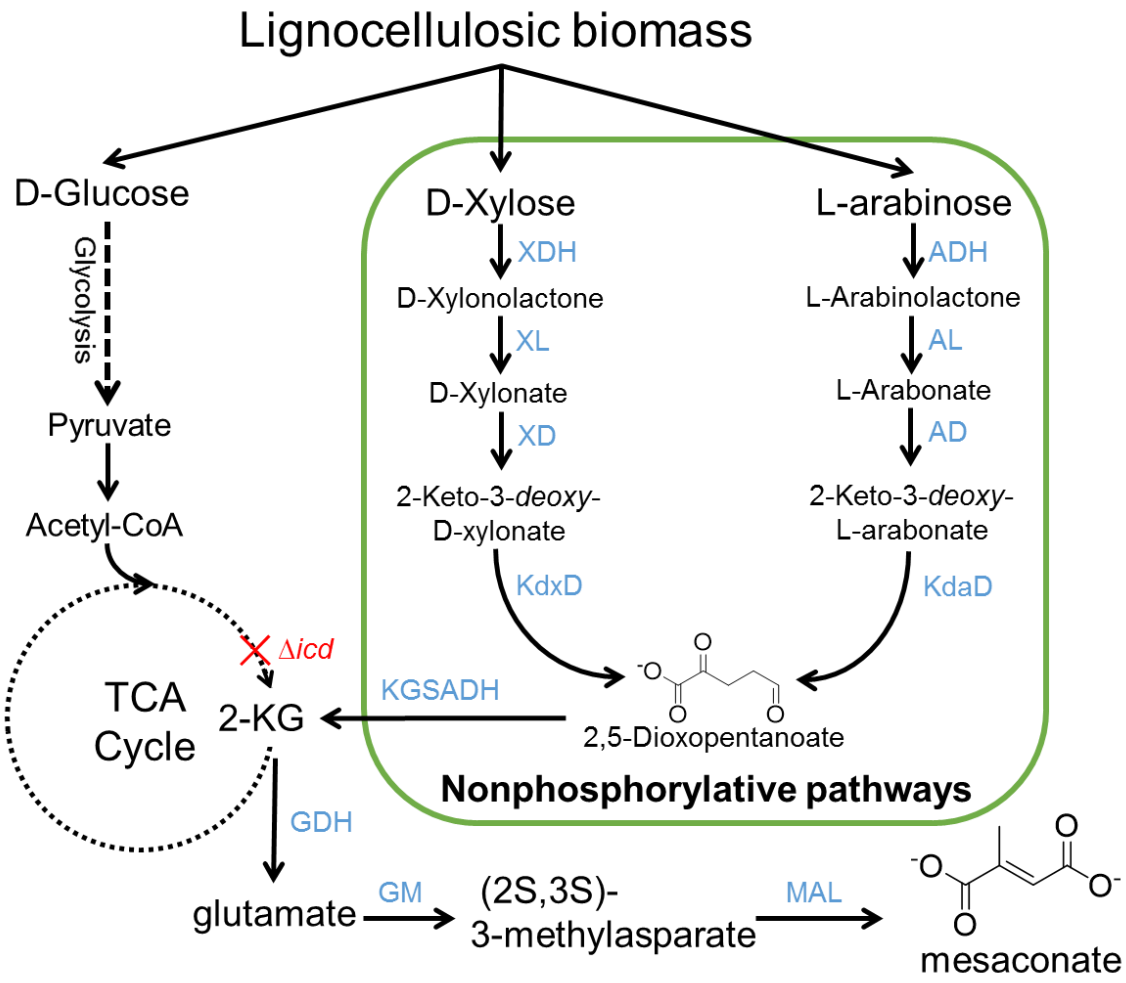

Figure 4.1| Metabolic pathways from lignocellulosic sugars to mesaconate via a nonphosphorylative metabolism. The pathway for D-xylose consists of D-xylose dehydrogenase (XDH), D-xylonolactonase (XL), D-xylonate dehydratase (XD), and 2-keto-3-deoxy-D-xylonate dehydratase (KdxD). The L-arabinose assimilation pathway is

composed of L-arabinose dehydrogenase (ADH), L-arabinolactonase (AL), L-arabonate dehydratase (AD), and 2-keto-3-deoxy-L-arabonate dehydratase (KdaD). The produced DOP is then converted into 2-KG by 2-ketoglutarate semialdehyde dehydrogenase (KGSADH). 2-KG is then transformed to mesaconate by glutamate dehydrogenase (GDH), glutamate mutase (GM), and 3-methylaspartate ammonia lyase (MAL).

Based on the pathway design, we constructed two strains, strain 1 and strain 2 (**Table 4.1**), to synthesize mesaconate from D-xylose and L-arabinose, respectively. In strain 1 (MX1, BW25113 Δ*xylA*Δ*yihH*Δ*yagE*Δ*icd*), a D-xylose operon from *B. xenovorans LB400* was overexpressed by a medium copy plasmid (pZA-*DR64_8447-8448-8449-8450*) to produce 2,5-dioxopentanoate (DOP), and DOP to mesaconate pathway genes were cloned into a high copy plasmid (pZE-*MAL-MutL-mutS-glmE-xylA*$_{CC}$). Finally, the regeneration and reactivation enzymes for coenzyme B12 were expressed by a low copy number plasmid (pZS-*btuB-btuR-fpr-fldA*) to maintain the activity of the B12-dependent glutamate mutase. Strain 2 (MA1, BW25113 Δ*icd*) contains an L-arabinose operon from *B. multivorans* a medium copy plasmid (pZA-*araC-araD-araA-araB*) and the same other two plasmids (pZE-*MAL-MutL-mutS-glmE-xylA*$_{CC}$ and pZS-*btuB-btuR-fpr-fldA*) as in strain 1. The two strains were then examined by fermentation for the production of mesaconate. After 48 h, strain 1 successfully produced 3.47 g/l mesaconate from 20 g/l of D-xylose and strain 2 enabled 3.08 g/l of mesaconate from 20 g/l of L-arabinose. Glucose was supplemented for cell growth, but did not contribute to mesaconate production due to the *icd* knockout. These preliminary results demonstrate an efficient conversion from the two pentoses D-xylose and L-arabinose to mesaconate via a nonphosphorylative metabolism.

Table 4.1| List of strains used in this study

Strain no.	*E. coli* stain	Plasmid 1	Plasmid 2	Plasmid 3
1	MX1	pZE-*MAL-MutL-mutS-glmE-xylA*$_{CC}$	pZA-*DR64_8447-8448-8449-8450*	pZS-*btuB-btuR-fpr-fldA*
2	MA1	pZE-*MAL-MutL-mutS-glmE-xylA*$_{CC}$	pZA-*araC-araD-araA-araB*	pZS-*btuB-btuR-fpr-fldA*
3	MX1	pZE-*MAL-MutL-mutS-glmE-xylA*$_{CC}$	pZA-*DR64_8447-8448-8449-8450*	pZS-*btuB-btuR-fpr-fldA-xylE*
4	MX1	pZE-*MAL-MutL-mutS-glmE-xylA*$_{CC}$	pZA-*DR64_8447-8448-8449-8450*	pZS-*btuB-btuR-fpr-fldA-xylFGH*
5	MX1	pZE-*MAL-MutL-mutS-glmE-xylA*$_{CC}$	pZA-*DR64_8447-8448-8449-8450*	pZS-*btuB-btuR-fpr-fldA-araE*
6	MA1	pZE-*MAL-MutL-mutS-glmE-xylA*$_{CC}$	pZA-*araC-araD-araA-araB*	pZS-*btuB-btuR-fpr-fldA-araE*
7	MA1	pZE-*MAL-MutL-mutS-glmE-xylA*$_{CC}$	pZA-*araC-araD-araA-araB*	pZS-*btuB-btuR-fpr-fldA-araFGH*
8	MA1	pZE-*MAL-MutL-mutS-glmE-xylA*$_{CC}$	pZA-*araC-araD-araA-araB*	pZS-*btuB-btuR-fpr-fldA-xylE*
9	MX1	pZE-*MAL-MutL-mutS-glmE-xylA*$_{CC}$	pZA-*xylB-xylC-xylD-xylX*	pZS-*btuB-btuR-fpr-fldA-araE*
10	MX1	pZE-*MAL-MutL-mutS-glmE-xylA*$_{CC}$	pZA-*xylB-xylC-xylD-DR64_8450*	pZS-*btuB-btuR-fpr-fldA-araE*
11	MA1	pZE-*MAL-MutL-mutS-glmE-xylA*$_{CC}$	pZA-*Bamb_4925-4923-4922-4918*	pZS-*btuB-btuR-fpr-fldA-araE*
12	MA1	pZE-*MAL-MutL-mutS-glmE-xylA*$_{CC}$	pZA-*BTH_II1632-1630-1629-1625*	pZS-*btuB-btuR-fpr-fldA-araE*
13	MX2	pZE-*MAL-MutL-mutS-glmE-xylA*$_{CC}$	pZA-*xylB-xylC-xylD-DR64_8450*	pZS-*btuB-btuR-fpr-fldA-araE*
14	MX2	pZE-*MAL-MutL-mutS-glmE-xylA*$_{CC}$	pZA-*xylB-xylC-xylD-DR64_8450*	pZS-*gdhA-btuB-btuR-fpr-fldA-araE*
15	MX2	pZE-*MAL-MutL-mutS-glmE-xylA*$_{CC}$	pZA-*xylB-xylC-xylD-DR64_8450*	pZS-*btuB-btuR-fpr-fldA-xylE*
16	MX2	pZE-*MAL-MutL-mutS-glmE-xylA*$_{CC}$	pZA-*xylB-xylC-xylD-DR64_8450*	pZS-*gdhA-btuB-btuR-fpr-fldA-xylE*
17	MA2	pZE-*MAL-MutL-mutS-glmE-xylA*$_{CC}$	pZA-*Bamb_4925-4923-4922-4918*	pZS-*btuB-btuR-fpr-fldA-araE*
18	MA2	pZE-*MAL-MutL-mutS-glmE-xylA*$_{CC}$	pZA-*Bamb_4925-4923-4922-4918*	pZS-*gdhA-btuB-btuR-fpr-fldA-araE*
19	MA2	pZE-*MAL-MutL-mutS-glmE-xylA*$_{CC}$	pZA-*Bamb_4925-4923-4922-4918*	pZS-*btuB-btuR-fpr-fldA-xylE*
20	MA2	pZE-*MAL-MutL-mutS-glmE-xylA*$_{CC}$	pZA-*Bamb_4925-4923-4922-4918*	pZS-*gdhA-btuB-btuR-fpr-fldA-xylE*

21	MX2	pZE-*MAL-MutL-mutS-glmE-xylA*$_{CC}$	pZA-*Bamb_4925-4923-4922-4918-xylB-xylC-xylD-DR64_8450*	pZS-*btuB-btuR-fpr-fldA-araE*

2.2 Overexpression of pentose transporters to enhance substrate uptakes

Since D-xylose and glucose mixtures (strain 1) or L-arabinose and glucose mixtures (strain 2) were used for mesaconate production, we observed CCR[154, 155] since glucose is a preferred substrate for *E. coli*. For strain 1, only 8.3 g/l of D-xylose was consumed after 48 h; for strain 2, only 9.3 g/l of L-arabinose was consumed, but glucose (20 g/l) was completely consumed in both experiments. Since this nonphosphorylative metabolism is not regulated by glucose, we believe that CCR can be alleviated by just enhancing pentose transportation. Thus, various pentose transporters were tested in the engineered strains for their ability to facilitate the pentose transportation and therefore alleviate CCR.

There are two pentose transporter systems in *E. coli*. One system contains ATP-binding cassette (ABC) transporters (XylFGH and AraFGH) which have a higher affinity but lower capacity. The other system contains pentose/proton symporters (XylE and AraE), which show a lower affinity but higher capacity[156]. The low-affinity transporters (XylE and AraE) are known to be promiscuous[157, 158] and each of them is able to transport both D-xylose and L-arabinose. Therefore, we constructed three strains (strains 3, 4, and 5) for D-xylose fermentation. These three strains based on MX1 strain were all transformed with the D-xylose to mesaconate pathway plasmids, pZA-*DR64_8447-8448-8449-8450* and pZE-*MAL-MutL-mutS-glmE-xylA*$_{CC}$, and different pentose transporters were cloned onto the pZS plasmid. XylE, XylFGH, and AraE were overexpressed in strain 3, strain 4, and strain 5, respectively. Due to the high-affinity nature of the ABC

transporter, AraFGH was not used for the D-xylose pathway. Fermentation results (**Fig. 4.2A**) showed that strain 5 (AraE) enabled the highest mesaconate production titer, 6.77 g/l after 48 h, from D-xylose. The ABC transporter XylFGH (strain 4) produced only slightly higher titer 3.57 g/l than strain 1 (no transporter) which enabled 3.47 g/l mesaconate. From the time curves (Supporting information, **Fig. 4.S1A, B, C, and D**) of the fermentation, we observe that XylFGH (strain 4) did not enhance D-xylose consumption. Besides, XylE (strain 3) improved D-xylose transportation and 20 g/l of D-xylose was completely consumed after 36 h. The final mesaconate production of strain 3 reached 5.92 g/l. We found that although XylE can transport D-xylose into cells faster than AraE, it did not result in a higher mesaconate production (5.92 g/l with XylE compared with 6.77 g/l with AraE) titer with D-xylose as the substrate.

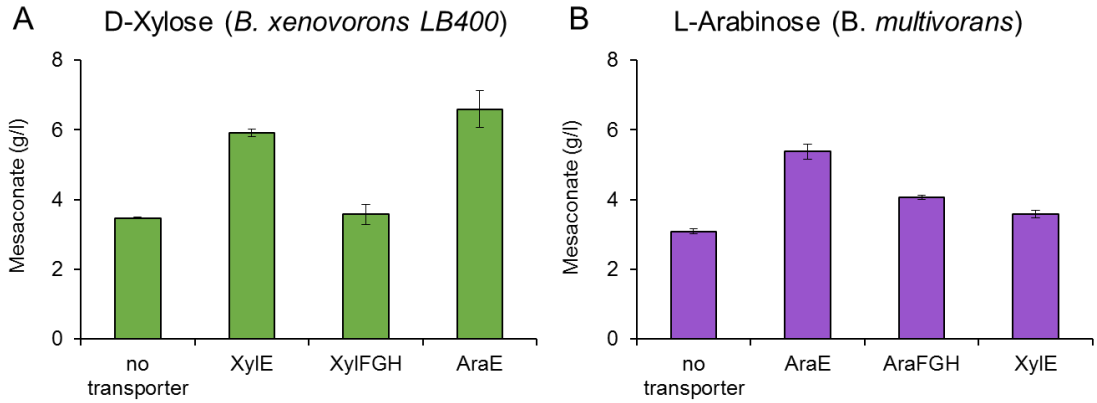

Figure 4.2| Overexpression of pentose transporters to improve mesaconate proudtion from D-xylose and L-arabinose. (A) Mesaconate production from D-xylose by strain 1 (no transporter), strain 3 (XylE), strain 4 (XylFGH), and strain 5 (AraE). XylE and AraE are proton symporters. XylFGH is a D-xylose specific ABC transporter. (B) Mesaconate production from L-arabinose by strain 2 (no transporter), strain 6 (AraE), strain 7 (AraFGH), and strain 8 (XylE). AraFGH is a L-arabinose specific ABC transporter. All error bars shown represent SD (n=3).

Other three strains (strains 6, 7, and 8) were constructed for L-arabinose. The three strains were MA1 strain transformed with plasmids pZA-*araC-araD-araA-araB*, pZE-*MAL-MutL-mutS-glmE-xylA*$_{CC}$, and the pZS plasmid containing B12 regeneration pathway and different pentose transporters. Strain 6 overexpressed the symporter AraE; strain 7 overexpressed the ABC transporter AraFGH; strain 8 overexpressed the D-xylose symporter XylE. After 48 h of fermentation (**Fig. 4.2B**), strain 6 performed best among the three and resulted in 5.37 g/l mesaconate. Due to the promiscuity of XylE, strain 8 also enhanced L-arabinose uptake and improved the mesaconate production titer to 3.71 g/l from 3.08 g/l from strain 2 (no transporter overexpression). Based on the time-course profiles (**Fig. 4.S2A, B, C, and D**), AraFGH only slightly improved the L-arabinose uptake rate (10.8 g/l of L-arabinose consumption by strain 7 compared to the 9.3 g/l of L-arabinose consumption by strain 2 with no transporter) and the resulted mesaconate titer is only 4.05 g/l.

2.3 Screening operons for mesaconate production

After we identified AraE as the most effective transporter for both D-xylose and L-arabinose, various operons of nonphosphorylative metabolism were screened for optimal mesaconate production. For D-xylose pathway, three operons were tested for their activity towards mesaconate production. In the previous section, strain 5 which contained the *DR64_8447-8448-8449-8450* operon from *B. xenovorans* LB400 (*B. xen*) was used to screen pentose transporters. For the other two operons, strain 9 contained the *xylB-xylC-xylD-xylX* operon from *C. crescentus* (*C. cre*) and strain 10 contained the *xylB-*

xylC-xylD-DR64_8250 operon which is a synthetic operon with the first three genes from *C. crescentus* (*xylB-xylC-xylD*) and the last gene (*DR64_8450*) from *B. xenovorans* LB400. We constructed this operon by combining the genes from two organisms since the enzyme KdxD from the *B. xenovorans* LB400 operon was reported to have a higher *in vitro* activity (DR64_8250, k_{cat}/K_M=0.53 $s^{-1}mM^{-1}$) than that from the *C. crescentus* operon (XylX, k_{cat}/K_M=0.26 $s^{-1}mM^{-1}$)[152]. On the other hand, *C. crescentus* operon has more active XDH and XD than the *B. xenovorans* LB400 operon. When the three strains were subjected to fermentation, strain 10 with the synthetic operon was the best performing strain and produced 7.60 g/l mesaconate after 48 h (**Fig. 4.3A**).

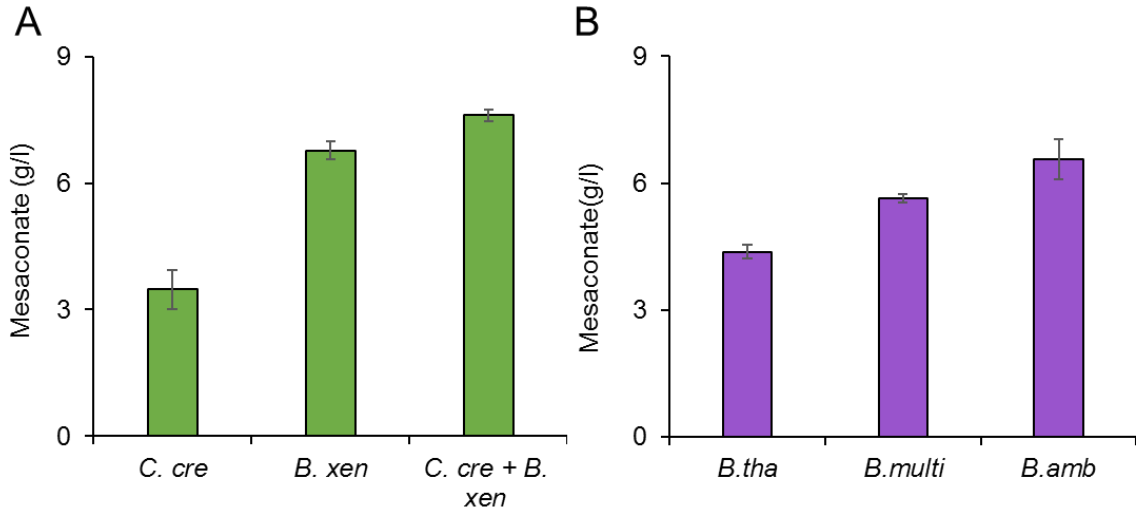

Figure 4.3| Screening nonphosphorylative metabolism operons for mesaconate production from D-xylose and L-arabinose. All strains overexpressed AraE to enhance pentose transportation. (A) Three D-xylose operons were examined. Strain 9 contained the *C. cre* operon (*xylB-xylC-xylD-xylX*). Strain 5 contained the *B. xen* operon (*DR64_8447-8448-8449-8450*). Strain 10 contained the synthetic *C. cre* + *B. xen* operon (*xylB-xylC-xylD-DR64_8250*). (B) Three L-arabinose operons were examined. Strain 12 contained the *B. tha* operon (*BTH_II1632-1630-1629-1625*). Strain 6 contained the *B. multi* operon (*araC-araD-araA-araB*). Strain 11 contained the *B. amb* operon (*Bamb_4925-4923-4922-4918*). All error bars shown represent SD (n=3).

Three L-arabinose operons were tested for mesaconate production via the nonphosphorylative metabolism. Strain 6 containing the *araC-araD-araA-araB* from *B. multivorans* (*B. multi*) was used in the previous section. Strain 11 contained the *B. ambifaria* operon *Bamb_4925-4923-4922-4918* (*B. amb*) and strain 12 contained the *B. thailandensis* (*B. tha*) operon *BTH_II1632-1630-1629-1625*. Among the three strains, strain 11 with *B. ambifaria* operon enabled the highest mesaconate production at 6.55 g/l (**Fig. 4.3B**). *B. thailandensis* operon was the least active and only produced 4.38 g/l mesaconate (**Fig. 4.3B**).

2.4 Optimization of mesaconate biosynthesis by metabolic engineering

To further optimize mesaconate production from D-xylose and L-arabinose via this nonphosphorylative metabolism, we applied metabolic engineering strategies to drive the carbon flux towards the desired metabolite. *E. coli* gene *sucA* encodes a subunit of 2-KG decarboxylase[159] which catalyzes the conversion of 2-KG to succinyl-CoA in the TCA cycle and diverted the carbon flux from glutamate production. Therefore, we knocked out *sucA* gene in the production strains MX1 and MA1 to generate strains MX2 (MX1 ⊿*sucA*) and MA2 (MA1 ⊿*sucA*), respectively. On the other hand, *E. coli* gene *gdhA* encoding glutamate dehydrogenase[160] which catalyzes the conversion of 2-KG into glutamate and can potentially enhance mesaconate production due to a larger glutamate pool. Therefore, the strategy was applied to optimize mesaconate production by cloning *gdhA* onto the pZS plasmids to generate plasmid pZS-*gdhA-btuB-btuR-fpr-fldA-araE*.

For D-xylose pathway, strain 13 (MX2 host strain transformed with pZE-*MAL-MutL-mutS-glmE-xylA*$_{CC}$, pZA-*xylB-xylC-xylD-DR64_8450*, and pZS-*btuB-btuR-fpr-fldA-araE*) produced 9.44 g/l mesaconate (**Fig. 4.4A**). This showed that the single *sucA* knockout enhanced mesaconate production by 24%. When *gdhA* was overexpressed in the pZS plasmid, strain 14 can further improve the mesaconate production to 12.53 g/l from 20 g/l D-xylose after 48 h. Similarly, *sucA* knockout (strain 17) improved mesaconate production from L-arabinose from 6.55 g/l to 11.30 g/l (**Fig. 4.4B**). Overexpression of *gdhA* (strain 18) further improved mesaconate titer to 13.25 g/l from 20 g/l L-arabinose. Time-course profiles of the best D-xylose and L-arabinose are shown in **Fig. 4.4C** and **4.4D**, respectively. For D-xylose pathway, strain 14 consumed all 20 g/l D-xylose in 48 h and mesaconate kept accumulating mesaconate during the time. Excitingly, the engineered cell simultaneously consumed glucose and D-xylose with no CCR phenomena observed. This showed that we can effectively use pentoses in lignocellulosic hydrolysates just by enhancing their transportation if this nonphosphorylative metabolism was applied. OD_{600} increased exponentially during the first 24 h and kept increasing to reach OD_{600}=23.02 at the end of fermentation. Acetate was accumulated to 2.4 g/l after 24 h and the concentration decreased to 1.4 g/l at 48 h. Similar trends were observed in the time-course profile of strain 18 for L-arabinose. The consumption rates of glucose and L-arabinose were the same and both were depleted after 48 h. There was less acetate production compared with strain 14 and all produced acetate was consumed by cells at the end of the fermentation.

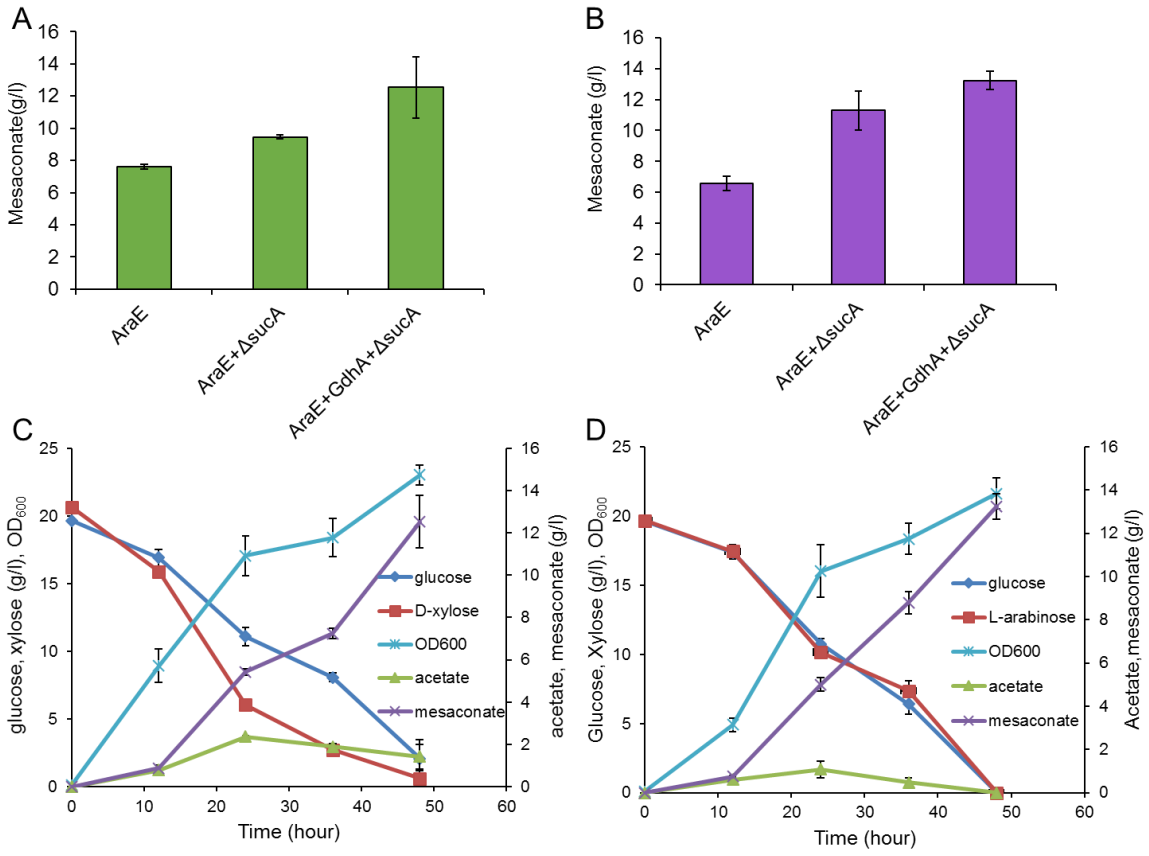

Figure 4.4| Optimization of mesaconate production from D-xylose and L-arabinose via a nonphosphorylative metabolism. (A) All three D-xylose strain were constructed based on the synthetic *C. cre* + *B. xen* operon and have AraE overexpression to enhance pentose transportation. Strain 13 was based on ⊿*sucA* strain and strain 14 was based ⊿*sucA* strain with *gdhA* overexpressed by the pZS plasmid. (B) All three L-arabinose strain were constructed based on the *B. amb* operon and have AraE overexpression to enhance pentose transportation. Strain 17 was based on ⊿*sucA* strain and strain 18 was based ⊿*sucA* strain with *gdhA* overexpressed by the pZS plasmid. (C) Time-coures profile of strain 14. (D) Time-coures profile of strain 18. Error bars are ± SD for n=3 independent fermentation experiments.

2.5 Mesaconate production by co-utilization of glucose, D-xylose and L-arabinose

After we successfully engineered the nonphosphorylative metabolism to produce mesaconate from D-xylose and L-arabinose, respectively, the next step is to construct the strain that can utilize D-xylose and L-arabinose simultaneously. Therefore, we constructed a plasmid (pZA-*Bamb_4925-4923-4922-4918-xylB-xylC-xylD-DR64_8450*) that contained the synthetic D-xylose operon and the *B. ambifaria* L-arabinose due to their highest activities among the tested operons for mesaconate production. AraE was chosen as the pentose transporter since it is promiscuous and is the most effective transporter both D-xylose and L-arabinose as shown in previous sections. Strain MX2 was thus transformed with plasmids *pZE-MAL-MutL-mutS-glmE-xylA*$_{CC}$, pZA-*Bamb_4925-4923-4922-4918-xylB-xylC-xylD-DR64_8450*, and *pZS-btuB-btuR-fpr-fldA-araE* to generate strain 21. During fermentation, 20 g/l glucose was supplemented for cell growth, and 10 g/l D-xylose and 10 g/l L-arabinose were fed for mesaconate production. The engineered strain 21 utilized three sugars simultaneously and produced 14.75 g/l mesaconate after 48 h (**Fig. 4.5**). From the time course, we can see that L-arabinose was the preferred pentose than D-xylose for *E. coli* and was completely consumed after 36 h, but the engineered strain was able to use all the D-xylose at 48 h. The yield of mesaconate was 0.74 g/g of combined D-xylose and L-arabinose which accounts for 85% of the theoretical yield.

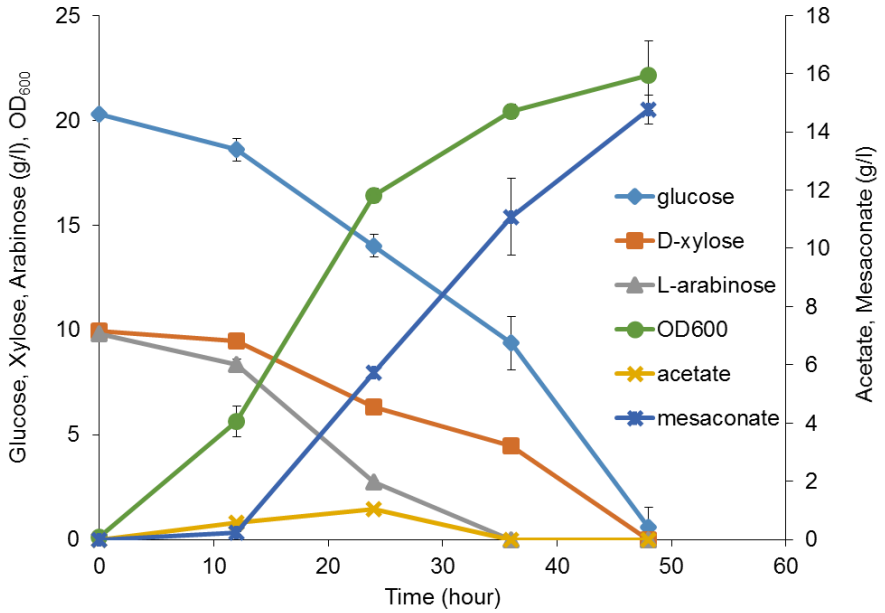

Figure 4.5| Time-coures profile of strain 21. The engineered strain co-utilized glucose, D-xylose, and L-arabinose for mesaconate production. Error bars are ±SD for n=3 independent fermentation experiments.

3. Conclusions

Successful conversion of D-xylose and L-arabinose, important sugars in hemicellulose, to a branched unsaturated dicarboxylic acid mesaconate via an efficient nonphosphorylative metabolism was demonstrated. To alleviate CCR in a mixture of glucose and pentose (D-xylose or L-arabinose), various pentose transporters were overexpressed and tested. AraE which is a proton symporter was found to be the most effective transporter for both D-xylose and L-arabinose. Three D-xylose operons and three L-arabinose operons were screened for mesaconate production. The synthetic D-xylose operon (*xylB-xylC-xylD-DR64*_8250) created by combining the first three genes (encode XDH, XL, and XD) from *C. crescentus* and the last gene from *B. xenovorans* LB400 (encodes KdxD) enabled the highest mesaconate production titer from D-xylose and the *B. ambifaria*

operon (*Bamb_4925-4923-4922-4918*) was the most active operon for L-arabinose. To further optimize mesaconate production, we applied metabolic engineering strategies by knocking our competing pathway gene *sucA* and overexpressing *gdhA* which encodes glutamate dehydrogenase to enlarge the glutamate pool. Mesaconate production was successfully improved from 7.60 g/l to 12.53 g/l from 20 g/l of D-xylose after implementing these two modifications. Similarly, mesaconate production titers were increased from 6.55 g/l to 13.24 g/l from 20 g/l L-arabinose. Finally, the two best-performing D-xylose and L-arabinose operons were integrated into a single plasmid and the engineered strain can thus utilize both D-xylose and L-arabinose simultaneously. By supplementing 10 g/l of D-xylose and 10 g/l of L-arabinose, strain 21 overexpressing the two operons was able to produce mesaconate at 14.75 g/l with a yield of 0.74 g/g of pentoses. Herein, we demonstrated a novel, efficient, and high-yield biosynthetic platform to produce mesaconate in *E. coli* from biomass pentoses.

4. Materials and Methods

4.1 Bacterial and growth conditions.

E. coli strains used in this study are listed in **Table 4.S1**. *E. coli* strain XL10-Gold (Stratagene) was used for cloning. Other strains were derived from the wildtype *E. coli* K-12 strain BW25113. The P1 phage of *sucA* was obtained from the Keio collection[87]. Phage was used to transfect the corresponding strains for construction of targeted knockout strains[161]. All the knockout strains were then transformed with pCP20 plasmid to remove the kanamycin marker. The correct knockouts were verified by colony PCR.

Unless otherwise stated, these *E. coli* strains were grown in test tubes at 37 °C in 2×YT rich medium (16 g/l tryptone, 10 g/l yeast extract, and 5 g/l NaCl) supplemented with appropriate antibiotics (100 mg/l ampicillin, 50 mg/l kanamycin, and/or 100 mg/l spectinomycin). Chemicals used in the study were purchased from Sigma-Aldrich unless otherwise specified.

4.2. Plasmids construction

All plasmids used in the study are listed in **Table 4.S1**. All primers used in this study were ordered from Eurofins MWG Operon and are listed in **Table 4.S2**. PCR reactions were carried out with Q5 High-Fidelity DNA polymerase (New England Biolabs) according to the manufacturer's instructions. FastDigest restriction enzymes were purchased from Thermo Scientific. Sequences of all the plasmids constructed were verified by restriction mapping and DNA sequencing.

The recombinant plasmid pM-3 was constructed as follows: gene *DR64_8450* was amplified from plasmid pM-1 using primer pairs DR64_8450-F and DR64_8450-R. The linearized pZA vector containing genes *xylB-xylC-xylD* was obtained by digesting plasmid pM-2 with restriction enzymes HindIII and BlpI. The amplified *DR64_8450* fragment was then ligated onto the linearized pZA vector using NEBuider HiFi DNA assembly master mix (New England Biolabs). The recombinant plasmid pM-10 was constructed as follows: *xylA* gene was amplified from plasmid pM-9 by PCR using xylA-F and xylA-R as primers. Gene fragment of *glmE* was amplified from plasmid pM-7 by PCR using glmE-F and glmE-R as primers. Amplified *xylA* PCR product was digested

with SdaI and XbaI, *glmE* PCR product was digested with SphI and SdaI, and then they were ligated into the linearized vector generated by digesting plasmid pM-7 with SphI and XbaI. The recombinant plasmid pM-11 was constructed as follows: *xylE* gene was amplified from *E. coli* BW25113 genomic DNA by PCR using xylE-F and xylE-R as primers. PCR product of *xylE* was digested by SphI and BamHI, and then ligated into the linearized vector generated by digesting pM-8 with the same enzymes. The construction of the recombinant plasmid pM-12 is similar to that of pM-11, but PCR product of *araE* was amplified using araE-F and araE-R as primers and was digested with SphI and BglII. The recombinant plasmid pM-15 was constructed as follows: *xylFGH* gene was amplified from *E. coli* BW25113 genomic DNA by PCR using xylFGH-F1 and xylFGH-R1 as primers. Then the PCR product was digested with KpnI and HindIII, and then ligated into the plasmid pM-13 digested by the same set of restriction enzymes. Then the plasmid pM-14 was obtained. Next, *xylFGH* fragment containing both promoter and terminator regions was amplified from plasmid pM-14 by PCR using xylFGH-F2 and xylFGH-R2 as primers. The fragment containing *btuB* gene was amplified from pM-8 by PCR using btuB-F and btuB-R. Then the two PCR fragments and the linearized pM-8 (digested KpnI and HindIII) were purified and ligated into the plasmid pM-8 between XhoI and PstI sites using NEBuider HiFi DNA assembly master mix. The construction of the recombinant plasmidspM-16and pM-17 was similar to that of pM-15, but the two primer sets used were AraFGH-F1 and AraFGH-R1, and AraFGH-F2 and AraFGH-R2. The recombinant plasmid pM-19 was constructed as follows: *gdhA* was amplified from *E. coli* BW25113 genomic DNA by

PCR using gdhA-F1 and gdhA-R1 as primers. Then the PCR product was digested by KpnI and HindIII, and then ligated into plasmid pM-13 digested by the same restriction enzymes to obtain plasmid pM-18. Next, *gdhA* fragment containing promoter and terminator regions was amplified from pM-18 by PCR using gdhA-F2 and gdhA-R2 as primers. The fragment containing *btuB* gene was amplified from pM-8 by PCR using btuB-F and btuB-R as primers. Then the two PCR fragments (*gdhA* and *btuB*) were purified and ligated into the linearized vector created by digesting plasmid pM-11 with XhoI and PstI using NEBuider HiFi DNA assembly master mix. The construction of the recombinant plasmid pM-20 was similar to that of pM-19, but the PCR products were ligated into the plasmid pM-12 instead of pM-11 between XhoI and PstI sites. The recombinant plasmid pM-21 was constructed as follows: L-arabinose operon containing the promoter and terminator was amplified from the plasmid pM-3 using araABCD-F and araABCD-R as primers. Xylose operon containing the promoter and terminator was amplified from the plasmid pM-4 using xylABCD-F and xylABCD-R as primers. pZAlac linear vector was amplified from plasmid pM-3 using pZA-F and pZA-R as primers. After purification, the three PCR fragments were ligated to form a recombinant plasmid pM-21 by using NEBuider HiFi DNA assembly master mix.

4.3 Shake flask batch fermentation

125-ml conical flasks with 0.5 g $CaCO_3$ (used to buffer the pH of media) were autoclaved and dried to perform all small-scale fermentations. The flasks were filled with 5 ml fermentation medium (M9 minimal media supplemented with 5 g/l yeast extract, 20

g/l glucose, 20 g/l D-xylose (or L-arabinose), 5μM coenzyme B12, 100 mg/l ampicillin, 50 mg/l kanamycin, and/or 100 mg/l spectinomycin). For *sucA* knocked strains MX2 and MA2, 5 mM succinic acid was supplemented. To start fermentation, 200 μl of overnight cultures incubated in 2×YT medium were transferred into the flasks. After adding 0.5 mM isopropyl-β-D-thiogalactoside (IPTG), the flasks were put into a shaker at 250 rpm and 30 °C, and the fermentation was performed for 48 h. The fermentation products were analyzed by HPLC. Error bars indicated the SD of the results obtained from three independent experiments (n=3) by picking three different colonies for fermentation.

4.4. Metabolite Analysis

Fermentation samples were analyzed using an Agilent 1260 Infinity HPLC system. The automated liquid sampler program and mobile phase gradient program were performed as manufacturer's instruction. The samples were analyzed using an Aminex HPX 87H column (Bio-Rad) and a refractive-index detector to detect carbohydrates. The mobile phase is 5 mM H_2SO_4 with a flow rate 0.6 ml/min. The column temperature and the RID detector temperature are 35°C and 50°C, respectively.

5. Supplementary Information

Table 4.S1| Strains and plasmids used in this study.

Name	Relevant genotype	Reference
Strains		
BW25113	*rrnB*$_{T14}$ ΔlacZ$_{WJ16}$*hsdR514* Δ*araBAD*$_{AH33}$ Δ*rhaBAD*$_{LD78}$	[70]
XL10-Gold	Tet^{R}Δ (*mcrA*)183 Δ (*mcrCB-hsaSMR-mrr*)173 *endA1supE*44 *thi-1 recA1*	Stratagene
MX1	BW25113 Δ*xylA*Δ*yjhH*Δ*yagE*Δ*icd*	[152]
MA1	BW25113 Δ*icd*	[152]
MX2	BW25113 Δ*xylA*Δ*yjhH*Δ*yagE*Δ*icd*ΔsucA	This work
MA2	BW25113 Δ*icd*ΔsucA	This work
Plasmids		
pM-1	P15A origin, KanR, PL*lacO*1: *DR64_8447-8448-8449-8450*	[152]
pM-2	P15A origin, KanR, PL*lacO*1: *xylB-xylC-xylD-xylX*	[152]
pM-3	P15A origin, KanR, PL*lacO*1: *xylB-xylC-xylD-DR64_8450*	This study
pM-4	P15A origin, KanR, PL*lacO*1: *Bamb_4925-4923-4922-4918*	[152]
pM-5	P15A origin, KanR, PL*lacO*1: *BTH_II1632-1630-1629-1625*	[152]
pM-6	P15A origin, KanR, PL*lacO*1: *araC-araD-araA-araB*	[152]
pM-7	ColE1 origin, AmpR, PL*lacO*1:*MAL-mutL-mutS-glmE*	[146]
pM-8	pUC origin, SpecR, PL*lacO*1: *btuB-btuR-fpr-fldA*	[146]
pM-9	ColE1 origin, AmpR, PL*lac*O1:xylA$_{CC}$	[152]
pM-10	ColE1 origin, AmpR, PL*lacO*1:*MAL-mutL-mutS-glmE-xylA*$_{CC}$	This study
pM-11	pUC origin, SpecR, PL*lacO*1: *btuB-btuR-fpr-fldA-xylE*	This study
pM-12	pUC origin, SpecR, PL*lacO*1: *btuB-btuR-fpr-fldA-araE*	This study
pM-13	pUC origin, SpecR, PL*lacO*1	Expressys
pM-14	pUC origin, SpecR, PL*lacO*1: *xylFGH*	This study
pM-15	pUC origin, SpecR, PL*lacO*1: *xylFGH*, PL*lacO*1:*btuB-btuR-fpr-fldA*	This study
pM-16	pUC origin, SpecR, PL*lacO*1: *araFGH*	This study
pM-17	pUC origin, SpecR, PL*lacO*1: *araFGH,* PL*lacO*1:*btuB-btuR-fpr-fldA*	This study
pM-18	pUC origin, SpecR, PL*lacO*1: *gdhA*	This study
pM-19	pUC origin, SpecR, PL*lacO*1: *gdhA*, PL*lacO*1:*gdhA-btuB-btuR-fpr-fldA-xylE*	This study
pM-20	pUC origin, SpecR, PL*lacO*1: *gdhA*, PL*lacO*1: *gdhA-btuB-btuR-fpr-fldA-araE*	This study
pM-21	P15A origin, KanR, PL*lacO*1: *Bamb_4925-4923-4922-4918-xylB-xylC-xylD- DR64_8450*	This study

Table 4.S2| Primers used in this study

Primers	Sequence (5' to 3')
DR64_8450-F	TGCCCCGCCACAACCACTAAAAGCTTAGGAGAAATTAACTATGTCCGCAACTTCTCCATC
DR64_8450-R	GTTTTATTTGATGCCTCTAGAGCTCAGCTTAGGCCGACGCAAGCAGCCCGCGTGCG
xylA-F	GCGTATCCTGCAGGATTAAAGAGGAGAAAGGTACCAT
xylA-R	CCCGGGTCTAGATTACGACCACGAGTAGGA
glmE-F	CCCGGGGCATGCAGGAGAAATTAACTATGGAACT
glmE-R	GCGTATCCTGCAGGCTTATTCTGGTCTTCCGATAAGTCT
xylFGH-F1	CCCGGGGGTACCATGAAAATAAAGAACATTCTACTC
xylFGH-R1	CCCGGGAAGCTTTCAAGAACGGCGTTTGGTTG
xylFGH-F2	ATCACGAGGCCCTTTCGTCTTCACC
xylFGH-R2	CCTAGGTCTAGGGCGGCGGATTTG
btuB-F	GACAAATCCGCCGCCCTAGACCTAGGAATTGTGAGCGGATAACAATTGACATTG
btuB-R	GAAGGTGTAGCTGCCAGACAAGGTGTATTCCCGTC
xylE-F	CCCGGGGCATGCAGGAGAAATTAACTATGAATACCCAGTATAATTCCAGTTA
xylE-R	CCCGGGGGATCCTTACAGCGTAGCAGTTTGTTGTGTTT
araFGH-F1	GAATTCATTAAAGAGGAGAAAGGTACCATGCACAAATTTACTAAAGCCCTGG
araFGH-R1	GCTGCAGGAATTCGATATCAAGCTTTCAGACAGTGCGTTTCGCTTTTTGCTTG
araFGH-F2	ATCACGAGGCCCTTTCGTCTTCACC
araFGH-R2	CCTAGGTCTAGGGCGGCGGATTTG
araE-F	CCCGGGGCATGCAGGAGAAATTAACTATGGTTACTATCAATACGGAATCTG
araE-R	CCCGGGAGATCTTCAGACGCCGATATTTCTCAACTTC
gdhA-F1	AGAAAGGTACCATGGATCAGACATATTCTCTGGAG
gdhA-R1	GATATCAAGCTTTTAAATCACACCCTGCGCCAGC
gdhA-F2	ATCACGAGGCCCTTTCGTCTTCACC
gdhA-R2	CCTAGGTCTAGGGCGGCGGATTTG
pZA-F	GGTACCTTTCTCCTCTTTAATGAATTCG
pZA-R	TCTAGAGGCATCAAATAAAACGAAAGGCTC
araABCD-F	CGAATTCATTAAAGAGGAGAAAGGTACCATGTCGGC
araABCD-R	CCTAGGTCTAGGGCGGCGGATTTG
xylBCDX-F	GACAAATCCGCCGCCCTAGACCTAGGAATTGTGAGCGGATAACAATTGACATTG
xylBCDX-R	GAGCCTTTCGTTTTATTTGATGCCTCTAG
DR64_8450-F	TGCCCCGCCACAACCACTAAAAGCTTAGGAGAAATTAACTATGTCCGCAACTTCTCCATC
DR64_8450-R	GTTTTATTTGATGCCTCTAGAGCTCAGCTTAGGCCGACGCAA

	GCAGCCCGCGTGCG
xylA-F	GCGTATCCTGCAGGATTAAAGAGGAGAAAGGTACCAT
xylA-R	CCCGGGTCTAGATTACGACCACGAGTAGGA
glmE-F	CCCGGGGCATGCAGGAGAAATTAACTATGGAACT
glmE-R	GCGTATCCTGCAGGCTTATTCTGGTCTTCCGATAAGTCT
xylFGH-F1	CCCGGGGGTACCATGAAAATAAAGAACATTCTACTC

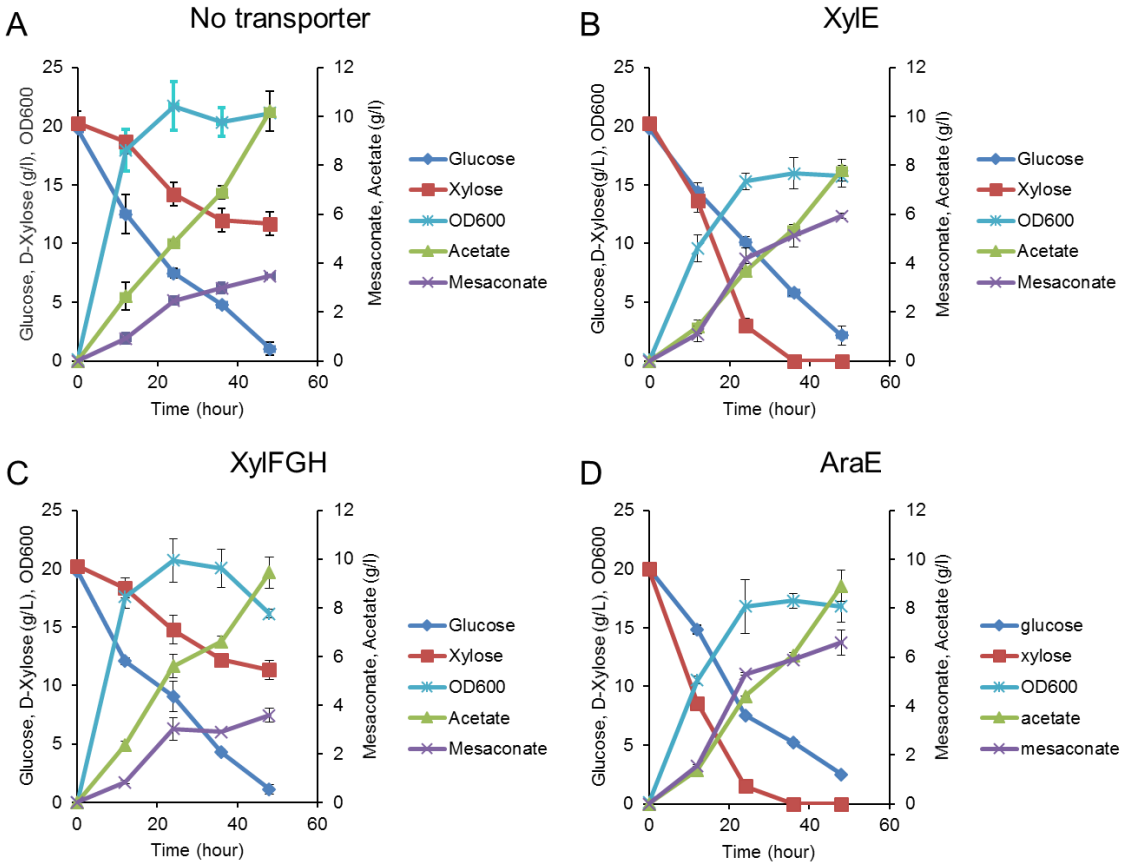

Figure 4S.1| Time-course profiles of D-xylose strains overexpressing different pentose transporters. All the strains here overexpressed *B. xen* operon for D-xylose conversion. (A) Strain 1 (no transporter) (B) Strain 3 (XylE) (C) Strain 4 (XylFGH) (D) Strain 5 (AraE). Error bars are ± SD for n=3 independent bioreactor fermentation experiments.

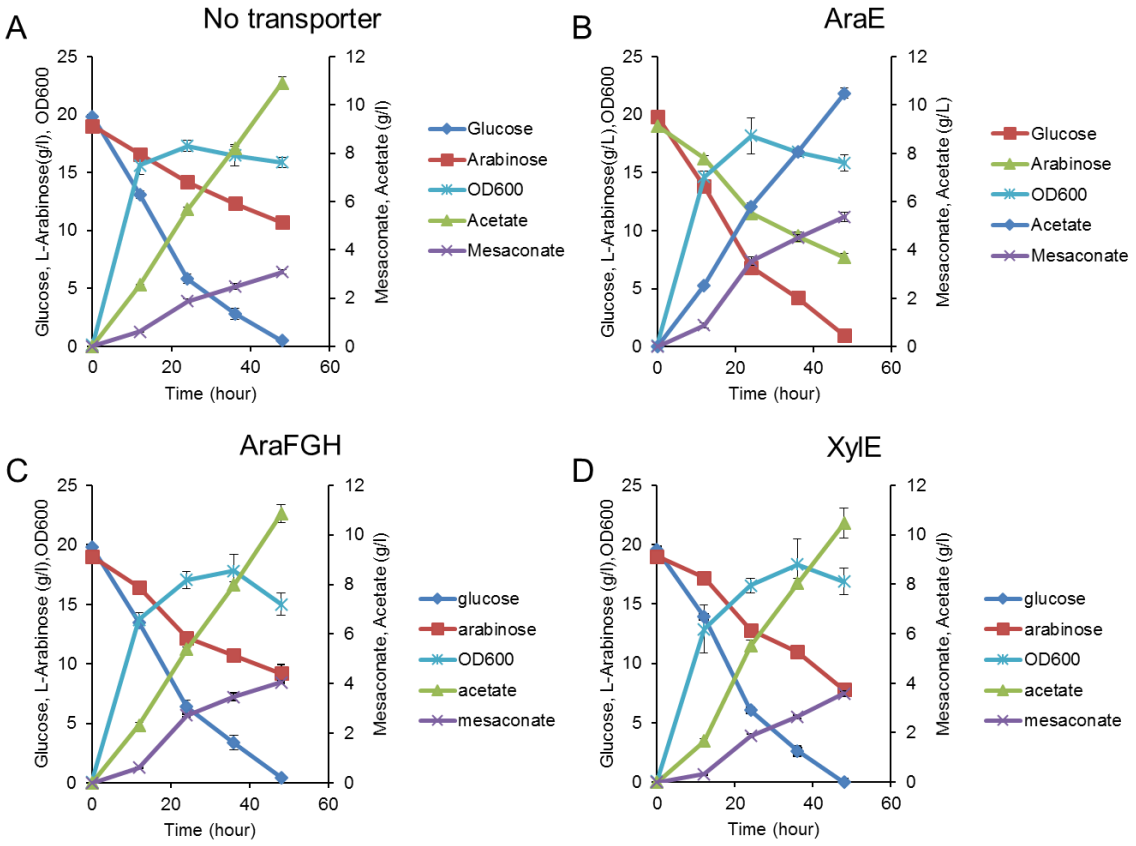

Figure 4S.2| Time-course profiles of L-arabinose strains overexpressing different pentose transporters. All the strains here overexpressed *B. multi* operon for L-arabinose conversion. (A) Strain 1 (no transporter) (B) Strain 3 (AraE) (C) Strain 4 (AraFGH) (D) Strain 5 (XylE). Error bars are ± SD for n=3 independent bioreactor fermentation experiments.

Chapter 5. Biosynthesis and Polymerization of Optically Active β-Methyl-δ-valerolactone

Summary

Chemo-enzymatic pathways were developed to prepare optically enriched (+)-β-methyl-δ-valerolactone and (-)-β-methyl-δ-valerolactone. Anhydromevalonolactone, synthesized by the acid-catalyzed dehydration of bio-derived mevalonate, was transformed to (+)-β-methyl-δ-valerolactone with 76% ee and 69% conversion using the mutant enoate reductase YqjM (C26D, I69T). With the same substrate but a different enoate reductase (OYE2), we obtained the other enantiomer ((-)-β-methyl-δ-valerolactone) with higher selectivity and yield (96% ee and a 92% conversion). The enzyme-docking program LibDock was used to help explain the origin of the divergent enatntioselectivity of the two reductases, and complementary *in vitro* experiments were used determine the turnover number and Michaelis constant for each. Finally, the effect of enantiopurity of β-methyl-δ-valerolactone monomer on the properties of the corresponding polyester was investigated. Like atactic poly((±)-β-methyl-δ-valerolactone), the isotactic polymer was determined to be amorphous with a low softening temperature (-52 °C).

1. Introduction

Medium sized lactones are a common structural motif in biologically active molecules including plant growth inhibitors, insect antifeedants, and antitumor agents[162, 163, 164]. In particular, the potential value of optically active δ-lactones as precursors for the synthesis of complex natural products has made the efficient asymmetric synthetic of these

molecules an important and longstanding research challenge for chemists and biochemists alike[165, 166]. More recently, these versatile molecules have also found additional use as monomers for the preparation of biodegradable aliphatic polyesters[167, 168, 169]. Importantly, it has been demonstrated that with many polyesters altering stereochemical composition can be used to tune key physical properties including degradation rate, thermal, and mechanical properties[167, 168].

Myriad synthetic strategies have been used for the synthesis of optically active δ-lactones, however only a few biocatalytic methods have been developed[165, 170]. Of these, the lipase-based resolution of racemic lactones has been most widely explored[171]. Notably, optically active polymers have also been prepared from the lipase-catalyzed polymerization of racemic ε-lactones. However, kinetic resolution strategies are problematic because, to achive high optical purity, the reaction must be stopped at low conversion[168]. Asymmetric synthesis method, such as lactonization of diols using dehydrogenases[172, 173, 174], oxidation of cyclic ketones using monooxygenase enzymes[175, 176], and reduction of unsaturated lactone precursors[164, 177, 178, 179, 180, 181, 182, 183], do not suffer from this limitation.

We recently developed a biosynthetic route for the production of β-methyl-δ-Valerolactone (MVL) from glucose[127]. The final step in our pathway utilizes an enoate reductase of the old yellow enzyme family (OYE2 or YqjM (C26D, I69T)) to reduce anhydromevalonolactone (AMVL). Because the titers of MVL prepared using biosynthetic route were low, we also developed a semisynthetic route whereby bioderived mevalonate is chemically dehydrated to AML and hydrogenated to prepare MVL[127].

Since the hydrogenation catalyst used is not steroselective, the semisynthetic route yeilds a racemic mixture of MVL. While we envisioned that our total biosynthetic routes could result in optically active products[174, 184, 185, 186], the stereoselectivities of reductases (YqjM (C26D, I69T) and OYE2) were not determined. We also hypothesized that the tacticity of PMVL might effect its thermal properties but were unable to test this hypothesis without optically pure (+)-MVL or (-)-MVL.

Here, AMVL prepared from the acid catalyzed dehydration of bioderived mevalonate is transformed into optically active MVL by either YqjM (C26D, I69T) or OYE2. After 72 h, OYE2 transformed anhydromevalonate to (-)-MVL with good conversion (91.5%) and steroselectivity (96% ee). Fermentation with YqjM (C26D, I69T) resulted in the production of (+)-MVL, albeit with slightly lower selectivity and conversion (76% enantiomeric excess (ee) and 68.9%, respectively). We discuss the mechanistic origins of selectivity of YqjM (C26D, I69T) and OYE2 and compare these enzymes to asymmetric hydrogenation catalysts previous used to prepare optically enriched MVL[187, 188]. Finally, we investigated the effect of polymer tacticity on the thermal properties of poly((-)-β-methyl-δ-valerolactone).

2. Results and Discussion

2.1 Stereoselective reduction of AMVL using enoate reductases

Previously, the dehydration of mevalonate to AMVL was found to be the rate-limiting step in the biosynthesis of MVL[127]. Here we performed the dehydration chemically by adding sulfuric acid directly to the mevalonate fermentation broth. After refluxing for 15

h, the solution was extracted with chloroform to obtain AMVL in high yields (typically 80-90% based on the starting concentration of mevalonate as monitored by GC). *E. coli* strains overexpressing an enoate reductase were used to convert AMVL to optically enriched β-methyl-δ-valerolactone. As described in **Scheme 5.1**, (-)-β-methyl-δ-valerolactone and (+)-β-methyl-δ-valerolactone were produced by strains expressing OYE2 and YqjM (C26D, I69T), respectively .

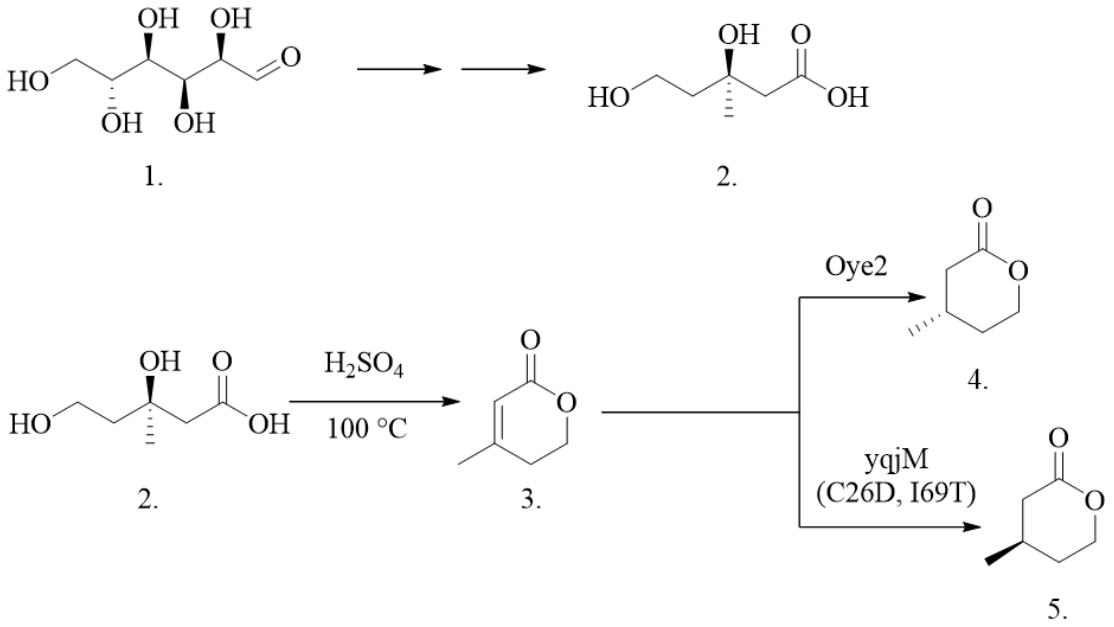

Scheme 5.1| Chemo-enzymatic synthesis of enantiopure β-methyl-δ-valerolactone Glucose. (1) is transformed biosynthetically to mevalonate (2); subsequent chemical dehydration yields AMVL (3). Enzymatic reduction with OYE2 or YqjM (C26D, I69T) yields (-)-β-methyl-δ-valerolactone or (+)-β-methyl-δ-valerolactone, respectively.

During the fermentation process, glucose (40 g/l) was supplied to support cell growth and provide cofactors/reducing power for the reduction of AMVL. However, since only the reductase was overexpressed, no glucose was directly converted to MVL. For the OYE2-overexpressing strain (**Fig. 5.1a**), the concentration of glucose gradually decreased (from 40 g/l to 9.7 g/l after 72 h). AMVL (1.1 g/l) was added to the fermentation broth as the substrate. After an initial lag period, MVL increased monotonically (to approximately 1.1 g/l). The overall conversion of anhydromevalonate reached 92% at the end of fermentation.

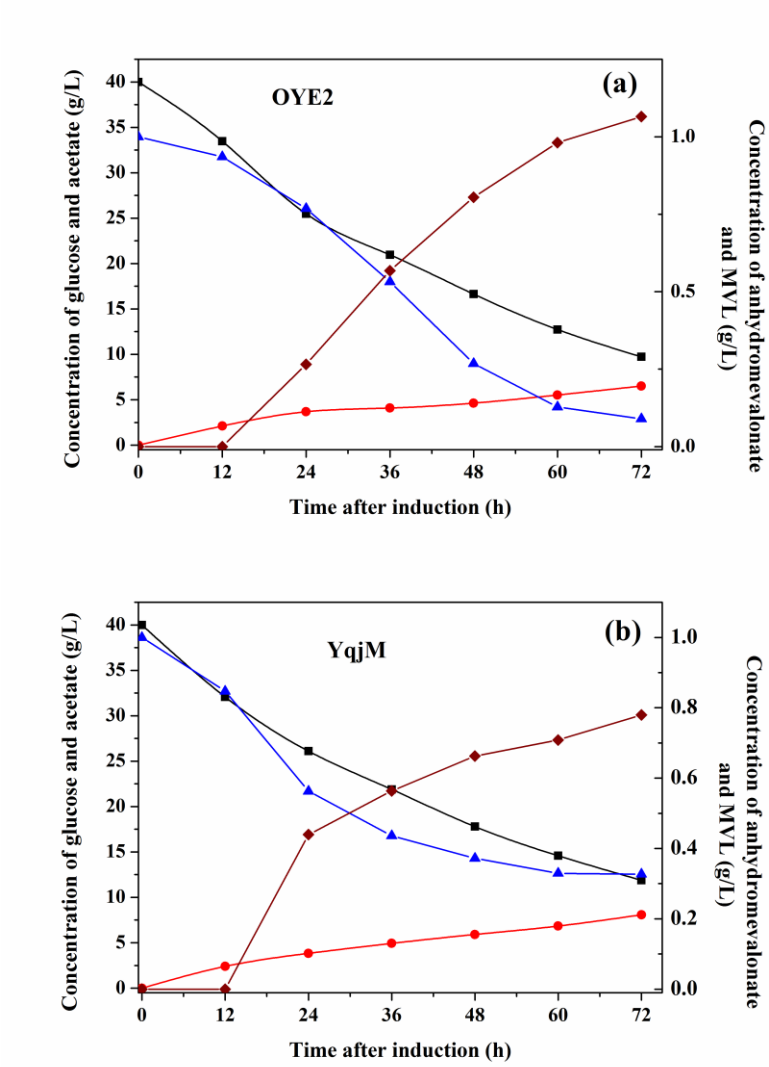

Figure 5.1| Shake flask fermentation results with (a) BW25113 transformed with pZE-OYE2 and (b) BW25113 transformed with pZE-YqjM (C26D, I69T) showing concentration of glucose (–■), acetate (–●), anhydromevalonolactone (–▲), and β-methyl-δ-valerolactone (–♦)

Fermentation with the YqjM (C26D, I69T)-overexpressing strain (**Fig. 5.1b**) was qualitatively similar. Again, no MVL was detected in the first 12 h while about 0.2 g/l AMVL was consumed in this period of time. The final concentration of MVL reached 0.8 g/l. After 72 h the overall conversion was 69%, slightly lower than that of the

fermentation with the OYE2-overexpressing strain. Comparatively, less glucose was consumed and more acetate accumulated (8.1 g/l was consumed after 72 h).

We then compared the *in vivo* activity of the respective enoate reductases to the *in vitro* activity. As shown in **Fig. 5.S8**, we first used SDS-PAGE to verify that OYE2 and YqjM were overexpressed by the respective recombinant cells. OYE2 and YqjM (C26D, I69T) were then extracted from the cells and purified; the activity of each enzyme was studied with a coupled assay. Using AMVL as the substrate we determined the kinetic parameters of OYE2 (K_M=90±5 mM and k_{cat}=0.04±0.02 s^{-1}) by monitoring the initial consumption rates of NADPH. Purified YqjM (C26D, I69T) has a faster turnover rate and a lower Michaelis constant (K_M as 61±6 mM and k_{cat}=0.3±0.05 s^{-1}). Although YqjM (C26D, I69T) showed better *in vitro* activity than OYE2, we found that OYE2 had a higher conversion in fermentation experiments.

2.2 Purification and characterization of β-methyl-δ-valerolactone

To isolate MVL, the fermentation broth was first washed with chloroform to remove residual AMVL. The solution was acidified with H_2SO_4 then washed with chloroform to extract MVL. The product was then concentrated and distilled. ^{1}H NMR spectroscopy and GC-MS were used to verify the purity of the product. The optical rotation of the isolated products was used to estimate the enantioselectivity of OYE and YqjM (C26D, I69T). Whereas fermentation with the strain transformed with pZE-OYE2 yielded (-)-MVL (96% ee), the strain transformed with pZE-YqjM (C26D, I69T) was selective for (+)-MVL (76% ee).

2.3 Scale-up synthesis of (-)-β-methyl-δ-valerolactone

Because the yield and selectivity of fermentation with the strain expressing pZE-OYE2 were higher than those of the strain transformed with pZE-YqjM (C26D, I69T), we chose to use WT strain transformed with pZE-OYE2 for a fed-batch biosynthesis. Scale-up synthesis of (-)-MVL was conducted in a 1.3-l bio-reactor. The fed-batch fermentation resulted in a final concentration of 1.0 g/l (-)-MVL after 48 h. The (-)-MVL thus obtained was purified and described previously and polymerized to examine the effect of optical purity on polymer properties.

2.4 Synthesis of poly((-)-β-methyl-δ-valerolactone)

To examine the impact of monomer optical purity on polymer properties, we prepared poly((-)-β-methyl-δ-valerolactone) from optically enriched (-)-MVL. Due to the low ceiling temperature of this monomer, the reaction was conducted at room temperature to ensure a high monomer conversion. Benzyl alcohol and diphenyl phosphate were used as an initiator and catalyst respectively. Using SEC the molecular weight of the polymer was estimated as 7.8 kg mol^{-1} while the molecular weight based on ^{1}H NMR end-group analysis was about 12.3 kg mol^{-1}. The molar mass of the isolated polymer was lower than the theoretical molar mass (M_N target = 21.4 kg mol^{-1}). As the polymer exhibits a narrow molecular weight distribution, we believe this discrepancy is most likely due to the presence of adventitious initiators in the monomer.

The thermal transitions of synthesized polyester were evaluated using differential scanning calorimetry. Initial experiments indicated that, like poly(±)-β-methyl-δ-

valerolactone, poly(-)-β-methyl-δ-valerolactone is fully amorphous with a low glass transition temperature (T_g = -52.5 °C) (**Fig. 5.2**). To verify these results was annealed 90 days at room temperature then retested; again no melting endotherm was observed on the initial heating ramp.

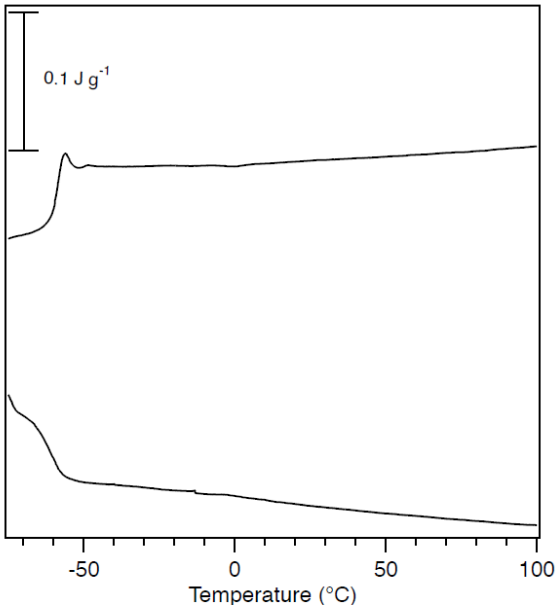

Figure 5.2| DSC thermogram (endotherm up) of poly(-)-β-methyl-δ-valerolactone. To ensure consistent thermal histories all samples were heated to 100 °C (rate of 5 °C min^{-1}) and cooled at the same rate. The two lines shown are the heating and cooling on the second cycle (ramp rate of 5 °C min^{-1}). To verify that the sample was amorphous, the sample was annealed 90 days at room temperature and heated again to 100 °C (rate of 5 °C min-1); no melting endotherm was observed on the initial heating ramp [data not shown].

3. Discussion

Enzymes in the Old Yellow Enzyme (OYE) family derive their yellow color from non-covalently bound flavin mononucleotide (FMN) cofactor. Both OYE2 and YqjM

catalyze alkene reduction reactions by the net trans-addition of H_2. During the reaction, N5 of the FMN cofactor is reduced by NADPH. Subsequently, a hydride is transferred from FMN to the β-carbon of the alkene substrate. The α-carbon is simultaneously protonated by the adjacent tyrosine (Y196 in OYE2 and Y169 in YqjM)[189]. Since the relative positions of FMN and the tyrosine residue are fixed in the active site, the orientation of the substrate in the binding pocket determines the stereoselectivity of the enzyme.

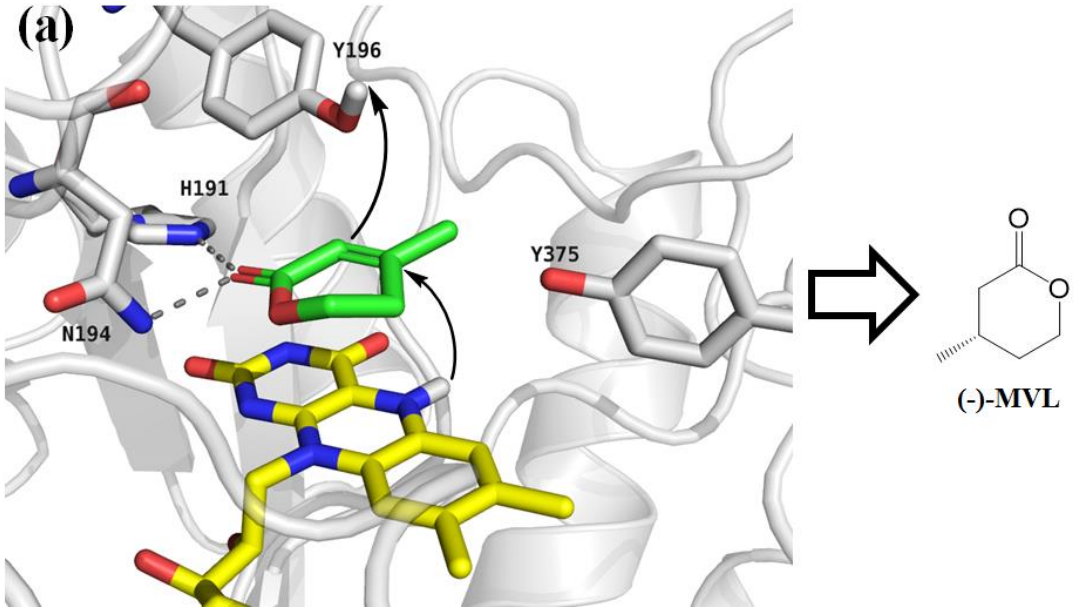

(Cont'd)

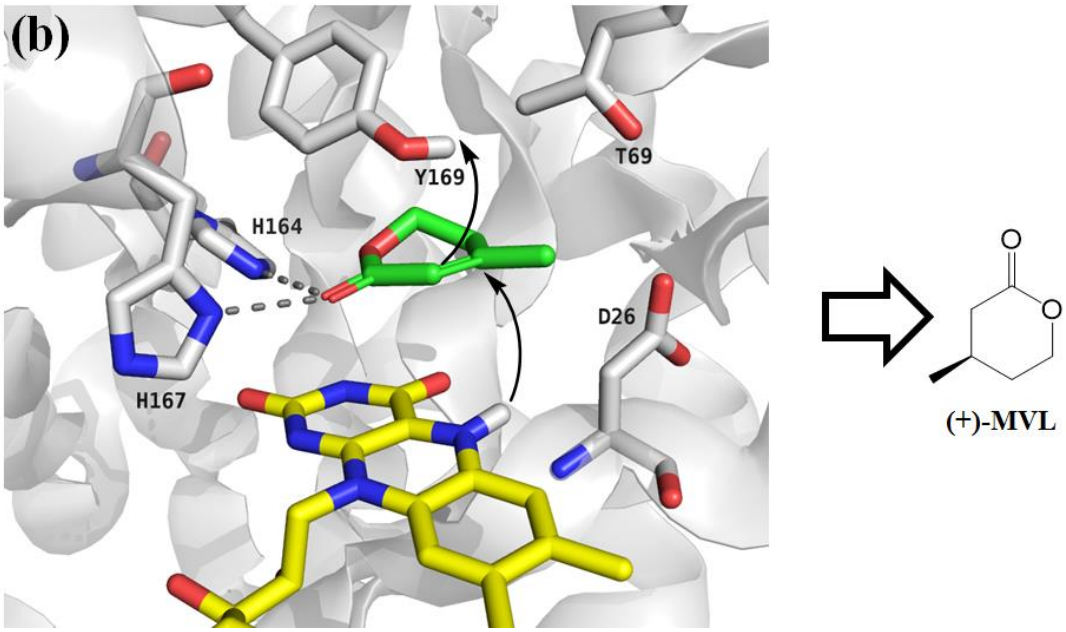

Figure 5.3| (a) The binding orientation AMVL in enzyme OYE2 and the resulting product (-)-MVL. N5 of the FMN cofactor adds a hydride to the β-carbon from bottom and Y196 adds another hydride to the α-carbon from top. PDB ID: 3TX9. **(b) The binding orientation AMVL in enzyme YqjM (C26D, I69T) and the resulting product (+)-MVL.** N5 of the FMN cofactor adds a hydride to the β-carbon from bottom and Y196 adds another hydride to the α-carbon from top.

Enzyme OYE2 binds different substrates with different orientations mainly because of the steric effects caused by amino acid residue Y375 or W116. In this study, we found that AMVL was reduced steroselectively by OYE2 to (-)-MVL (96% ee); this observation suggests that OYE2 binds AMVL in the orientation shown in **Fig. 5.3a**. Amino acid residues H191 and N194 hydrogen bonded with the carbonyl group and help fix the substrate. Because AMVL does not have a bulky side chain, this result suggests the internal oxygen atom may play an important role in determining the binding orientation.

YqjM, another member of the old yellow enzyme family, was first isolated from *B. subtilis* where it plays a role in the oxidative stress response[190]. The YqjM crystal structure, determined with p-hydroxybenzaldehyde and p-nitrophenol substrates, suggests H164 and H167 are necessary for fixation and activation of carbonyl while Y169 is responsible for α-carbon protonation[191]. YqjM has been extensively studied by directed evolution utilizing iterative saturation mutagenesis to broaden its substrate spectrum[192]. Our experiment results show that YqjM (C26D, I69T) can transform anhydromevalonate into (+)-MVL with 76% ee, which suggests AMVL may prefer a flipped binding mode in YqjM mutant compared with that in OYE2 as shown in **Fig. 5.3b**. Docking experiments, performed to gain insight on the stereoselectivity of YqjM (C26D, I69T), confirm this idea. Indeed, a flipped binding mode for AMVL was identified in YqjM (C26D, I69T). In this mode FMN is positioned below AMVL, where the reduced form can transfer a hydride from N5 to the β carbon of AMVL. In the binding mode, the α-carbon deprotonates the Y169 residue positioned above the substrate. This results in selective production of (+)-MVL.

Previously, the asymmetric conjugate reduction of AMVL has been studied using copper/BIPHEMP catalysts with polymethylhydrosiloxane as a stoichiometric reductant. Using this method, (-)-MVL has been prepared from in moderate yield and enantioselectivity (70 % and 82 %, respectively)[187]. Additionally, the asymmetric hydrogenation of a number of heterocyclic alkenes has been investigated using homogenous iridium complexes. In the hydrogenation of AMVL the authors report moderate selectivity (79 %) for (-)-MVL[188]. Like OYE2 and YqiM, the

enantioselectivities of these organometallic catalysts are determined by the preferred binding orientation of the substrate to an active coordination site. Because the coordination of a trisubstituted alkene is most favorable when the alkene hydrogen is oriented closest to the most sterically encumbered position, the absolute configuration of the product depends primarily on configuration and position of the chiral ligand. Like OYE2, the iridium and copper catalysts described in previous works are selective for (-)-MVL[187, 188]; however, OYE2 shows improved selectivity. Although the YqjM studied in this work only gives modest enatioselectivity it is a notable method to produce (+)-MVL from anhydromevalonate; heretofore no transition metal hydrogenation catalysts have been reported to be selective for this enantiomer.

With optically active monomer in hand we investigated properties of optically enriched poly(MVL). Although we have previously demonstrated good molar mass control for the polymerization of racemic MVL, in this work we obtained a lower molar mass polymer than expected. Because the dispersity was relatively narrow we believe this discrepancy is probably due to the presence of adventitious initiators in the monomer. It is probable that use of higher purity monomer could result in better control, however this was not practical at the current scale. Like poly(±)-β-methyl-δ-valerolactone, poly(-)-β-methyl-δ-valerolactone is fully amorphous. Although this behavior is similar to that previously reported for poly-((-)-4-methyl caprolactone)[168], it is still somewhat surprising because it has been reported that the constitutional isomer, poly-((+)-γ-methyl-δ-valerolactone is semicrystalline[193]. We are actively exploring the interesting effects optical purity and monomer structure have on polymer thermal properties.

4. Conclusions

Optically active lactones have enormous potential applications in pharmaceutical, fine chemical and polymer material industries. In this work we use a biocatalytic strategy to prepare both enantiomers of MVL from AMVL, an unsaturated precursor that can be produced efficiently on a lage scale via the dehydration of bioderived mevalonate. Specifically, reduction with OYE2 yields (-)-β-methyl-δ-valerolactone (96% e.e. and 91.5% conversion), and reduction with YqjM (C26D, I69T) yields (+)-β-methyl-δ-valerolactone (76% ee and 68.9% yield). Reduction of AMVL with OYE2 results in higher yield and enatioselectivity than reductions with transition metal catalysts.[187] [188] Interestingly, polymerization of optically active (-)-β-methyl-δ-valerolactone yielded an isotactic polymer was, like its atactic analog, fully amorphous.

This investigation is significant for the following reasons. First, optically active MVL is a potentially useful for synthetic chemistry and pharmaceutical applications[194]. We have developed a method to produce both enantiomers from the same renewable precursor and have also shown that reduction of AMVL with OYE2 results in higher yield and enatioselectivity than reductions with transition metal catalysts[187] [188]. Secondly we have expanded the substrate scope of OYE2 and YqjM (C26D, I69T), and investigated the binding mechanism of both enzymes. Finally, we have shown that, unlike poly((+)-γ-methyl-δ-valerolactone) which rapidly crystallizes[193], isotactic poly((-)-β-methyl-δ-valerolactone) is fully amorphous. This interesting result suggests that substituent position can have a dramatic effect on the physical properties of optically active aliphatic polyesters.

5. Materials and Methods

5.1 Materials

Benzyl alcohol (Sigma Aldrich) was purchased and used as received. Diphenyl phosphate (Sigma Aldrich) was purchased, dried in a vacuum oven at room temperature for 96 h. Both benzyl alcohol and diphenyl phosphate were handled and stored in a glovebox with a nitrogen atmosphere. Reagent grade chloroform and methanol were purchased from Fisher Scientific and used as received. Reagents used in fermentation and culture processes were purchased from Sigma-Aldrich unless otherwise specified. FastDigest restriction enzymes were purchased from Thermo Scientific. Quick ligation and Phusion high-fidelity PCR kits were supplied by New England Biolabs. Oligonucleotides were ordered from Eurofins MWG Operon.

5.2 Characterization

Fermentation products were analyzed using an Agilent 1260 Infinity HPLC equipped with an Aminex HPX 87H column and a refractive index detector. The mobile phase was 5 mM aqueous H_2SO_4 at a flow rate of 0.6 ml/min. The column and detector temperatures were 35 °C and 50 °C, respectively. The purity of anhydromevalonate precursor and β-methyl-δ-valerolactone monomer was verified using tandem gas chromatography/low resolution mass spectrometry (GC/MS) and ^{1}H NMR (more details are described below). GC/MS was performed on a mass selective detector that used electron impact (EI) ionization. Samples were prepared in ethyl acetate with a concentration of ~0.1 mg/ml.

Optical rotations of (+)-β-methyl-δ-valerolactone and (-)-β-methyl-δ-valerolactone were identified using a digital polarimeter with a 100 mm cell. Samples were prepared in chloroform and data were collected at room temperature. A reference optical rotation of $[\alpha^{23}]_D$ = -27.55 was used to calculate ee[195]. The identity of each previously characterized compound used in this work was established by ^{1}H NMR spectroscopy.^{1}H NMR Spectra were collected from $CDCl_3$ solution on a Varian INOVA-500 spectrometer operating at 500 MHz. ^{1}H NMR spectra are reported as the average of at least 24 scans and were acquired using a 5 second acquisition time and a 10 second delay, chemical shifts are referenced to the protic solvent peak at 7.26 ppm.

Polymer mass-average molar mass (M_w) and dispersity (Đ) were determined using a size exclusion chromatography instrument with THF as the mobile phase at 25 °C and a flow rate of 1 mL min^{-1}. Size exclusion was performed with three successive Phenomenex Phenogel-5 columns. The mass average molar mass and dispersity were identified using the known concentration of the sample in THF and the assumption of 100% mass recovery to calculate dn/dc from the RI signal. Differential scanning calorimetry was conducted on a TA Instruments Q-1000 DSC. Samples were analyzed in hermetically sealed aluminum pans. The samples were equilibrated at -80 °C, heated to 100 at 10 °C min^{-1}, cooled to -80 at 5 °C min^{-1}, and then reheated to 100 °C at the same rate. In a separate experiment, a polymer sample was heated to 100 °C at 5 °C min^{-1} and cooled to 20 at 5 °C min^{-1}, and annealed at room temperature (20 ± 3 °C) for 90 days. The sample was then heated to 100 °C at a rate of 5 °C min^{-1}.

5.3 Bacterial strains and plasmid construction

Bacterial strains and plasmids used in this study are described in **Table 5.S1**. *E. coli* strain XL10-Gold was used in plasmid construction processes. *E. coli* strain BW25113 was used in fermentation experiments. *E. coli* strain BL21 was used in protein expression and purification experiments. Enoate reductases OYE2 from *S. cerevisiae* and YqjM from *Bacillus subtilis* were used for biosynthesis of enantiopure MVL. The OYE2 fragment was first amplified from *S. cerevisiae* genomic DNA with primers OYE2-EcoRI-F (cacacagaattcattaaagaggagaaattaactATGCCATTTGTTAAGGACTTTAAGCC) and OYE2-XbaI-R (gctgcttctagaTTAATTTTTGTCCCAACCGAGTTTTA), and then cloned into a pZE vector at EcoRI and XbaI sites to form the plasmid pZE-OYE2. YqjM (C26D, I69T) was PCR amplified with primers YqjM-EcoRI-F (gctgctgaattcattaaagaggagaaaggtaccatgGCCAGAAAATTATTTACACCTAT) and YqjM-XbaI-R (gctgcttctagagctagcTTACCAGCCTCTTTCGTATTGAACAG) using pMVL-4 as the template, and then cloned into a pZE vector at EcoRI and XbaI sites to form the plasmid pZE-yqjM (C26D, I69T).

Vectors (pZE-his6-OYE2 and pZE-his6-yqjM (C26D, I69T)) containing an *n*-terminal Hexa-Histidine (6His) affinity tag were constructed for enzyme purification and characterization. OYE2 gene was amplified by PCR with primers hisOYE2-BamHI-F (ggatcgcatcaccatcaccatcacggatccATGCCATTTGTTAAGGACTTTAAGCCACAg) and hisOYE2-XbaI-R (ttttatttgatgcctctagaTTAATTTTTGTCCCAACCGA) and then inserted into a pZE vector to form pZE-his6-OYE2. YqjM (C26D, I69T) was amplified by PCR with primers hisYqjM-BamHI-F

(ggatcgcatcaccatcaccatcacggatccatgGCCAGAAAATTATTTACACCTATTACA) and hisYqjM-XbaI-R (ttttatttgatgcctctagattaCCAGCCTCTTTCGTATT) using pMVL-4 as the template, and then cloned into a pZE vector to form the plasmid pZE-his6-yqjM (C26D, I69T).

5.4 Fermentation methods

5.4.1 Batch Fermentations:

Anhydromevalonate, used as a substrate for all fermentation reactions and enzyme assays, was produced using the methods previously described[127]. For shake flask fermentation, 125 ml conical flasks containing 0.5 g $CaCO_3$ were autoclaved and dried. Then 5.0 ml of M9 medium supplemented with yeast extract (5 g/l), glucose (to a final concentration of 40 g/l), IPTG (0.1mM), anhydromevalonate (1 g/l), and ampicillin (100 mg/l) were added to the sterilized shake flask. The additional glucose was supplied to support cell growth and to provide the reducing power for reductases OYE2 or YqjM (C26D, I69T). The shaker flasks were inoculated with overnight cultures of the appropriate recombinant strain in 2×YT medium (200 µl) and then incubated in a 30 °C shaker for 72 h with a shaker speed of 250 rpm.

5.4.2 Fed-batch Fermentations:

Fed-batch fermentations were conducted in 1.3-L bench-top bioreactor (New Brunswick Bioflo® 115). The primary culture media used for fed batch fermentations was composed of glucose (10 g/l), K_2HPO_4 (7.5 g/l), $MgSO_4 \cdot 7H_2O$ (2 g/l), citric acid monohydrate (2

g/l), ferric ammonium citrate (0.3 g/l), yeast extract (20 g/l), sulfuric acid (98%, 0.8 ml L^{-1}), ampicillin (0.1 g/l), 1000X modified trace metal solution (1 ml L^{-1}), and vitamin solution (1ml L^{-1}). The 1000X modified trace metal solution contained NaCl (10 g/l), citric acid (40 g/l), $ZnSO_4 \cdot 7H_2O$ (1.0 g/l), $MnSO_4 \cdot H_2O$ (30 g/l), $CuSO_4 \cdot 5H_2O$ (0.1 g/l), H_3BO_3 (0.1 g/l), $Na_2MoO_4 \cdot 2H_2O$ (0.1 g/l), $FeSO_4 \cdot 7H_2O$ (1 g/l), and $CoCl_2 \cdot 6H_2O$ (1 g/l). The vitamin solution was composed of thiamine hydrochloride (1 g/l), (+)-biotin (1 g/l), nicotinic acid (1 g/l), pyridoxine hydrochloride (4 g/l). Inoculum was prepared by adding 1% overnight pre-culture to a sterile shake flask containing 50 ml LB medium and 0.1g/l ampicillin. This flask was incubated at 37 °C until the contents reached an optical density (OD_{600}) of 1.0. The cell solution was then transferred to the bench-top bioreactor and culture media was added to bring the initial volume to 0.5 liter. The reactor was incubated in batch mode at 37°C until the OD_{600} reached 6.0, Then the temperature was decreased to 30 °C and IPTG (to a concentration of 0.3 mM) was added. Following induction with IPTG, a substrate solution containing AMVL (100 g/l) in water was fed into the bioreactor to reach a concentration of 1 g/l. A second solution comprised of glucose (600 g/l), K_2HPO_4 (7.4 g/l), ampicillin (0.1 g/l), and IPTG (0.3 mM), modified trace metal solution (1 ml/l), and vitamin solution (8 ml/l), was fed at a rate determined by the dissolved oxygen (DO) level. Throughout the fermentation, the pH was maintained (at ~6.8) via addition of a 26 wt.% aqueous NH_4OH solution. The DO level was maintained above 10% by adjusting agitation rate (from 300 to 800 rpm). The airflow rate was maintained at 0.5 vvm in order to provide oxygen for cells.

Throughout the fermentation, concentrations of starting materials and of metabolites were monitored using HPLC.

5.5 Protein expression and purification

The BL21 *E. coli* strain was transformed with the His-tagged plasmids, pZE-his6-OYE2 or pZE-his6-yqjM (C26D, I69T). The recombinant cells were inoculated from an overnight pre-culture at 1/100 dilution and grown in 500 ml of LB medium containing ampicillin (100 mg/l) at 30 °C. After the OD_{600} reached 0.6, IPTG (0.5mM) was added. Following induction, the cells were incubated at 30 °C overnight. Then the cells were harvested by centrifugation. All the subsequent steps were carried out at 4 °C to prevent protein degradation. To lyse the cells, the pellets were resuspended in ~15 ml lysis buffer (composed of 50 mM Tris-HCl, 100 mM NaCl, 10 mM imidazole, 5% glycerol, 1 mM DTT, pH=7.6) and sonicated using a Heat Systems Ultrasonics W-225 Sonicator. The extracts were clarified by centrifuging at 10,733 rcf for 15 minutes. The supernatants were passed through a gravity column containing 4 ml of HisPur Ni-NTA resin (Thermo Scientific). The resin was washed twice with 10 ml of wash buffer (50 mM Tris-HCl, 100 mM NaCl, and 25mM imidazole, pH=7.6). The bound protein was eluted with 15 ml of elution buffer (50 mM Tris-HCl, 250 mM NaCl, and 250 mM imidazole, pH=8.0). The final protein sample was then purified using buffer-exchanged with Amicon Ultra centrifugal filters (Millipore) and a storage buffer (50M Tris-HCl, 2mM $MgSO_4$, 20% glycerol, pH=8.0). The purified protein concentration was determined by a Quick Start Bradford protein assay kit (Bio-Rad Laboratories).

5.6 Enzymatic activity assays

The reductase activities of OYE2 and YqjM (C26D, I69T) were assessed using NADPH initial consumption rates as determined using a coupled assay. The assay solution was comprised of 1mM NADPH, and 0.1-100 mM AMVL in 100 μl of 100 mM Tris-HCl buffer (pH=7.5) with 5 mM $MgSO_4$. Purified enzyme (100 nM of either OYE2 or YqjM (C26D, I69T)) was added to start the reaction and the NADPH consumption rate was monitored spectroscopically. For each enzyme, three replicate assays were conducted. These data were used to fit the parameters of the Michaelis-Menten kinetic model, k_{cat} and K_M, by nonlinear least-squares regression using the intrinsic *nlinfit* function of the Matlab software program.

5.7 Enzyme ligand docking

All molecular and enzyme docking was performed with Libdock utilizing Discovery Studio 4.1 software. Both PDB files of OYE2 (PDB ID:4GXM) and YqjM (PDB ID:1Z42) were downloaded from protein data bank[196]. The active sites denoted in crystal structure were defined as the binding site for Libdock. Since the crystal structure of YqjM (C26D, I69T) has not been reported, we used sequence alignment and homology modeling in Discovery Studio 4.1 software to build the structure of this mutant YqjM. Subsequently, Libdock was used to analyze the interaction between OYE2 or YqjM (C26D, I69T) and anhydromevalonolactone.

5.8 Synthetic methods

5.8.1 Anhydromevalonolactone

The pathway for enzymatic synthesis of mevalonate from glucose has previously been reported[127]. The mevalonate fermentation broth (containing 28 g/l mevalonate as determined by HPLC) was filtered through activated charcoal to remove cell debris and colored impurities. Then concentrated H_2SO_4 (200 ml) was slowly charged into the filtered fermentation broth (2 l) under vigorous stirring. The acid solution was refluxed for 15 h, then cooled and extracted with chloroform. The chloroform was removed under reduced pressure and the crude product distilled to yield pure AMVL (39 grams, 82% gravimetric yield).

5.8.2 Purification of (-)-β-methyl-δ-valerolactone

To the fermentation broth (1l) chloroform (200 ml) was added to extract residual AMVL. Among numerous potential green solvents, ethyl acetate or isobutanol may be viable, less toxic, alternatives to chloroform. The aqueous layer was carefully acidified with H_2SO_4 (to pH ~2), then extracted using chloroform (3X 200 ml). The organic layer was dried with $MgSO_4$, filtered, and concentrated under reduced pressure to obtain crude (-)-MVL (0.5 g). Prior to polymerization this monomer was dried over calcium hydride and distilled. ^{1}H NMR: 4.47-4.36 ppm (m, 1H $CH_2C\mathbf{H_2}OR$) 4.47-4.36 ppm (m, 1H $CH_2C\mathbf{H_2}OR$) 2.76-2.60 ppm (m, 1H $CO_2C\mathbf{H_2}CHCH_3$), 2.180-2.05 (m, 1H $CO_2CH_2CHCH_3C\mathbf{H_2}$), 1.97-1.87 ppm (m, 1H $CO_2C\mathbf{H_2}CHCH_3$), 1.60-1.44 ppm (m, 1H $CH_2C\mathbf{H}CH_3CH_2$), 1.1 ppm (d, 3H $CO_2CH_2CH\mathbf{CH_3}$), $[\alpha^{23}]_D$ = -25.7 ($CHCl_3$).

5.8.3 (+)-β-methyl-δ-valerolactone

(+)-MVL was obtained using the method described above except the crude MVL was purified by column chromatography (silica gel, 30:70 ethyl acetate: hexanes), dried over $MgSO_4$, and filtered. ^{1}H NMR: 4.47-4.36 ppm (m, 1H $CH_2C\mathbf{H_2}OR$) 4.47-4.36 ppm (m, 1H $CH_2C\mathbf{H_2}OR$) 2.76-2.60 ppm (m, 1H $CO_2C\mathbf{H_2}CHCH_3$), 2.180-2.05 (m, 1H $CO_2CH_2CHCH_3C\mathbf{H_2}$), 1.97-1.87 ppm (m, 1H $CO_2C\mathbf{H_2}CHCH_3$), 1.60-1.44 ppm (m, 1H $CH_2C\mathbf{H}1CH_2$), 1.1 ppm (d, 3H $CO_2CH_2CH\mathbf{CH_3}$), $[\alpha^{23}]_D$ = +20.9 ($CHCl_3$).

5.8.4 Synthesis of poly((-)-β-methyl-δ-valerolactone)

Benzyl alcohol (2.7 mg) was mixed with (-)-MVL (0.5345 grams) in a glass vial with magnetic stirring. When fully dissolved diphenyl phosphate (1.7 mg) was added to initiate the polymerization. The reaction was stirred for 8 h at room temperature. The obtained polymer was purified by precipitation in methanol from dichloromethane/chloroform and subsequently dried. ^{1}H NMR: kg mol^{-1}; 7.37-7.33 ppm (m, 5H Ar-**H**), 5.14 ppm (s, 2H Ar-$C\mathbf{H_2}O$), 4.19-4.05 ppm (170 H, $C\mathbf{H_2}OR$), 3.73-3.62 ppm (3.3 H, $C\mathbf{H_2}OH$), 2.36-2.30 ppm (m, 80H $CO_2C\mathbf{H_2}CH$), 2.20-2.15 ppm (m, 80H $CO_2C\mathbf{H_2}CH_2$), 2.14-2.03 ppm (m, 95H, $CH_2C\mathbf{H}CH_3CH_2$), 1.74-1.65 ppm (m, 87H $CH_2CHCH_3\mathbf{CH_2}$), 1.57-1.48 ppm (m, 87H $CH_2CHCH_3\mathbf{CH_2}$), 1.03 ppm (d, 259H $CH_2CHC\mathbf{H_3}CH_2$); MALLS-SEC: M_n = 7.8 kg mol^{-1}, Đ = 1.03; $[\alpha^{23}]_D$ = -7.5 ($CHCl_3$); DSC: T_g = -52.5 °C.

6. Supporting Information

Table 5.S1| Strains and plasmids used in this study.

Name	Relevant Genotype	Reference
Strains		
BW25113	*rrnB*$_{T14}$ ΔlacZ$_{WJ16}$*hsdR514* Δ*araBAD*$_{AH33}$ Δ*rhaBAD*$_{LD78}$	
XL10-Gold	Tet^{R}Δ (*mcrA*)183 Δ (*mcrCB-hsaSMR-mrr*)173 *endA1supE*44 *thi-1 recA1*	Stratagene
BL21	*E. coli* B F- *dcmompThsdS*(r_B- m_B-) gal [malB$^+$]$_{K-12}$(λ^S)	[71]
Plasmids		
pMEV-1	ColE1 origin, Amp^R, P$_L$*lacO*$_1$: *atoB-mvaS-mvaE*	[127]
pMVL-4	P15A origin, Kan^R, P$_L$*lacO*$_1$: *sidI-sidH-yqjM (C26D, I69T)*	[127]
pZE-OYE2	ColE1 origin, Amp^R, P$_L$*lacO*$_1$: *OYE2*	This study
pZE-yqjM (C26D, I69T)	ColE1 origin, Amp^R, P$_L$*lacO*$_1$: *yqjM (C26D, I69T)*	This study
pZE-his6-OYE2	ColE1 origin, Amp^R, P$_L$*lacO*$_1$: 6xhis-*OYE2*	This study
pZE-his6-yqjM (C26D, I69T)	ColE1 origin, Amp, P$_L$*lacO*$_1$: 6xhis- *yqjM (C26D, I69T)*	This study

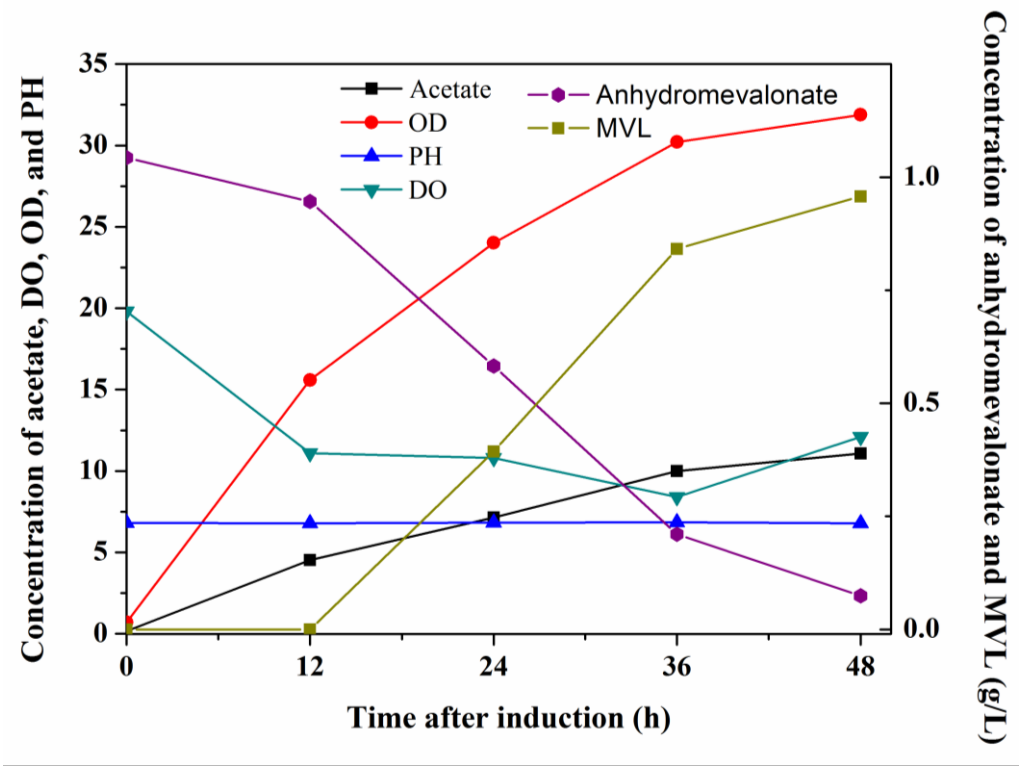

Figure 5.S1| Scale-up fermentation results with OYE2 in a 1.3-l bioreactor.

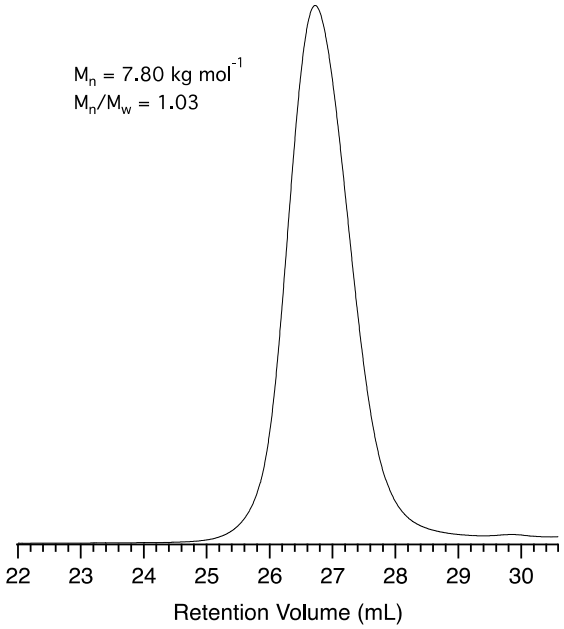

Figure 5.S2| MALLS-SEC of poly(-)-MVL prepared from polymerization of (-)-MVL.

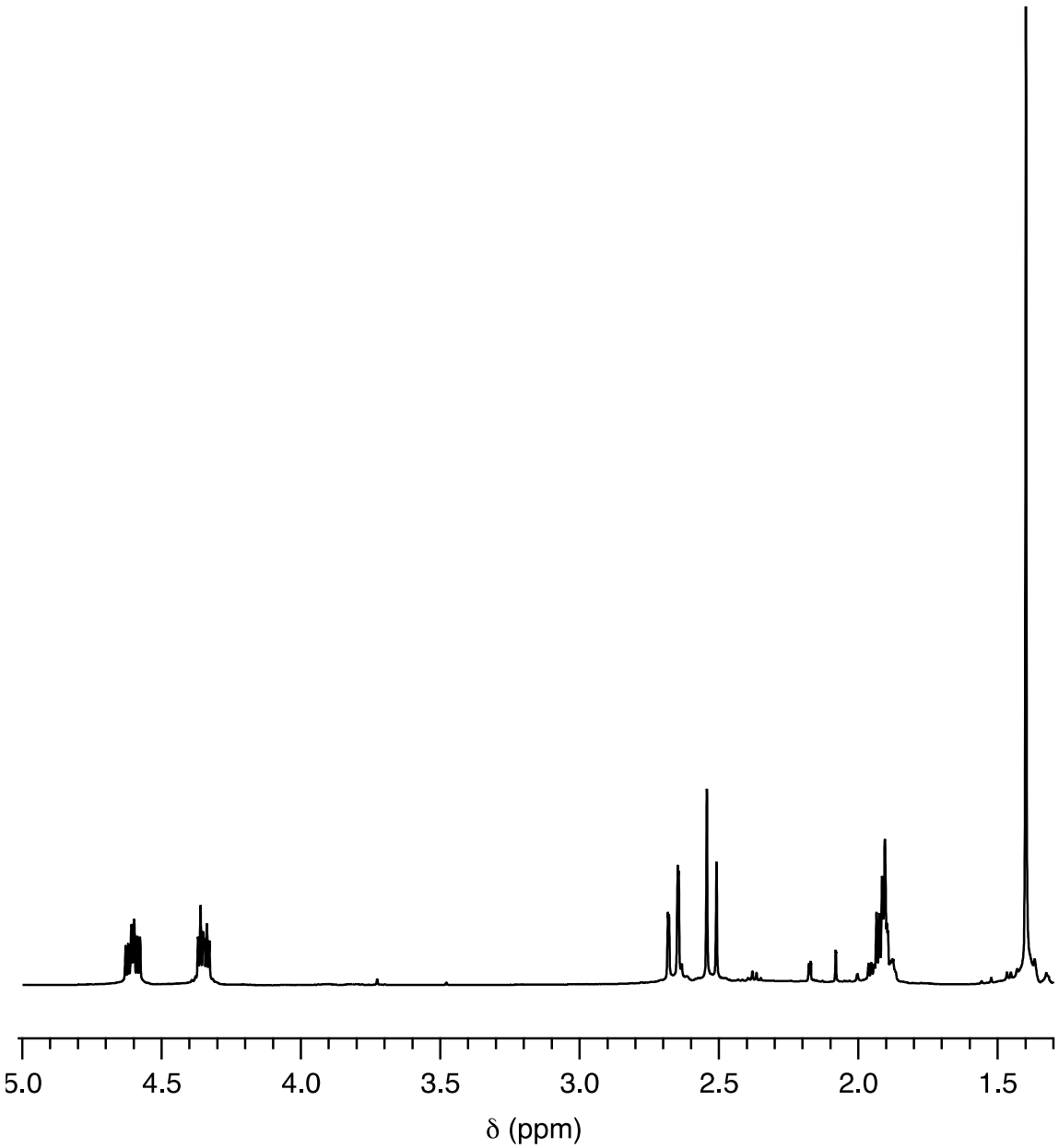

Figure 5.S3| ^{1}H NMR spectra of mevalonolactone isolated by extraction from fermentation broth.

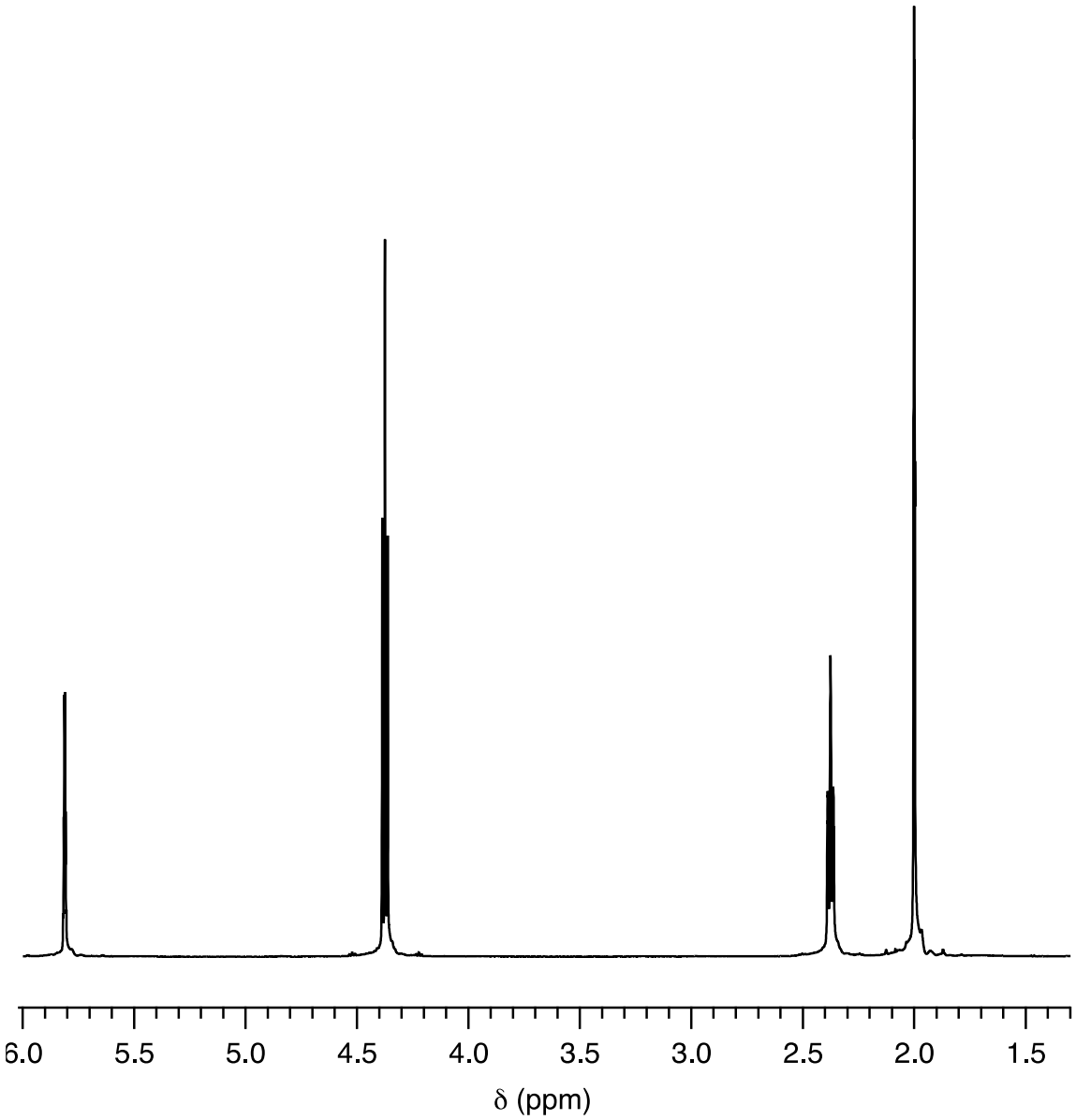

Figure 5.S4| ^{1}H NMR spectra of anhydromevalonolactone prepared by acid catalyzed dehydration of mevalonolactone.

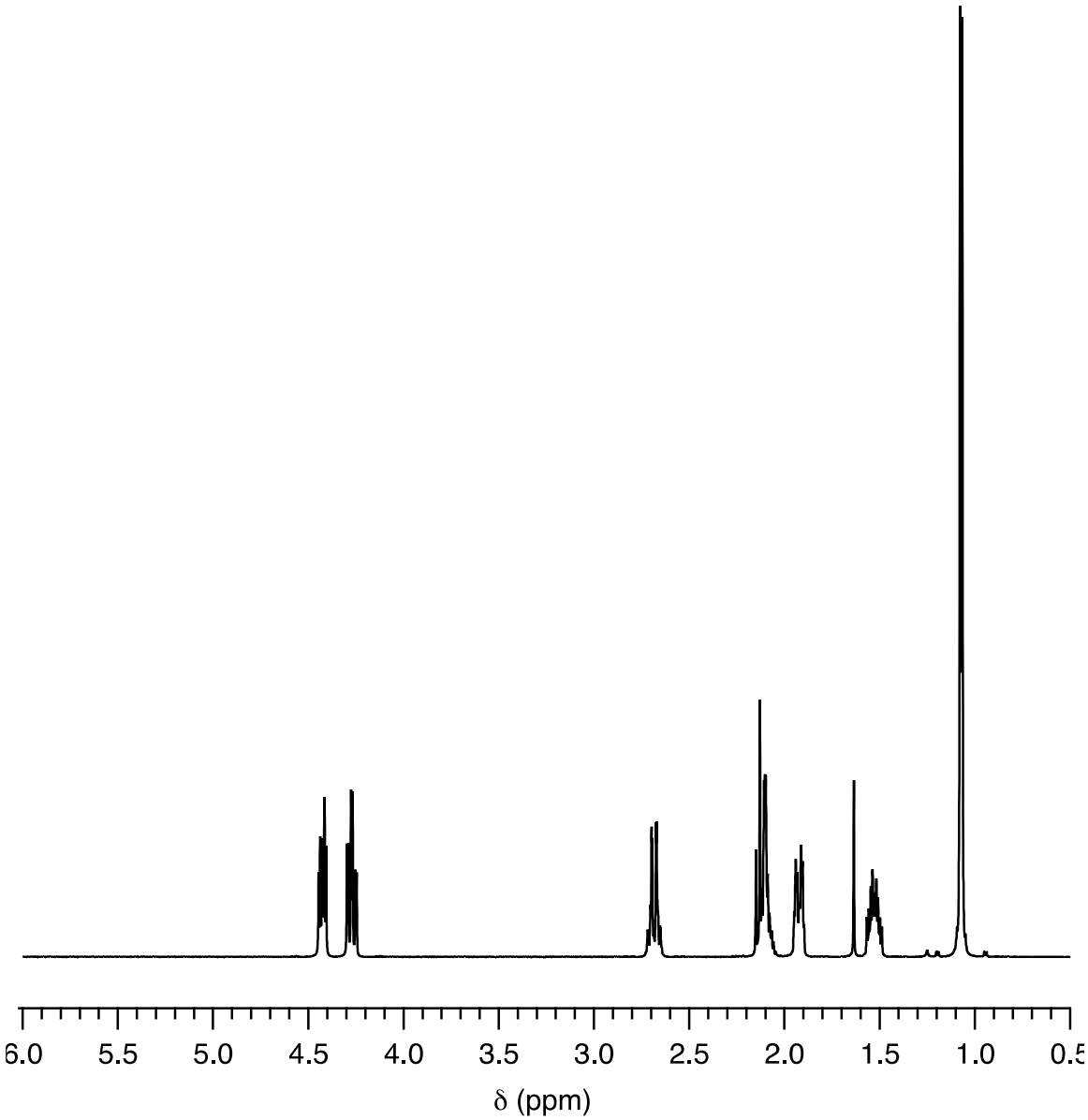

Figure 5.S5| ^{1}H NMR spectra of (±)-MVL prepared by hydrogenation of mevalonolactone.

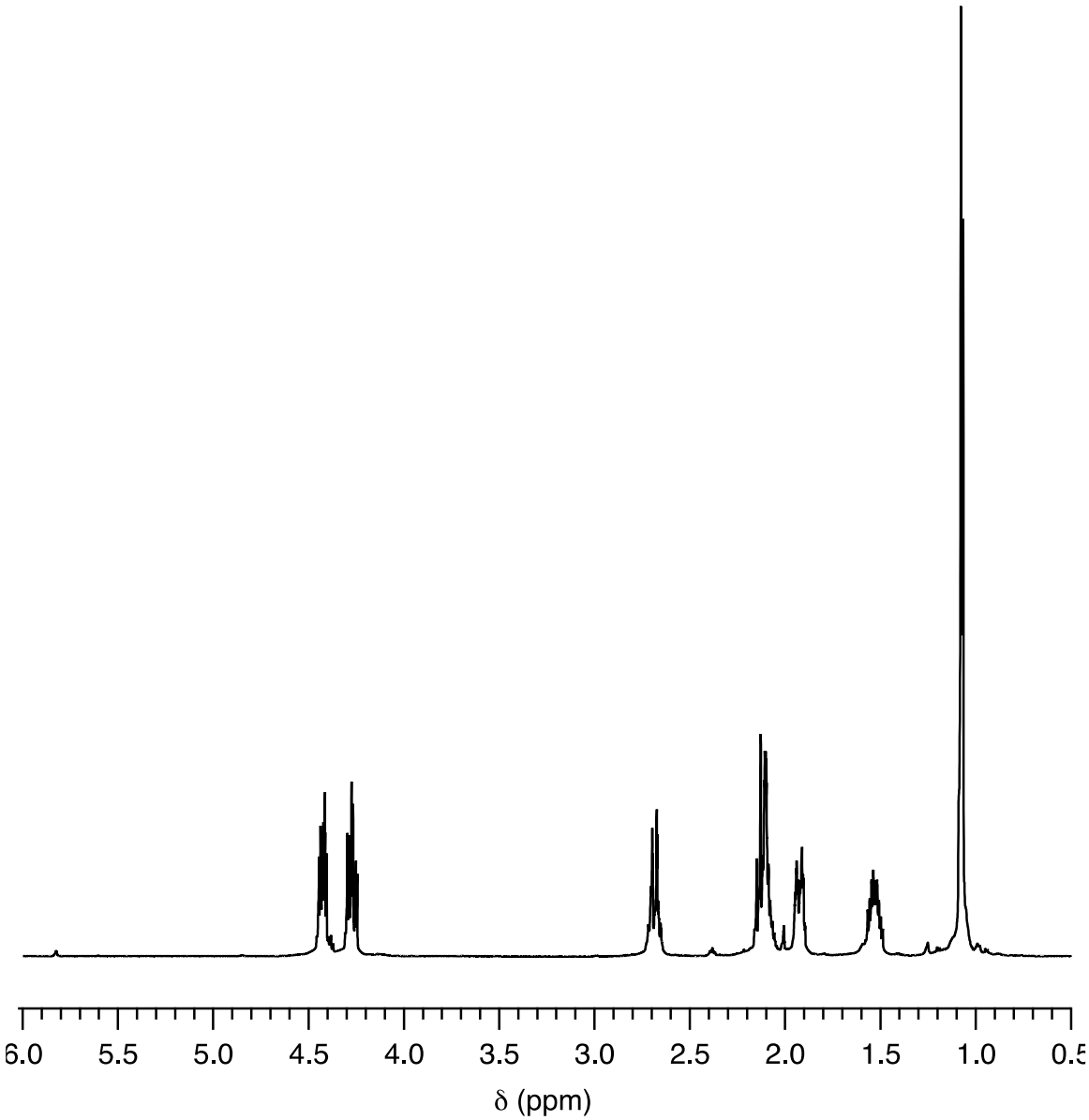

Figure 5.S6| ^{1}H NMR spectra of (-)-MVL prepared from anhydromevalonolactone using OYE2.

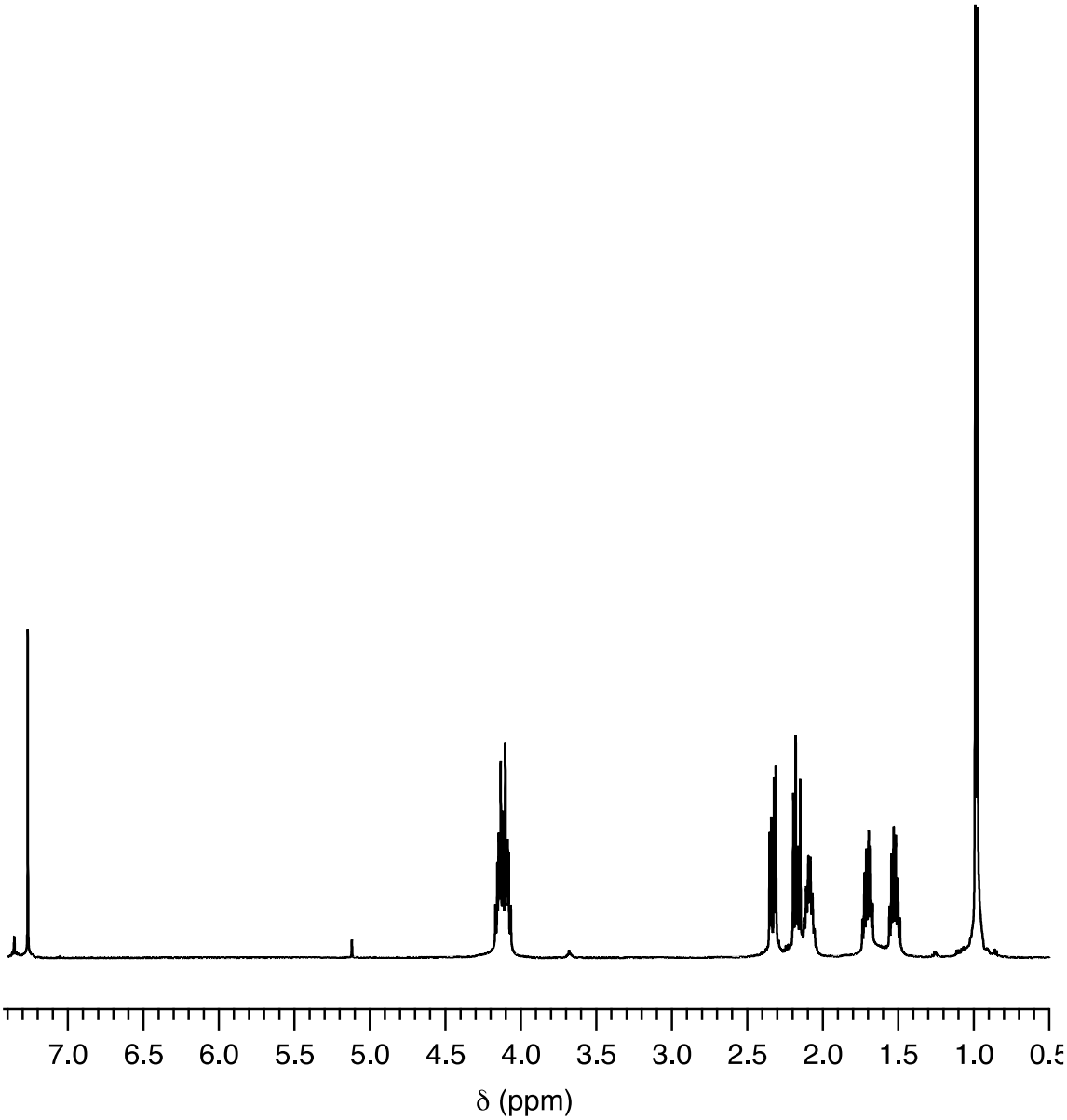

Figure 5.S7| ^{1}H NMR spectra of poly(-)-MVL prepared from polymerization of (-)-MVL.

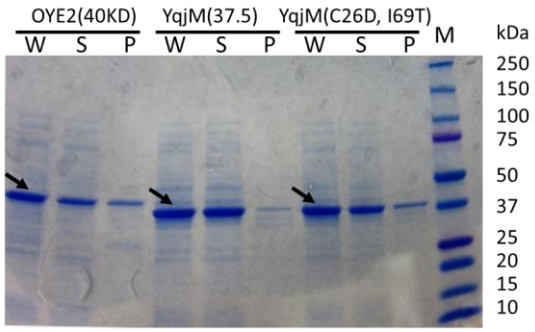

Figure 5.S8| Picture of SDS-PAGE with protein OYE2, YqjM and YqjM (C26D, I69T). these proteins were expressed in BW25113 bearing pZE-OYE2, pZE-YqjM and pZE-YqjM (C26D, I69T) respectively. After induction, the cell was collected and sonicated to release all the proteins, and then centrifuged to separate soluble proteins in supernatant and insoluble proteins in pellet. The target protein is indicated by arrow. W: all the proteins from the whole cell; S: the soluble proteins from the supernatant; P: the insoluble proteins from the pellet. M: Bio-Rad Precision Plus Duel Color Standards;

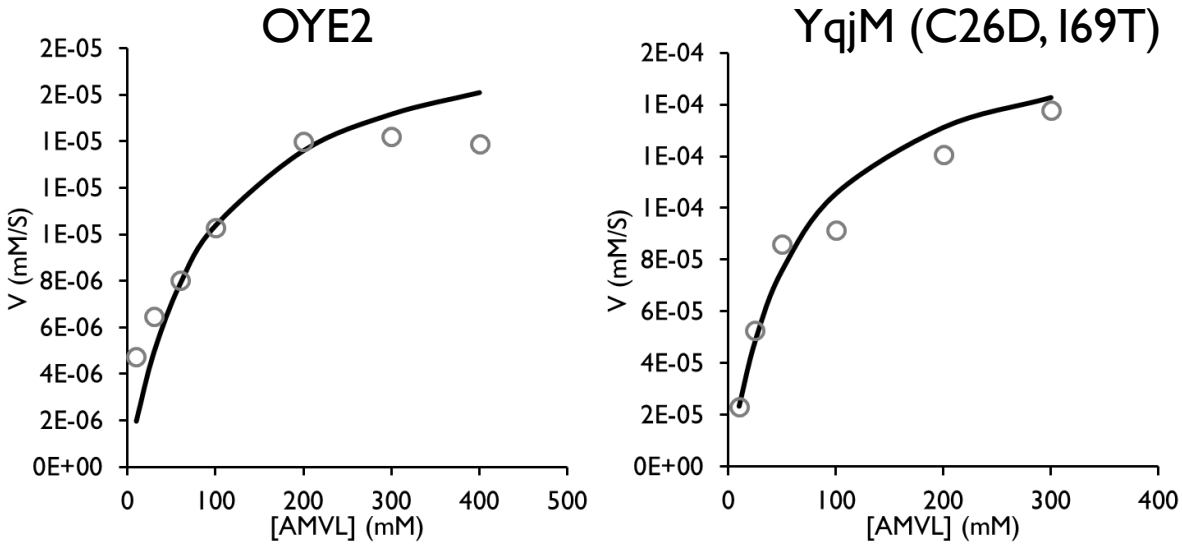

Figure 5.S9| Representative Michaelis- Menten plots of OYE2 and YqjM (C26D, I69T). Purified OYE2 and YqjM (C26D, I69T) were used at a concentration of 0.5 μM with varying AMVL concentrations and the NADPH consumption rate was used to determine the reaction rate. From the representative plots, the kinetic parameters for OYE are: k_{cat}=0.04 s^{-1} and K_m=90 mM and the kinetic parameters for YqjM (C26D, I69T) are: k_{cat}=0.35 s^{-1} and K_m=64.1 mM.

Chapter 5. Concluding Remarks

Petroleum is the major material basis of modern society. With increasing demand and dwindling reserves, there is a pressing need to find alternative resources for fuels and chemicals. Metabolic engineering has the potential to be a key player in facilitating the transition from traditional chemical production to a green and sustainable process[197, 198, 199]. For the past decade, this powerful biotechnology has been successful in converting renewable sugars into various fuels[8, 9, 54, 200, 201] and chemicals[8, 202, 203, 204, 205, 206, 207, 208]. However, the intrinsic microbial metabolism can only be used to produce a limited amount of products. My thesis work aimed to expand the capabilities of metabolism to enable biosynthesis of valuable daily chemicals by designing and constructing novel biosynthetic pathways in *E. coli*.

I have engineered a total biosynthetic platform in *E. coli* for ester production which was demonstrated by isobutyl acetate (IBAc) and isoamyl acetate (IAAc) production. To fulfill the platform, the key enzyme is AAT which catalyzes the esterification reaction. Most AAT enzymes have not been well characterized before. Therefore, through extensive investigation in metabolic reaction databases, I identified five AAT candidates from floral plants, baker's yeast, and strawberries. Small-scale fermentation was carried out to examine the activities of these AATs. Among them, a highly efficient AAT, ATF1 from *S. cerevisiae* was found which enabled successful production of both IBAc and IAAc with the highest product concentrations. These results are the earliest demonstrations of direct esters production from renewable sugars by engineered *E. coli*. To further test the production platform in a larger scale, I used the

optimized IBAc producing strain in a 1.3-L bench-top bioreactor and 36 g/l of IBAc was produced in 72 h. This proved the feasibility for the production scale-up of this valuable chemical.

To efficiently convert lignocellulosic feedstock into TCA cycle derivatives, I engineered an unconventional "shortcut" metabolism into *E. coli* and exploited to produce value-added chemicals such as BDO and mesaconate. Conventionally, pentoses derived from lignocellulosic biomass were converted via lengthy and complex glycolysis and PPP which result in low production yield. These alternative pathways for pentose assimilation have been discovered in some rare bacteria or archaea species which can convert pentoses into a TCA cycle intermediate, 2-ketoglutarate, in only 5 reaction steps with higher yield. Nonetheless, the detailed genetic and biochemical information of gene clusters involved in the "shortcut" metabolism is scattered and incomplete, limiting the understanding and engineering of these new pathways.

Therefore, my research project focused on characterizing the enzymes and introducing these nonphosphorylative pathways into *E. coli*. To demonstrate the viability of these novel metabolic pathways as a generally useful biosynthetic platform, BDO and mesaconate production from two pentoses, D-xylose and L-arabinose, was examined. Before applying these "shortcut" pathways for production, I purified and characterized the key enzymes to confirm the desired activities and provide important kinetic parameters. Then the production pathway was designed by diverting from the intermediates. I screened different combinations of upstream and downstream enzymes and performed protein engineering and metabolic engineering to improve the production.

In summary, I achieved high-level productions of BDO from both D-xylose (12 g/l) and L-arabinose (15.6 g/l) in 1.3-l bioreactors. Similarly, mesaconate was successfully produced via this metabolism at 14.8 g/l from a mixture of D-xylose and L-arabinose. Hence, I demonstrated not only the practicability but also the high efficiency of these newly designed pathways.

Zhang lab has previously developed a synthetic pathway to produce the promising monomer MVL; however, the properties of the polymers produced from optically active monomers have not been investigated yet. Therefore, I helped develop a chemo-enzymatic process to produce (+)-MVL and (-)-MVL by two different enol reductases OYE2 and YqjM (C26D, I69T). I investigated the bindings of these two enzymes to further understand the mechanisms. (-)-MVL production from OYE2 was scaled up due to its higher selectivity and conversion (96% ee and 99% conversion). We found that the isotactic polymer produced from (-)-MVL was amorphous with a low glass transition temperature at -52 °C.

Overall, the work shown in this thesis demonstrates the design and implementation of novel metabolic pathways for biosynthesis of various commodity chemicals. Multiple strategies have been presented throughout the body of this thesis for future perspectives of this research. The ester production platform can be further expanded to produce other esters and more AATs should be screened and optimized for the production of each specific target ester. The nonphosphorylative metabolism can be applied for biosynthesis of other TCA cycle derivatives by different downstream modification. For upstream part, other substrates such as pentoses and hydroxyl-proline

can be utilized by introducing their respective nonphosphorylative pathway. Finally, besides deeper understanding of key pathway enzymes, further optimization of total biosynthesis of MVL is critical for an economically feasible process. In conclusion, my thesis research on expanding *E. coli* metabolism has realized the production of a variety of value-added new bioproducts such as esters, BDO, mesaconate, and optically active MVL which has helped lay the foundation of future development of economically feasible bioproducts.

Bibliography

1. Ren, N.; Wang, A.; Cao, G.; Xu, J.; Gao, L. Bioconversion of lignocellulosic biomass to hydrogen: Potential and challenges. *Biotechnol. Adv.* **2009,** *27* (6), 1051-1060.

2. Schubert, C. Can biofuels finally take center stage? *Nat. Biotechnol.* **2006,** *24* (7), 777-784.

3. Legras, J. L.; Merdinoglu, D.; Cornuet, J. M.; Karst, F. Bread, beer and wine: Saccharomyces cerevisiae diversity reflects human history. *Mol. Ecol.* **2007,** *16* (10), 2091-2102.

4. Kardos, N.; Demain, A. L. Penicillin: the medicine with the greatest impact on therapeutic outcomes. *Appl. Microbiol. Biotechnol.* **2011,** *92* (4), 677-687.

5. Atsumi, S.; Higashide, W.; Liao, J. C. Direct photosynthetic recycling of carbon dioxide to isobutyraldehyde. *Nat. Biotechnol.* **2009,** *27* (12), 1177-1180.

6. Stephanopoulos, G.; Aristidou, A. A.; Nielsen, J. H.; Nielsen, J. *Metabolic engineering: principles and methodologies*; Academic Press 1998.

7. Demain, A. L. Microbial biotechnology. *Trends Biotechnol.* **2000,** *18* (1), 26-31.

8. Atsumi, S.; Hanai, T.; Liao, J. C. Non-fermentative pathways for synthesis of branched-chain higher alcohols as biofuels. *Nature* **2008,** *451* (7174), 86-89.

9. Steen, E. J.; Kang, Y.; Bokinsky, G.; Hu, Z.; Schirmer, A.; McClure, A.; Del Cardayre, S. B.; Keasling, J. D. Microbial production of fatty-acid-derived fuels and chemicals from plant biomass. *Nature* **2010,** *463* (7280), 559-562.

10. Holm, M. S.; Saravanamurugan, S.; Taarning, E. Conversion of sugars to lactic acid derivatives using heterogeneous zeotype catalysts. *Science* **2010,** *328* (5978), 602-605.

11. Zha, W.; Shao, Z.; Frost, J. W.; Zhao, H. Rational pathway engineering of type I fatty acid synthase allows the biosynthesis of triacetic acid lactone from D-glucose in vivo. *J. Am. Chem. Soc.* **2004,** *126* (14), 4534-4535.

12. Yan, Y.; Chemler, J.; Huang, L.; Martens, S.; Koffas, M. A. G. Metabolic engineering of anthocyanin biosynthesis in Escherichia coli. *Appl. Environ. Microbiol.* **2005,** *71* (7), 3617-3623.

13. Pfeifer, B. A.; Admiraal, S. J.; Gramajo, H.; Cane, D. E.; Khosla, C. Biosynthesis of complex polyketides in a metabolically engineered strain of E. coli. *Science* **2001,** *291* (5509), 1790-2.

14. Causey, T. B.; Zhou, S.; Shanmugam, K. T.; Ingram, L. O. Engineering the metabolism of Escherichia coli W3110 for the conversion of sugar to redox-neutral and oxidized products: Homoacetate production. *Proc. Natl. Acad. Sci. U.S.A.* **2003,** *100* (3), 825-832.

15. Ikeda, M. Amino acid production processes. *Adv. Biochem. Eng. Biotechnol.* **2002,** *79*, 1-35.

16. Leuchtenberger, W.; Huthmacher, K.; Drauz, K. Biotechnological production of amino acids and derivatives: current status and prospects. *Appl. Microbiol. Biotechnol.* **2005,** *69* (1), 1-8.

17. Hazelwood, L. A.; Daran, J. M.; van Maris, A. J. A.; Pronk, J. T.; Dickinson, J. R. The Ehrlich pathway for fusel alcohol production: a century of research on Saccharomyces cerevisiae metabolism? *Appl. Environ. Microbiol.* **2008,** *74* (8), 2259-2266.

18. Connor, M. R.; Cann, A. F.; Liao, J. C. 3-Methyl-1-butanol production in Escherichia coli: random mutagenesis and two-phase fermentation. *Appl. Microbiol. Biotechnol.* **2010,** *86* (4), 1155-1164.

19. Atsumi, S.; Wu, T.-Y.; Eckl, E.-M.; Hawkins, S.; Buelter, T.; Liao, J. Engineering the isobutanol biosynthetic pathway in Escherichia coli by comparison of three aldehyde reductase/alcohol dehydrogenase genes. *Appl. Microbiol. Biotechnol.* **2010,** *85* (3), 651-657.

20. Cann, A. F.; Liao, J. C. Production of 2-methyl-1-butanol in engineered Escherichia coli. *Appl. Microbiol. Biotechnol.* **2008,** *81* (1), 89-98.

21. Zhang, K.; Sawaya, M. R.; Eisenberg, D. S.; Liao, J. C. Expanding metabolism for biosynthesis of nonnatural alcohols. *Proc. Natl. Acad. Sci. U.S.A.* **2008,** *105* (52), 20653-20658.

22. Marcheschi, R. J.; Li, H.; Zhang, K.; Noey, E. L.; Kim, S.; Chaubey, A.; Houk, K.; Liao, J. C. A synthetic recursive "+ 1" pathway for carbon chain elongation. *ACS Chem. Biol.* **2012,** *7* (4), 689-697.

23. Dhande, Y. K. Biosynthetic routes to short-chain carboxylic acids and their hydroxy derivatives. University of Minnesota 2013.

24. Xiong, M.; Yu, P.; Wang, J.; Zhang, K. Improving engineered Escherichia coli strains for high-level biosynthesis of isobutyrate. *AIMS Bioeng.* **2015,** *2* (2), 60-74.

25. Baez, A.; Cho, K. M.; Liao, J. C. High-flux isobutanol production using engineered Escherichia coli: a bioreactor study with in situ product removal. *Appl. Microbiol. Biotechnol.* **2011,** *90* (5), 1681-1690.

26. Kalscheuer, R.; Stölting, T.; Steinbüchel, A. Microdiesel: Escherichia coli engineered for fuel production. *Microbiol.* **2006,** *152* (9), 2529-2536.

27. Liu, T.; Vora, H.; Khosla, C. Quantitative analysis and engineering of fatty acid biosynthesis in E. coli. *Metab. Eng.* **2010,** *12* (4), 378-386.

28. Schirmer, A.; Rude, M. A.; Li, X.; Popova, E.; del Cardayre, S. B. Microbial biosynthesis of alkanes. *Science* **2010,** *329* (5991), 559-562.

29. Rude, M. A.; Baron, T. S.; Brubaker, S.; Alibhai, M.; Del Cardayre, S. B.; Schirmer, A. Terminal olefin (1-alkene) biosynthesis by a novel P450 fatty acid decarboxylase from Jeotgalicoccus species. *Appl. Environ. Microbiol.* **2011,** *77* (5), 1718-1727.

30. Picataggio, S.; Rohrer, T.; Deanda, K.; Lanning, D.; Reynolds, R.; Mielenz, J.; Eirich, L. D. Metabolic engineering of Candida tropicalis for the production of long-chain dicarboxylic acids. *Nat. Biotech.* **1992,** *10* (8), 894-898.

31. Lu, W.; Ness, J. E.; Xie, W.; Zhang, X.; Minshull, J.; Gross, R. A. Biosynthesis of monomers for plastics from renewable oils. *J. Am. Chem. Soc.* **2010**.

32. Dellomonaco, C.; Clomburg, J. M.; Miller, E. N.; Gonzalez, R. Engineered reversal of the β-oxidation cycle for the synthesis of fuels and chemicals. *Nature* **2011,** *476* (7360), 355-359.

33. Shen, C. R.; Lan, E. I.; Dekishima, Y.; Baez, A.; Cho, K. M.; Liao, J. C. Driving forces enable high-titer anaerobic 1-butanol synthesis in Escherichia coli. *Appl. Environ. Microbiol.* **2011,** *77* (9), 2905-2915.

34. Dekishima, Y.; Lan, E. I.; Shen, C. R.; Cho, K. M.; Liao, J. C. Extending carbon chain length of 1-butanol pathway for 1-hexanol synthesis from glucose by engineered Escherichia coli. *J. Am. Chem. Soc.* **2011**.

35. Chappell, J. Biochemistry and molecular biology of the isoprenoid biosynthetic pathway in plants. *Annu. Rev. Plant Physiol. Mol. Biol.* **1995,** *46*, 521-547.

36. McGarvey, D. J.; Croteau, R. Terpenoid metabolism. *Plant Cell* **1995,** *7*, 1015-1026.

37. Withers, S. T.; Gottlieb, S. S.; Bonny Lieu, F.; Newman, J. D.; Keasling, J. D. Identification of isopentenol biosynthetic genes from Bacillus subtilis by a screening method based on isoprenoid precursor toxicity. *Appl. Environ. Microbiol.* **2007,** *73* (19), 6277-6283.

38. Wang, C. L.; Yoon, S. H.; Shah, A. A.; Chung, Y. R.; Kim, J. Y.; Choi, E. S.; Keasling, J. D.; Kim, S. W. Farnesol production from Escherichia coli by harnessing the exogenous mevalonate pathway. *Biotechnol. Bioeng.* **2010,** *107* (3), 421-429.

39. Miller, B.; Oschinski, C.; Zimmer, W. First isolation of an isoprene synthase gene from poplar and successful expression of the gene in Escherichia coli. *Planta* **2001,** *213* (3), 483-497.

40. Zhang, F.; Rodriguez, S.; Keasling, J. D. Metabolic engineering of microbial pathways for advanced biofuels production. *Curr. Opin. Biotechnol.* **2011,** *22* (6), 775-783.

41. Martin, D. M.; Fäldt, J.; Bohlmann, J. Functional characterization of nine Norway spruce TPS genes and evolution of gymnosperm terpene synthases of the TPS-d subfamily. *Plant Physiol.* **2004,** *135* (4), 1908-1927.

42. Peralta-Yahya, P. P.; Ouellet, M.; Chan, R.; Mukhopadhyay, A.; Keasling, J. D.; Lee, T. S. Identification and microbial production of a terpene-based advanced biofuel. *Nat. Commun.* **2011,** *2*, 483.

43. Ajikumar, P. K.; Xiao, W.-H.; Tyo, K. E. J.; Wang, Y.; Simeon, F.; Leonard, E.; Mucha, O.; Phon, T. H.; Pfeifer, B.; Stephanopoulos, G. Isoprenoid pathway optimization for taxol precursor overproduction in Escherichia coli. *Science* **2010,** *330* (6000), 70-74.

44. Leonard, E.; Ajikumar, P. K.; Thayer, K.; Xiao, W. H.; Mo, J. D.; Tidor, B.; Stephanopoulos, G.; Prather, K. L. J. Combining metabolic and protein engineering of a

terpenoid biosynthetic pathway for overproduction and selectivity control. *Proc. Natl. Acad. Sci. U.S.A.* **2010,** *107* (31), 13654-13659.

45. Ro, D. K.; Paradise, E. M.; Ouellet, M.; Fisher, K. J.; Newman, K. L.; Ndungu, J. M.; Ho, K. A.; Eachus, R. A.; Ham, T. S.; Kirby, J. Production of the antimalarial drug precursor artemisinic acid in engineered yeast. *Nature* **2006,** *440* (7086), 940-943.

46. Westfall, P. J.; Pitera, D. J.; Lenihan, J. R.; Eng, D.; Woolard, F. X.; Regentin, R.; Horning, T.; Tsuruta, H.; Melis, D. J.; Owens, A. Production of amorphadiene in yeast, and its conversion to dihydroartemisinic acid, precursor to the antimalarial agent artemisinin. *Proc. Natl. Acad. Sci. U.S.A.* **2012,** *109* (3), E111-E118.

47. Beekwilder, J.; Alvarez-Huerta, M.; Neef, E.; Verstappen, F. W. A.; Bouwmeester, H. J.; Aharoni, A. Functional characterization of enzymes forming volatile esters from strawberry and banana. *Plant Physiol.* **2004,** *135* (4), 1865-1878.

48. Panda, H. *Perfumes and flavours technology handbook*; Asia Pacific Business Press Inc. 2010.

49. Linak, E. Global solvent report: the green impact. *SRI Consulting* **2006**, 44-46 and 233-234.

50. Vadali, R. V.; Bennett, G. N.; San, K. Y. Applicability of CoA/acetyl-CoA manipulation system to enhance isoamyl acetate production in Escherichia coli. *Metab. Eng.* **2004,** *6* (4), 294-299.

51. Lange, J. P.; Price, R.; Ayoub, P. M.; Louis, J.; Petrus, L.; Clarke, L.; Gosselink, H. Valeric biofuels: a platform of cellulosic transportation fuels. *Angew. Chem.-Int. Edit.* **2010,** *49* (26), 4479-4483.

52. Perry, R. H.; Green, D. W. *Perry's Chemical Engineers' Handbook*; 7th ed.; McGraw-Hill New York, 1997. p 2640.

53. Luli, G. W.; Jarboe, L.; Ingram, L. O. *The development of ethanologenic cacteria for fuel ethanol production*; Amer Soc Microbiology: Washington, 2008. p 129-137.

54. Sheng, J. Y.; Feng, X. Y. Metabolic engineering of yeast to produce fatty acid-derived biofuels: bottlenecks and solutions. *Front. Microbiol.* **2015,** *6*.

55. Alleman, T. L.; Fouts, L.; McCormick, R. L. Quality analysis of wintertime B6-B20 biodiesel blend samples collected in the United States. *Fuel Process. Technol.* **2011,** *92* (7), 1297-1304.

56. Chulalaksananukul, W.; Condoret, J. S.; Combes, D. Kinetics of geranyl acetate synthesis by lipase-catalysed transesterification in n-hexane. *Enzyme Microb. Technol.* **1992,** *14* (4), 293-298.

57. Rojas, V.; Gil, J. V.; Pinaga, F.; Manzanares, P. Studies on acetate ester production by non-Saccharomyces wine yeasts. *Int. J. Food Microbiol* **2001,** *70* (3), 283-289.

58. Watanabe, M.; Fukuda, K.; Asano, K.; Ohta, S. Mutants of bakers yeasts producing a large amount of isobutyl alcohol or isoamyl alcohol, flavor components of bread. *Appl. Microbiol. Biotechnol.* **1990,** *34* (2), 154-159.

59. San, K. Y.; Bennett, G. N.; Berrios-Rivera, S. J.; Vadali, R. V.; Yang, Y. T.; Horton, E.; Rudolph, F. B.; Sariyar, B.; Blackwood, K. Metabolic engineering through cofactor manipulation and its effects on metabolic flux redistribution in Escherichia coli. *Metab. Eng.* **2002,** *4* (2), 182-192.

60. Vadali, R. V.; Horton, C. E.; Rudolph, F. B.; Bennett, G. N.; San, K. Y. Production of isoamyl acetate in ackA-pta and/or ldh mutants of Escherichia coli with overexpression of yeast *ATF2*. *Appl. Microbiol. Biotechnol.* **2004,** *63* (6), 698-704.

61. Rodriguez, G. M.; Tashiro, Y.; Atsumi, S. Expanding ester biosynthesis in Escherichia coli. *Nat. Chem. Biol.* **2014,** *10* (4), 259-265.

62. Zhang, K.; Woodruff, A. P.; Xiong, M. Y.; Zhou, J.; Dhande, Y. K. A synthetic metabolic pathway for production of the platform chemical isobutyric acid. *Chemsuschem* **2011,** *4* (8), 1068-1070.

63. Dhande, Y. K.; Xiong, M.; Zhang, K. Production of C5 carboxylic acids in engineered Escherichia coli. *Process Biochem.* **2012,** *47* (12), 1965-1971.

64. Renna, M. C.; Najimudin, N.; Winik, L. R.; Zahler, S. A. Regulation of the Bacillus Subtilis alsS, alsD, and alsR genes involved in post-exponential-phase production of acetoin *J. Bacteriol.* **1993,** *175* (12), 3863-3875.

65. Daniels, D. L.; Plunkett, G.; Burland, V.; Blattner, F. R. Analysis of the *Escherichia coli* genome DNA sequence of the region from 84.5 to 86.5 minutes. *Science* **1992,** *257* (5071), 771-778.

66. Derrick, S.; Large, P. J. Activities of the enzymes of the Ehrlich pathway and formation of branched-chain alcohols in Saccharomyces cerevisiae and Candida utilis grown in continuous culture on valine or ammonium as sole nitrogen source. *J. Gen. Microbiol.* **1993,** *139*, 2783-2792.

67. Sulzenbacher, G.; Alvarez, K.; van den Heuvel, R. H. H.; Versluis, C.; Spinelli, M.; Campanacci, V.; Valencia, C.; Cambillau, C.; Eklund, H.; Tegoni, M. Crystal structure of E.

coli alcohol dehydrogenase YqhD: evidence of a covalently modified NADP coenzyme. *J. Mol. Biol.* **2004,** *342* (2), 489-502.

68. Connor, M. R.; Liao, J. C. Engineering of an Escherichia coli strain for the production of 3-methyl-1-butanol. *Appl. Environ. Microbiol.* **2008,** *74* (18), 5769-5775.

69. Lutz, R.; Bujard, H. Independent and tight regulation of transcriptional units in Escherichia coli via the LacR/O, the TetR/O and AraC/I-1-I-2 regulatory elements. *Nucleic Acids Res.* **1997,** *25* (6), 1203-1210.

70. Datsenko, K. A.; Wanner, B. L. One-step inactivation of chromosomal genes in Escherichia coli K-12 using PCR products. *Proc. Natl. Acad. Sci. U.S.A.* **2000,** *97* (12), 6640-5.

71. Studier, F. W.; Moffatt, B. A. Use of bacteriophage T7 RNA polymerase to direct selective high-level expression of cloned genes. *J. Mol. Biol.* **1986,** *189* (1), 113-130.

72. Xiong, M.; Deng, J.; Woodruff, A. P.; Zhu, M.; Zhou, J.; Park, S. W.; Li, H.; Fu, Y.; Zhang, K. A bio-catalytic approach to aliphatic ketones. *Sci. Rep.* **2012,** *2*.

73. D'Auria, J. C.; Chen, F.; Pichersky, E. Characterization of an acyltransferase capable of synthesizing benzylbenzoate and other volatile esters in flowers and damaged leaves of Clarkia breweri. *Plant Physiol.* **2002,** *130* (1), 466-476.

74. Fujii, T.; Nagasawa, N.; Iwamatsu, A.; Bogaki, T.; Tamai, W.; Hamachi, M. Molecular cloning, sequence analysis, and expression of the yeast alcohol acetyltransferase gene. *Appl. Environ. Microbiol.* **1994,** *60* (8), 2786-2792.

75. Fujii, T.; Yoshimoto, H.; Tamai, Y. Acetate ester production by Saccharomyces cerevisiae lacking the *ATF1* gene encoding the alcohol acetyltransferase. *J. Ferment. Bioeng.* **1996,** *81* (6), 538-542.

76. Nagasawa, N.; Bogaki, T.; Iwamatsu, A.; Hamachi, M.; Kumagai, C. Cloning and nucleotide sequence of the alcohol acetyltransferase II gene (*ATF2*) from Saccharomyces cerevisiae Kyokai No. 7. *Biosci. Biotechnol. Biochem.* **1998,** *62* (10), 1852-1857.

77. Orlova, I.; Marshall-Colon, A.; Schnepp, J.; Wood, B.; Varbanova, M.; Fridman, E.; Blakeslee, J. J.; Peer, W. A.; Murphy, A. S.; Rhodes, D.; Pichersky, E.; Dudareva, N. Reduction of benzenoid synthesis in petunia flowers reveals multiple pathways to benzoic acid and enhancement in auxin transport. *Plant Cell* **2006,** *18* (12), 3458-3475.

78. Aharoni, A.; Keizer, L. C. P.; Bouwmeester, H. J.; Sun, Z. K.; Alvarez-Huerta, M.; Verhoeven, H. A.; Blaas, J.; van Houwelingen, A.; De Vos, R. C. H.; van der Voet, H.; Jansen, R. C.; Guis, M.; Mol, J.; Davis, R. W.; Schena, M.; van Tunen, A. J.; O'Connell, A. P. Identification of the *SAAT* gene involved in strawberry flavor biogenesis by use of DNA microarrays. *Plant Cell* **2000,** *12* (5), 647-661.

79. Kanehisa, M.; Goto, S. KEGG: Kyoto Encyclopedia of Genes and Genomes. *Nucleic Acids Res.* **2000,** *28* (1), 27-30.

80. Dittrich, C. R.; Bennett, G. N.; San, K. Y. Characterization of the acetate-producing pathways in Escherichia coli. *Biotechnol. Prog.* **2005,** *21* (4), 1062-1067.

81. Bunch, P. K.; MatJan, F.; Lee, N.; Clark, D. P. The *ldhA* gene encoding the fermentative lactate dehydrogenase of Escherichia coli. *Microbiol.* **1997,** *143*, 187-195.

82. Yang, Y. T.; San, K. Y.; Bennett, G. N. Redistribution of metabolic fluxes in Escherichia coli with fermentative lactate dehydrogenase overexpression and deletion. *Metab. Eng.* **1999,** *1* (2), 141-52.

83. Schneider, K.; Dimroth, P.; Bott, M. Biosynthesis of the prosthetic group of citrate lyase. *Biochemistry* **2000,** *39* (31), 9438-9450.

84. Geiger, O.; Gonzalez-Silva, N.; Lopez-Lara, I. M.; Sohlenkamp, C. Amino acid-containing membrane lipids in bacteria. *Prog. Lipid Res.* **2010,** *49* (1), 46-60.

85. Zhang, K.; Xiong, M.; Tai, Y.-S. Cells and methods for producing medium-chain esters. **2013,** *PCT/US2013/031470*, WO/2013/180810.

86. Guo, D. Y.; Zhu, J.; Deng, Z. X.; Liu, T. G. Metabolic engineering of *Escherichia coli* for production of fatty acid short-chain esters through combination of the fatty acid and 2-keto acid pathways. *Metab. Eng.* **2014,** *22*, 69-75.

87. Baba, T.; Ara, T.; Hasegawa, M.; Takai, Y.; Okumura, Y.; Baba, M.; Datsenko, K. A.; Tomita, M.; Wanner, B. L.; Mori, H. Construction of Escherichia coli K-12 in-frame, single-gene knockout mutants: the Keio collection. *Mol. Sys. Biol.* **2006,** *2*.

88. Sambrook, J.; Russell, D. W. *Molecular cloning : a laboratory manual*; Cold Spring Harbor Laboratory: Cold Spring Harbor, 2011.

89. Khorana, H. G.; Agarwal, K. L.; Buchi, H.; Caruthers, M. H.; Gupta, N. K.; Kleppe, K.; Kumar, A.; Otsuka, E.; RajBhandary, U. L.; Van de Sande, J. H.; Sgaramella, V.; Terao, T.; Weber, H.; Yamada, T. Studies on polynucleotides. 103. Total synthesis of the structural gene for an alanine transfer ribonucleic acid from yeast. *J. Mol. Biol.* **1972,** *72* (2), 209-17.

90. Schneider, C. A.; Rasband, W. S.; Eliceiri, K. W. NIH Image to ImageJ: 25 years of image analysis. *Nat. Methods.* **2012,** *9* (7), 671-675.

91. Graham-Rowe, D. Agriculture: Beyond food versus fuel. *Nature* **2011,** *474* (7352), S6-S8.

92. Perlack, R. D.; Wright, L. L.; Turhollow, A. F.; Graham, R. L.; Stokes, B. J.; Erbach, D. C. *Biomass as feedstock for a bioenergy and bioproducts industry: the technical feasibility of a billion-ton annual supply*: Oak Ridge National Laboratory 2005.

93. Li, C.; Cheng, G.; Balan, V.; Kent, M. S.; Ong, M.; Chundawat, S. P.; Melnichenko, Y. B.; Dale, B. E.; Simmons, B. A.; Singh, S. Influence of physico-chemical changes on enzymatic digestibility of ionic liquid and AFEX pretreated corn stover. *Bioresour. Technol.* **2011,** *102* (13), 6928-6936.

94. Himmel, M. E.; Baker, J. O.; Overend, R. P. *Enzymatic conversion of biomass for fuels production*; American Chemical Society: Washington, DC, 1994.

95. Wei, N.; Quarterman, J.; Kim, S. R.; Cate, J. H.; Jin, Y. S. Enhanced biofuel production through coupled acetic acid and xylose consumption by engineered yeast. *Nat. Commun.* **2013,** *4*, 2580.

96. Shaw, A. J.; Podkaminer, K. K.; Desai, S. G.; Bardsley, J. S.; Rogers, S. R.; Thorne, P. G.; Hogsett, D. A.; Lynd, L. R. Metabolic engineering of a thermophilic bacterium to produce ethanol at high yield. *Proc. Natl. Acad. Sci. U.S.A.* **2008,** *105* (37), 13769-13774.

97. Gao, D.; Chundawat, S. P.; Sethi, A.; Balan, V.; Gnanakaran, S.; Dale, B. E. Increased enzyme binding to substrate is not necessary for more efficient cellulose hydrolysis. *Proc. Natl. Acad. Sci. U.S.A.* **2013,** *110* (27), 10922-7.

98. Edwards, M. C.; Henriksen, E. D.; Yomano, L. P.; Gardner, B. C.; Sharma, L. N.; Ingram, L. O.; Peterson, J. D. Addition of genes for cellobiase and pectinolytic activity in Escherichia coli for fuel ethanol production from pectin-rich lignocellulosic biomass. *Appl. Environ. Microbiol.* **2011,** *77* (15), 5184-5191.

99. Cirino, P. C.; Chin, J. W.; Ingram, L. O. Engineering Escherichia coli for xylitol production from glucose-xylose mixtures. *Biotechnol. Bioeng.* **2006,** *95* (6), 1167-76.

100. Niu, W.; Molefe, M. N.; Frost, J. W. Microbial synthesis of the energetic material precursor 1,2,4-butanetriol. *J. Am. Chem. Soc.* **2003,** *125* (43), 12998-9.

101. Yim, H.; Haselbeck, R.; Niu, W.; Pujol-Baxley, C.; Burgard, A.; Boldt, J.; Khandurina, J.; Trawick, J. D.; Osterhout, R. E.; Stephen, R. Metabolic engineering of Escherichia coli for direct production of 1, 4-butanediol. *Nat. Chem. Biol.* **2011,** *7* (7), 445-452.

102. Pharkya, P.; Burgard, A. P.; Maranas, C. D. Exploring the overproduction of amino acids using the bilevel optimization framework OptKnock. *Biotechnol. Bioeng.* **2003,** *84* (7), 887-899.

103. Weimberg, R. Pentose oxidation by Pseudomonas fragi. *J. Biol. Chem.* **1961,** *236* (3), 629-635.

104. Stephens, C.; Christen, B.; Fuchs, T.; Sundaram, V.; Watanabe, K.; Jenal, U. Genetic analysis of a novel pathway for D-xylose metabolism in Caulobacter crescentus. *J. Bacteriol.* **2007,** *189* (5), 2181-2185.

105. Brouns, S. J. J.; Walther, J.; Snijders, A. P. L.; de Werken, H.; Willemen, H.; Worm, P.; de Vos, M. G. J.; Andersson, A.; Lundgren, M.; Mazon, H. F. M.; van den Heuvel, R. H. H.; Nilsson, P.; Salmon, L.; de Vos, W. M.; Wright, P. C.; Bernander, R.; van der Oost, J. Identification of the missing links in prokaryotic pentose oxidation pathways - Evidence for enzyme recruitment. *J. Biol. Chem.* **2006,** *281* (37), 27378-27388.

106. Novick, N. J.; Tyler, M. E. L-Arabinose metabolism in Azospirillum brasiliense. *J. Bacteriol.* **1982,** *149* (1), 364-367.

107. Boer, H.; Maaheimo, H.; Koivula, A.; Penttila, M.; Richard, P. Identification in Agrobacterium tumefaciens of the d-galacturonic acid dehydrogenase gene. *Appl. Microbiol. Biotechnol.* **2010,** *86* (3), 901-909.

108. Andberg, M.; Maaheimo, H.; Boer, H.; Penttila, M.; Koivula, A.; Richard, P. Characterization of a novel Agrobacterium tumefaciens galactarolactone cycloisomerase

enzyme for direct conversion of D-galactarolactone to 3-deoxy-2-keto-L-threo-hexarate. *J. Biol. Chem.* **2012,** *287* (21), 17662-17671.

109. Hosoya, S.; Yamane, K.; Takeuchi, M.; Sato, T. Identification and characterization of the Bacillus subtilis D-glucarate/galactarate utilization operon ycbCDEFGHJ. *FEMS Microbiol. Lett.* **2002,** *210* (2), 193-199.

110. Liu, H. W.; Lu, T. Autonomous production of 1,4-butanediol via a de novo biosynthesis pathway in engineered Escherichia coli. *Metab. Eng.* **2015,** *29*, 135-141.

111. Liu, H. W.; Ramos, K. R. M.; Valdehuesa, K. N. G.; Nisola, G. M.; Lee, W. K.; Chung, W. J. Biosynthesis of ethylene glycol in Escherichia coli. *Appl. Microbiol. Biotechnol.* **2013,** *97* (8), 3409-3417.

112. Meijnen, J. P.; de Winde, J. H.; Ruijssenaars, H. J. Establishment of oxidative D-xylose metabolism in Pseudomonas putida S12. *Appl. Environ. Microbiol.* **2009,** *75* (9), 2784-2791.

113. Radek, A.; Krumbach, K.; Gatgens, J.; Wendisch, V. F.; Wiechert, W.; Bott, M.; Noack, S.; Marienhagen, J. Engineering of Corynebacterium glutamicum for minimized carbon loss during utilization of D-xylose containing substrates. *J. Biotechnol.* **2014,** *192*, 156-160.

114. Lin, Y. H.; Shen, X. L.; Yuan, Q. P.; Yan, Y. J. Microbial biosynthesis of the anticoagulant precursor 4-hydroxycoumarin. *Nat. Commun.* **2013,** *4*.

115. Djurdjevic, I.; Zelder, O.; Buckel, W. Production of glutaconic acid in a recombinant Escherichia coli strain. *Appl. Environ. Microbiol.* **2011,** *77* (1), 320-2.

116. Zhang, K.; Xiong, M. Biosynthetic pathways and methods for TCA derivatives. **2014,** *PCT/US2013/076118, WO 2014/100173*.

117. Moore, R. A.; Reckseidler-Zenteno, S.; Kim, H.; Nierman, W.; Yu, Y.; Tuanyok, A.; Warawa, J.; DeShazer, D.; Woods, D. E. Contribution of gene loss to the pathogenic evolution of Burkholderia pseudomallei and Burkholderia mallei. *Infect. Immun.* **2004,** *72* (7), 4172-4187.

118. Stoolmiller, A. C.; Abeles, R. H. Formation of α-ketoglutaric semialdehyde from l-2-keto-3-deoxyarabonic acid and isolation of l-2-keto-3-deoxyarabonate dehydratase from Pseudomonas saccharophila. *J. Biol. Chem.* **1966,** *241* (24), 5764-5771.

119. Duncan, M. J. L-Arabinose metabolism in Rhizobia. *J. Gen. Microbiol.* **1979,** *113*, 177-179.

120. Yoon, S. H.; Moon, T. S.; Iranpour, P.; Lanza, A. M.; Prather, K. J. Cloning and characterization of uronate dehydrogenases from two pseudomonads and Agrobacterium tumefaciens strain C58. *J. Bacteriol.* **2009,** *191* (5), 1565-73.

121. de la Plaza, M.; Fernandez de Palencia, P.; Pelaez, C.; Requena, T. Biochemical and molecular characterization of alpha-ketoisovalerate decarboxylase, an enzyme involved in the formation of aldehydes from amino acids by Lactococcus lactis. *FEMS Microbiol. Lett.* **2004,** *238* (2), 367-74.

122. Iding, H.; Dunnwald, T.; Greiner, L.; Liese, A.; Muller, M.; Siegert, P.; Grotzinger, J.; Demir, A. S.; Pohl, M. Benzoylformate decarboxylase from Pseudomonas putida as stable catalyst for the synthesis of chiral 2-hydroxy ketones. *Chem-Eur. J.* **2000,** *6* (8), 1483-1495.

123. Bastian, S.; Liu, X.; Meyerowitz, J. T.; Snow, C. D.; Chen, M. M. Y.; Arnold, F. H. Engineered ketol-acid reductoisomerase and alcohol dehydrogenase enable anaerobic 2-methylpropan-1-ol production at theoretical yield in Escherichia coli. *Metab. Eng.* **2011,** *13* (3), 345-352.

124. Larroy, C.; Fernandez, M. R.; Gonzalez, E.; Pares, X.; Biosca, J. A. Characterization of the Saccharomyces cerevisiae YMR318C (ADH6) gene product as a broad specificity NADPH-dependent alcohol dehydrogenase: relevance in aldehyde reduction. *Biochem. J.* **2002,** *361*, 163-172.

125. Oshima, T.; Biville, F. Functional identification of ygiP as a positive regulator of the ttdA-ttdB-ygjE operon. *Microbiol.* **2006,** *152* (7), 2129-2135.

126. Berthold, C. L.; Gocke, D.; Wood, M. D.; Leeper, F. J.; Pohl, M.; Schneider, G. Structure of the branched-chain keto acid decarboxylase (KdcA) from Lactococcus lactis provides insights into the structural basis for the chemoselective and enantioselective carboligation reaction. *Acta. Cryst.* **2007,** *63* (Part 12), 1217-1224.

127. Xiong, M. Y.; Schneiderman, D. K.; Bates, F. S.; Hillmyer, M. A.; Zhang, K. Scalable production of mechanically tunable block polymers from sugar. *Proc. Natl. Acad. Sci. U.S.A.* **2014,** *111* (23), 8357-8362.

128. Eiteman, M. A.; Altman, E. Overcoming acetate in Escherichia coli recombinant protein fermentations. *Trends Biotechnol.* **2006,** *24* (11), 530-536.

129. Gorke, B.; Stulke, J. Carbon catabolite repression in bacteria: many ways to make the most out of nutrients. *Nat. Rev. Microbiol.* **2008,** *6* (8), 613-24.

130. Engler, C.; Kandzia, R.; Marillonnet, S. A one pot, one step, precision cloning method with high throughput capability. *PloS one* **2008,** *3* (11), e3647.

131. Watanabe, S.; Shimada, N.; Tajima, K.; Kodaki, T.; Makino, K. Identification and characterization of L-arabonate dehydratase, L-2-keto-3-deoxyarabonate dehydratase, and L-arabinolactonase involved in an alternative pathway of L-arabinose metabolism - Novel evolutionary insight into sugar metabolism. *J. Biol. Chem.* **2006,** *281* (44), 33521-33536.

132. Perez, J. M.; Arenas, F. A.; Pradenas, G. A.; Sandoval, J. M.; Vasquez, C. C. Escherichia coli YqhD exhibits aldehyde reductase activity and protects from the harmful effect of lipid peroxidation-derived aldehydes. *J. Biol. Chem.* **2008,** *283* (12), 7346-7353.

133. Bechthold, I.; Bretz, K.; Kabasci, S.; Kopitzky, R.; Springer, A. Succinic acid: a new platform chemical for biobased polymers from renewable resources. *Chem. Eng. Technol.* **2008,** *31* (5), 647-654.

134. Hong, U. G.; Park, H. W.; Lee, J.; Hwang, S.; Kwak, J.; Yi, J.; Song, I. K. Hydrogenation of succinic acid to 1,4-butanediol over rhenium catalyst supported on copper-containing mesoporous carbon. *J. Nanosci. Nanotechnol.* **2013,** *13* (11), 7448-7453.

135. Sato, K.; Aoki, M.; Noyori, R. A "green" route to adipic acid: Direct oxidation of cyclohexenes with 30 percent hydrogen peroxide. *Science* **1998,** *281* (5383), 1646-1647.

136. Lopez-Garzon, C. S.; Straathof, A. J. J. Recovery of carboxylic acids produced by fermentation. *Biotechnol. Adv.* **2014,** *32* (5), 873-904.

137. Blair, A. H.; Barker, H. A. Assay and purification of (+)-citramalate hydro-lyase components from Clostridium tetanomorphum. *J. Biol. Chem.* **1966,** *241* ((2)), 400-408.

138. Kronen, M.; Sasikaran, J.; Berg, I. A. Mesaconase cctivity of class I fumarase contributes to mesaconate utilization by Burkholderia xenovorans. *Appl. Environ. Microbiol.* **2015,** *81* (16), 5632-5638.

139. Uzum, O. B.; Karadag, E. Equilibrium swelling studies of highly swollen acrylamide/mesaconic acid hydrogels. *J. Appl. Polym. Sci.* **2005,** *96* (6), 2253-2259.

140. White, J. D.; Sheldon, B. G. Intramolecular Diels-Alder reactions of sorbyl citraconate and sesaconate esters. *J. Org. Chem.* **1981,** *46* (11), 2273-2280.

141. Gillham, H. C.; Sherr, A. E. Flame-retardant agents for thermoplastic products. U.S. **1969,** *PCT/US3431324A*.

142. Guccione, E.; Hitchcock, A.; Hall, S. J.; Mulholland, F.; Shearer, N.; van Vliet, A. H. M.; Kelly, D. J. Reduction of fumarate, mesaconate and crotonate by Mfr, a novel oxygen-regulated periplasmic reductase in Campylobacter jejuni. *Environ. Microbiol.* **2010,** *12* (3), 576-591.

143. Sonntag, F.; Buchhaupt, M.; Schrader, J. Thioesterases for ethylmalonyl-CoA pathway derived dicarboxylic acid production in Methylobacterium extorquens AM1. *Appl. Microbiol. Biotechnol.* **2014,** *98* (10), 4533-4544.

144. Sonntag, F.; Müller, J. E. N.; Kiefer, P.; Vorholt, J. A.; Schrader, J.; Buchhaupt, M. High-level production of ethylmalonyl-CoA pathway-derived dicarboxylic acids by Methylobacterium extorquens under cobalt-deficient conditions and by polyhydroxybutyrate negative strains. *Appl. Microbiol. Biotechnol.* **2015,** *99* (8), 3407-3419.

145. Buckel, W.; Barker, H. A. Two pathways of glutamate fermentation by anaerobic bacteria *J. Bacteriol.* **1974,** *117* (3), 1248-1260.

146. Wang, J.; Zhang, K. Production of mesaconate in Escherichia coli by engineered glutamate mutase pathway. *Metab. Eng.* **2015,** *30*, 190-196.

147. Jojima, T.; Omumasaba, C. A.; Inui, M.; Yukawa, H. Sugar transporters in efficient utilization of mixed sugar substrates: current knowledge and outlook. *Appl. Microbiol. Biotechnol.* **2010,** *85* (3), 471-480.

148. Weber, C.; Farwick, A.; Benisch, F.; Brat, D.; Dietz, H.; Subtil, T.; Boles, E. Trends and challenges in the microbial production of lignocellulosic bioalcohol fuels. *Appl. Microbiol. Biotechnol.* **2010,** *87* (4), 1303-1315.

149. Feldmann, S. D.; Sahm, H.; Sprenger, G. A. Cloning and expression of the genes for xylose isomerase and xylulokinase from Klebsiella pneumoniae 1033 in Escherichia coli K12. *Mol. Gen. Genet.* **1992,** *234* (2), 201-210.

150. Bruckner, R.; Titgemeyer, F. Carbon catabolite repression in bacteria: choice of the carbon source and autoregulatory limitation of sugar utilization. *FEMS Microbiol. Lett.* **2002,** *209* (2), 141-148.

151. Dien, B. S.; Nichols, N. N.; Bothast, R. J. Fermentation of sugar mixtures using Escherichia coli catabolite repression mutants engineered for production of L-lactic acid. *J. Ind. Microbiol. Biotechnol.* **2002,** *29* (5), 221-227.

152. Tai, Y.-S.; Xiong, M.; Jambunathan, P.; Wang, J.; Wang, J.; Stapleton, C.; Zhang, K. Engineering nonphosphorylative metabolism to generate lignocellulose-derived products. *Nat. Chem. Biol.* **2016,** *12* (4), 247-253.

153. Dagley, S.; Trudgill, P. W. The metabolism of galactarate, D-glucarate and various pentoses by species of Pseudomonas. *Biochem. J.* **1965,** *95* ((1)), 48-58.

154. Stülke, J.; Hillen, W. Carbon catabolite repression in bacteria. *Curr. Opin. Microbiol.* **1999,** *2* (2), 195-201.

155. Desai, T. A.; Rao, C. V. Regulation of arabinose and xylose metabolism in Escherichia coli. *Appl. Environ. Microbiol.* **2010,** *76* (5), 1524-1532.

156. Hasona, A.; Kim, Y.; Healy, F. G.; Ingram, L. O.; Shanmugam, K. T. Pyruvate formate lyase and acetate kinase are essential for anaerobic growth of Escherichia coli on xylose. *J. Bacteriol.* **2004,** *186* (22), 7593-7600.

157. Shamanna, D. K.; Sanderson, K. E. Uptake and catabolism of D-xylose in Salmonella typhimurium Lt2. *J. Bacteriol.* **1979,** *139* (1), 64-70.

158. Song, S. G.; Park, C. Utilization of D-ribose through D-xylose transporter. *FEMS Microbiol. Lett.* **1998,** *163* (2), 255-261.

159. Buck, D.; Spencer, M. E.; Guest, J. R. Cloning and Expression of the Succinyl-Coa Synthetase Genes of Escherichia coli-K12. *J. Gen. Microbiol.* **1986,** *132*, 1753-1762.

160. Sakamoto, N.; Kotre, A. M.; Savageau, M. A. Glutamate dehydrogenase from Escherichia coli: purification and properties. *J. Bacteriol.* **1975,** *124* (2), 775-783.

161. Miller, J. H. *Experiments in molecular genetics*; Cold Spring Harbor Laboratory1972.

162. Kamal, A.; Sandbhor, M.; Shaik, A. A. Application of a one-pot lipase resolution strategy for the synthesis of chiral gamma- and delta-lactones. *Tetrahedron: Asymmetry* **2003,** *14* (11), 1575-1580.

163. Davies-Coleman, M. T.; Rivett, D. E. A. Naturally occurring 6-substituted 5,6-dihydro-α-pyrones. In *Fortschritte der Chemie organischer Naturstoffe / Progress in the Chemistry of Organic Natural Products*, Herz, W.; Grisebach, H.; Kirby, G. W.; Tamm, C., Eds.; Springer Vienna, 1989; Vol. 55, pp 1-35.

164. Korpak, M.; Pietruszka, J. Chemoenzymatic one-pot synthesis of gamma-butyrolactones. *Adv. Synth. Catal.* **2011,** *353* (9), 1420-1424.

165. Paryzek, Z.; Skiera, W. Synthesis and cleavage of lactones and thiolactones. Applications in organic synthesis. A review. *Org. Prep. Proced. Int.* **2007,** *39* (3), 203-296.

166. Wang, S. Z.; Kayser, M. M.; Jurkauskas, V. Access to optically pure 4-and 5-substituted lactones: A case of chemical-biocatalytical cooperation. *J. Org. Chem.* **2003,** *68* (16), 6222-6228.

167. Li, S. M.; McCarthy, S. Influence of crystallinity and stereochemistry on the enzymatic degradation of poly(lactide)s. *Macromolecules* **1999,** *32* (13), 4454-4456.

168. Xiao, Y.; Cummins, D.; Palmans, A. R. A.; Koning, C. E.; Heise, A. Synthesis of biodegradable chiral polyesters by asymmetric enzymatic polymerization and their formulation into microspheres. *Soft Matter* **2008,** *4* (3), 593-599.

169. Childers, M. I.; Longo, J. M.; Van Zee, N. J.; LaPointe, A. M.; Coates, G. W. Stereoselective epoxide polymerization and copolymerization. *Chem. Rev.* **2014,** *114* (16), 8129-8152.

170. Takii, K.; Kanbayashi, N.; Onitsuka, K. Modular synthesis of optically active lactones by Ru-catalyzed asymmetric allylic carboxylation and ring-closing metathesis reaction. *Chem. Commun.* **2012,** *48* (32), 3872-3874.

171. Evans, D. A.; Johnson, J. S.; Olhava, E. J. Enantioselective synthesis of dihydropyrans. Catalysis of hetero Diels-Alder reactions by bis(oxazoline) copper(II) complexes. *J. Am. Chem. Soc.* **2000,** *122* (8), 1635-1649.

172. Ohta, H.; Tetsukawa, H.; Noto, N. Enantiotopically selective oxidation of alpha, omega-diols with the enzyme systems of microorganisms. *J. Org. Chem.* **1982,** *47* (12), 2400-2404.

173. Honda, Y.; Morita, E.; Ohshiro, K.; Tsuchihashi, G. 1,3-Asymmetric Induction In Acyclic Systems by Practical Application Of Dithioacetal Group. *Chem. Lett.* **1988,** (1), 21-24.

174. Osa, T.; Kashiwagi, Y.; Yanagisawa, Y. Electroenzymatic oxidation of alcohols on a poly(acrylic acid)-coated graphite felt electrode terimmobilizing ferrocene, diaphorase and alcohol dehydrogenase. *Chem. Lett.* **1994,** (2), 367-370.

175. Kamerbeek, N. M.; Janssen, D. B.; van Berkel, W. J. H.; Fraaije, M. W. Baeyer-Villiger monooxygenases, an emerging family of flavin-dependent biocatalysts. *Adv. Synth. Catal.* **2003,** *345* (6-7), 667-678.

176. Kayser, M. M.; Chen, G.; Stewart, J. D. Enantio- and regioselective Baeyer-Villiger oxidations of 2- and 3-substituted cyclopentanones using engineered bakers' yeast. *J. Org. Chem.* **1998,** *63* (20), 7103-7106.

177. Shimoda, K.; Kubota, N. Asymmetric reduction of 2-substituted 2-butenolides with reductase from Marchantia polymorpha. *Tetrahedron: Asymmetry* **2004,** *15* (24), 3827-3829.

178. Shimoda, K.; Kubota, N.; Hirata, T.; Kondo, Y.; Hamada, H. Stereoselective reduction of 2-butenolides to chiral butanolides by reductases from cultured cells of Glycine max. *Tetrahedron Lett.* **2007,** *48* (8), 1345-1347.

179. Fischer, T.; Pietruszka, J. Alcohol dehydrogenase-catalyzed synthesis of enantiomerically pure delta-lactones as versatile intermediates for natural product synthesis. *Adv. Synth. Catal.* **2012,** *354* (13), 2521-2530.

180. Classen, T.; Korpak, M.; Scholzel, M.; Pietruszka, J. Stereoselective enzyme cascades: an efficient synthesis of chiral gamma-butyrolactones. *ACS Catal.* **2014,** *4* (5), 1321-1331.

181. Brenna, E.; Gatti, F. G.; Monti, D.; Parmeggiani, F.; Sacchetti, A.; Valoti, J. Substrate-engineering approach to the stereoselective chemo-multienzymatic cascade synthesis of Nicotiana tabacum lactone. *J. Mol. Catal. B-Enzym.* **2015,** *114*, 77-85.

182. Turrini, N. G.; Hall, M.; Faber, K. Enzymatic synthesis of optically active lactones via asymmetric bioreduction using ene-reductases from the old yellow enzyme Family. *Adv. Synth. Catal.* **2015,** *357* (8), 1861-1871.

183. Takabe, K.; Hiyoshi, H.; Sawada, H.; Tanaka, M.; Miyazaki, A.; Yamada, T.; Katagiri, T.; Yoda, H. Baker's yeast reduction of 3-phenylthiomethyl-2-butanolide and its derivatives-synthesis of versatile chiral C5-building blocks for terpenoid synthesis. *Tetrahedron: Asymmetry* **1992,** *3* (11), 1399-1400.

184. Paddon, C. J.; Westfall, P. J.; Pitera, D. J.; Benjamin, K.; Fisher, K.; McPhee, D.; Leavell, M. D.; Tai, A.; Main, A.; Eng, D.; Polichuk, D. R.; Teoh, K. H.; Reed, D. W.; Treynor, T.; Lenihan, J.; Fleck, M.; Bajad, S.; Dang, G.; Dengrove, D.; Diola, D.; Dorin, G.; Ellens, K. W.; Fickes, S.; Galazzo, J.; Gaucher, S. P.; Geistlinger, T.; Henry, R.; Hepp, M.; Horning, T.; Iqbal, T.; Jiang, H.; Kizer, L.; Lieu, B.; Melis, D.; Moss, N.; Regentin, R.; Secrest, S.; Tsuruta, H.; Vazquez, R.; Westblade, L. F.; Xu, L.; Yu, M.; Zhang, Y.; Zhao, L.; Lievense, J.; Covello, P. S.; Keasling, J. D.; Reiling, K. K.; Renninger, N. S.; Newman, J. D. High-level semi-synthetic production of the potent antimalarial artemisinin. *Nature* **2013,** *496* (7446), 528-532.

185. Martin, V. J. J.; Pitera, D. J.; Withers, S. T.; Newman, J. D.; Keasling, J. D. Engineering a mevalonate pathway in Escherichia coli for production of terpenoids. *Nat. Biotechnol.* **2003,** *21* (7), 796-802.

186. Drueckhammer, D. G.; Riddle, V. W.; Wong, C. H. Fmn reductase catalyzed regeneration of NAD(P) for use In enzymatic-synthesis. *J. Org. Chem.* **1985,** *50* (25), 5387-5389.

187. Hughes, G.; Kimura, M.; Buchwald, S. L. Catalytic enantioselective conjugate reduction of lactones and lactams. *J. Am. Chem. Soc.* **2003,** *125* (37), 11253-11258.

188. Verendel, J. J.; Li, J. Q.; Quan, X.; Peters, B.; Zhou, T. G.; Gautun, O. R.; Govender, T.; Andersson, P. G. Chiral hetero- and carbocyclic compounds from the asymmetric hydrogenation of cyclic alkenes. *Chem. Eur. J.* **2012,** *18* (21), 6507-6513.

189. Padhi, S. K.; Bougioukou, D. J.; Stewart, J. D. Site-saturation mutagenesis of tryptophan 116 of Saccharomyces pastorianus old yellow enzyme uncovers stereocomplementary variants. *J. Am. Chem. Soc.* **2009,** *131* (9), 3271-3280.

190. Fitzpatrick, T. B.; Amrhein, N.; Macheroux, P. Characterization of YqjM, an old yellow enzyme homolog from Bacillus subtilis involved in the oxidative stress response. *J. Biol. Chem.* **2003,** *278* (22), 19891-19897.

191. Kitzing, K.; Fitzpatrick, T. B.; Wilken, C.; Sawa, J.; Bourenkov, G. P.; Macheroux, P.; Clausen, T. The 1.3 A crystal structure of the flavoprotein YqjM reveals a novel class of old yellow enzymes. *J. Biol. Chem.* **2005,** *280* (30), 27904-27913.

192. Bougioukou, D. J.; Kille, S.; Taglieber, A.; Reetz, M. T. Directed evolution of an enantioselective enoate-reductase: testing the utility of iterative saturation mutagenesis. *Adv. Synth. Catal.* **2009,** *351* (18), 3287-3305.

193. Ishmuratov, G. Y.; Yakovleva, M. P.; Zaripova, G. V.; Botsman, L. P.; Muslukhov, R. R.; Tolstikov, G. A. Novel synthesis of (4R)-4-methylpentanolide from (L)-(-)-menthol. *Chem. Nat. Compd.* **2004,** *40* (6), 548-551.

194. Kim, K. H.; Shin, Y. J.; Choi, S. U.; Lee, K. R. New cytotoxic delta-valerolactones from Cornus walteri. *B. Korean. Chem. Soc.* **2011,** *32* (7), 2443-2445.

195. Irwin, A. J.; Jones, J. B. Asymmetric syntheses via enantiotopically selective horse liver alcohol dehydrogenase catalyzed oxidations of diols containing a prochiral center. *J. Am. Chem. Soc.* **1977,** *99* (2), 556-561.

196. Berman, H. M.; Westbrook, J.; Feng, Z.; Gilliland, G.; Bhat, T. N.; Weissig, H.; Shindyalov, I. N.; Bourne, P. E. The Protein Data Bank. *Nucleic Acids Res.* **2000,** *28* (1), 235-242.

197. Connor, M. R.; Liao, J. C. Microbial production of advanced transportation fuels in non-natural hosts. *Curr. Opin. Biotechnol.* **2009,** *20* (3), 307-315.

198. Keasling, J. D. Manufacturing molecules through metabolic engineering. *Science* **2010,** *330* (6009), 1355-1358.

199. Stephanopoulos, G. Challenges in engineering microbes for biofuels production. *Science* **2007,** *315* (5813), 801-804.

200. Lennen, R. M.; Pfleger, B. F. Engineering Escherichia coli to synthesize free fatty acids. *Trends Biotechnol.* **2012,** *30* (12), 659-667.

201. Xu, P.; Gu, Q.; Wang, W. Y.; Wong, L.; Bower, A. G. W.; Collins, C. H.; Koffas, M. A. G. Modular optimization of multi-gene pathways for fatty acids production in E. coli. *Nat. Commun.* **2013,** *4*.

202. Tseng, H. C.; Prather, K. L. Controlled biosynthesis of odd-chain fuels and chemicals via engineered modular metabolic pathways. *Proc. Natl. Acad. Sci. U.S.A.* **2012,** *109* (44), 17925-30.

203. Achkar, J.; Xian, M.; Zhao, H.; Frost, J. Biosynthesis of phloroglucinol. *J. Am. Chem. Soc.* **2005,** *127* (15), 5332-5333.

204. Cheong, S.; Clomburg, J. M.; Gonzalez, R. Energy- and carbon-efficient synthesis of functionalized small molecules in bacteria using non-decarboxylative Claisen condensation reactions. *Nat Biotechnol.* **2016,** *34* (5), 556-561.

205. Handke, P.; Lynch, S. A.; Gill, R. T. Application and engineering of fatty acid biosynthesis in Escherichia coli for advanced fuels and chemicals. *Metab. Eng.* **2011,** *13* (1), 28-37.

206. Yan, Y. J.; Kohli, A.; Koffas, M. A. G. Biosynthesis of natural flavanones in Saccharomyces cerevisiae. *Appl. Environ. Microbiol.* **2005,** *71* (9), 5610-5613.

207. Alper, H.; Miyaoku, K.; Stephanopoulos, G. Construction of lycopene-overproducing E. coli strains by combining systematic and combinatorial gene knockout targets. *Nat. Biotechnol.* **2005,** *23* (5), 612-616.

208. Zhu, Y. H.; Eiteman, M. A.; Altman, R.; Altman, E. High glycolytic flux improves pyruvate production by a metabolically engineered Escherichia coli strain. *Appl. Environ. Microbiol.* **2008,** *74* (21), 6649-6655.